MNRAS **430,** 1125–1157 (2013) doi:10.1093/mnras/sts681

The RMS survey: near-IR spectroscopy of massive young stellar objects

H. D. B. Cooper,[1]★ S. L. Lumsden,[1] R. D. Oudmaijer,[1] M. G. Hoare,[1] A. J. Clarke,[1] J. S. Urquhart,[2] J. C. Mottram,[3] T. J. T. Moore[4] and B. Davies[4]

[1]*School of Physics & Astronomy, University of Leeds, Leeds LS2 9JT, UK*
[2]*Max-Planck-Institut für Radioastronomie, D-53121 Bonn, Germany*
[3]*Leiden Observatory, Leiden University, NL-2300 RA Leiden, the Netherlands*
[4]*Astrophysics Research Institute, Liverpool John Moores University, Twelve Quays House, Egerton Wharf, Birkenhead CH41 1LD, UK*

Accepted 2012 December 20. Received 2012 December 20; in original form 2012 June 10

ABSTRACT

Near-infrared *H*- and *K*-band spectra are presented for 247 objects, selected from the Red MSX Source (RMS) survey as potential young stellar objects (YSOs). 195 (∼80 per cent) of the targets are YSOs, of which 131 are massive YSOs ($L_{\rm BOL} > 5 \times 10^3$ L$_\odot$, $M > 8$ M$_\odot$). This is the largest spectroscopic study of massive YSOs to date, providing a valuable resource for the study of massive star formation. In this paper, we present our exploratory analysis of the data. The YSOs observed have a wide range of embeddedness ($2.7 < A_V < 114$), demonstrating that this study covers minimally obscured objects right through to very red, dusty sources. Almost all YSOs show some evidence for emission lines, though there is a wide variety of observed properties. The most commonly detected lines are Brγ, H_2, fluorescent Fe II, CO bandhead, [Fe II] and He I 2–1 ^{1}S–^{1}P, in order of frequency of occurrence. In total, ∼40 per cent of the YSOs display either fluorescent Fe II 1.6878 μm or CO bandhead emission (or both), indicative of a circumstellar disc; however, no correlation of the strength of these lines with bolometric luminosity was found. We also find that ∼60 per cent of the sources exhibit [Fe II] or H_2 emission, indicating the presence of an outflow. Three quarters of all sources have Brγ in emission. A good correlation with bolometric luminosity was observed for both the Brγ and H_2 emission line strengths, covering $1 < L_{\rm BOL} < 3.5 \times 10^5$ L$_\odot$. This suggests that the emission mechanism for these lines is the same for low-, intermediate- and high-mass YSOs, i.e. high-mass YSOs appear to resemble scaled-up versions of low-mass YSOs.

Key words: line: identification – stars: formation – stars: pre-main-sequence – ISM: jets and outflows.

1 INTRODUCTION

Massive stars (>8 M$_\odot$, i.e. >5 × 10^3 L$_\odot$) have a profound influence on their surroundings due to their intense ionizing radiation, strong stellar winds and powerful outflows. However, despite the fact that low-mass star formation is broadly understood (Shu, Adams & Lizano 1987), relatively little is known about the conditions and processes that influence high-mass star formation. The study of massive star formation is hindered by the rarity of massive stars, their short evolutionary time-scales and the dust extinction which renders the stars invisible at short wavelengths for most of their formation.

The massive young stellar object (MYSO) phase is of particular interest for the study of massive star formation. In this relatively brief phase (10$^{4–5}$ yr; Davies et al. 2011; Mottram et al. 2011a), fusion has begun in the central star, but it has not yet ionized its surroundings to form an H II region. Accretion may be disrupted or completely halted, in which case the final mass of the star would be set in this phase. MYSOs typically have strong, ionized stellar winds (Bunn, Hoare & Drew 1995) and bipolar molecular outflows (Shepherd & Churchwell 1996), both of which have an important feedback effect on the surrounding molecular cloud.

Whilst these properties mean that the MYSO stage is crucial to the understanding of massive star formation, their observation is not without difficulties. Dust extinction hinders optical and infrared (IR) studies, their lack of H II regions means that radio emission is either weak or non-existent, and although MYSOs are often associated with masers, no single maser transition can be guaranteed to be present (Beuther et al. 2002).

Most of the bolometric luminosity of MYSOs is found in the thermal IR, so that is where they are most easily observed. Previous attempts to produce a large sample of MYSOs have been made using *IRAS* (e.g. Molinari et al. 1996; Sridharan et al. 2002). The low

★ E-mail: pyhdc@leeds.ac.uk

spatial resolution of *IRAS* (3 arcmin × 5 arcmin at 100 μm) meant that in star clusters and in the dense environment of the Galactic plane sources were often confused. Since most massive stars form in clusters and exist within the Galactic plane, the MYSOs in these studies may not be representative of all massive stars. The small number of MYSOs that have been identified so far means that there is a lack of statistical evidence with which to improve our understanding of high-mass star formation.

The Red MSX Source survey (RMS; Hoare et al. 2005; Urquhart et al. 2008a) is a valuable tool with which to address these issues, having taken both imaging and spectroscopic data from near-IR to radio wavelengths on a comprehensive, uniformly selected sample of MYSOs. The MSX point source catalogue (Egan et al. 2003) and near-IR 2 Micron All Sky Survey (2MASS; Skrutskie et al. 2006) data were used to find sources with IR excess. The MSX survey has a much better spatial resolution than *IRAS*, thus eliminating the bias against dense environments (Hoare et al. 2004). The reddest, most embedded objects were selected as targets using colour cuts defined by Lumsden et al. (2002). However, ultracompact H II (UCHII) regions, planetary nebulae (PN) and dusty evolved stars also have similar colours to MYSOs, so classification of the sources has been a major part of the project. A campaign of follow-up observations has been undertaken to achieve this (see Urquhart et al. 2008a). We combined radio, mid-IR and near-IR images with kinematic distances and far-IR data to characterize our sources (Mottram et al. 2007, 2010, 2011a; Urquhart et al. 2007a,b, 2008b, 2009a,b, 2011a,b, 2012). The full classification criteria are discussed in Lumsden et al. (in preparation).

Near-IR spectroscopy is the final classification stage, separating the MYSOs from the remaining sources. To date, ∼90 per cent of the ∼2000 objects from the original survey have been classified, identifying ∼600 MYSOs and ∼500 UCHII regions.[1] In total, we have spectroscopic observations of ∼450 objects. The data for the ∼200 objects observed in the Southern hemisphere are still in the analysis process, and will be presented in a future paper. In this paper, we present near-IR spectra and classifications of 247 objects observed in the Northern hemisphere, i.e. ∼12 per cent of the objects in the survey.

2 OBSERVATIONS

Spectroscopic observations of the YSO candidates were made using the UIST instrument at the United Kingdom Infra-Red Telescope (UKIRT) observatory from 2002 to 2008. 247 objects were successfully observed over 84 nights. Sources were selected from the ∼2000 candidate MYSOs found using the MSX catalogue in the preceding stages of the RMS survey. Initially, no radio or luminosity data were available, so the criteria for the spectroscopic observations were that the objects satisfy the colour cuts laid out in Lumsden et al. (2002), and that they were bright enough to be seen at the *K* band in 2MASS to enable correct identification of the counterpart. Once luminosity estimates were available, a loose luminosity cut of $L_{21\,\mu m} \geq 500\ L_{\odot}$ (which corresponds to $L_{BOL} \geq 10\,000\ L_{\odot}$, see Mottram et al. 2011a) was imposed. Therefore fewer low-luminosity sources were observed in the later runs. We targeted our source selection to observe all objects we believed to be YSOs with the appropriate luminosity, plus the 10 per cent of the ∼2000 candidates whose classifications were ambiguous. A full list of observational parameters for each individual object is shown in Tables A1 and A2 (see Appendix A).

UIST is a 1–5 μm imager spectrometer with a 1024 × 1024 InSb array and a camera with 0.12 arcsec/pixel resolution in spectroscopy mode. The HK grism (1.395–2.506 μm) was used, with a 0.48 arcsec × 120 arcsec long slit. This produces a fairly low spectral resolution of $\lambda/\Delta\lambda \sim 500$, but meant that in ideal conditions a high signal-to-noise ratio could be achieved with relatively short exposure time. This allowed identification of faint lines whilst maximizing the number of objects that could be observed in the time awarded. In practice, a large number of the observations were done in poor weather conditions and with typical seeing of 1 arcsec, so the signal-to-noise ratio was not always very high, and flux calibration was unreliable on some nights. Exposure times for each object are shown in Table A1.

Many of the observations were taken before the near-IR counterparts had been accurately identified. As a result, finding charts was frequently done at the telescope using UIST in imaging mode so that the counterpart could be identified prior to taking the spectrum. In a few instances, such spectra were repeated later if subsequent high spatial resolution thermal IR images suggested that a different source was the correct counterpart. The position angle for the slit (also shown in Table A1) was derived from such images, as well as from 2MASS images for brighter, isolated sources, or GLIMPSE[2] for complex embedded sources. The aim was to avoid very bright, unrelated stars nearby, and if possible to align the slit on other interesting objects and extended emission nearby. This proved a useful technique as several fields of view had more than one MYSO within the field, and many have extended emission. In the tables, multiple objects within the same field of view are denoted by G*** – 1, G*** – 2, etc.

Standard stars with spectral types ranging from A0 to B9.5 were observed before each object for flux calibration, and the objects were nodded along the slit to minimize the effect of bad pixels and aid sky subtraction. The spectrum of an argon lamp was taken each night for wavelength calibration.

The standard star and object spectra were all reduced using the UKIRT pipeline ORAC-DR and the Starlink package FIGARO. To prevent confusion between emission lines in the object spectra and the H I absorption lines in the standard star spectra, the lines in the standards were fitted with Gaussian functions and removed before flux calibrating the object spectra. Flux calibration was done using the FIGARO routine IRFLUX. This routine uses a blackbody model for the standard star, normalized to the star's flux at *K*. The *K*-band magnitudes and spectral types of the standard stars were taken from the SIMBAD data base. The temperatures corresponding to the spectral types were taken from Schmidt-Kaler (1982).

3 PHOTOMETRY

We compared our magnitude data with the 2MASS Point Source Catalogue (2MASS PSC; Skrutskie et al. 2006) and UKIDSS Galactic Plane Survey (GPS) data base release 8.[3] The choice of catalogue

[1] See RMS data base http://www.ast.leeds.ac.uk/RMS/, Lumsden et al. (in preparation).

[2] GLIMPSE: the Galactic Legacy Infrared Mid-Plane Survey Extraordinaire – a Spitzer legacy science programme which imaged the Galactic mid-plane at 3.6, 4.5, 5.8 and 8 μm.

[3] The UKIDSS project is defined in Lawrence et al. (2007). UKIDSS uses the UKIRT Wide Field Camera (WFCAM; Casali et al. 2007) and a photometric system described in Hewett et al. (2006). The pipeline processing and science archive are described in Irwin (2008) and Hambly et al. (2008).

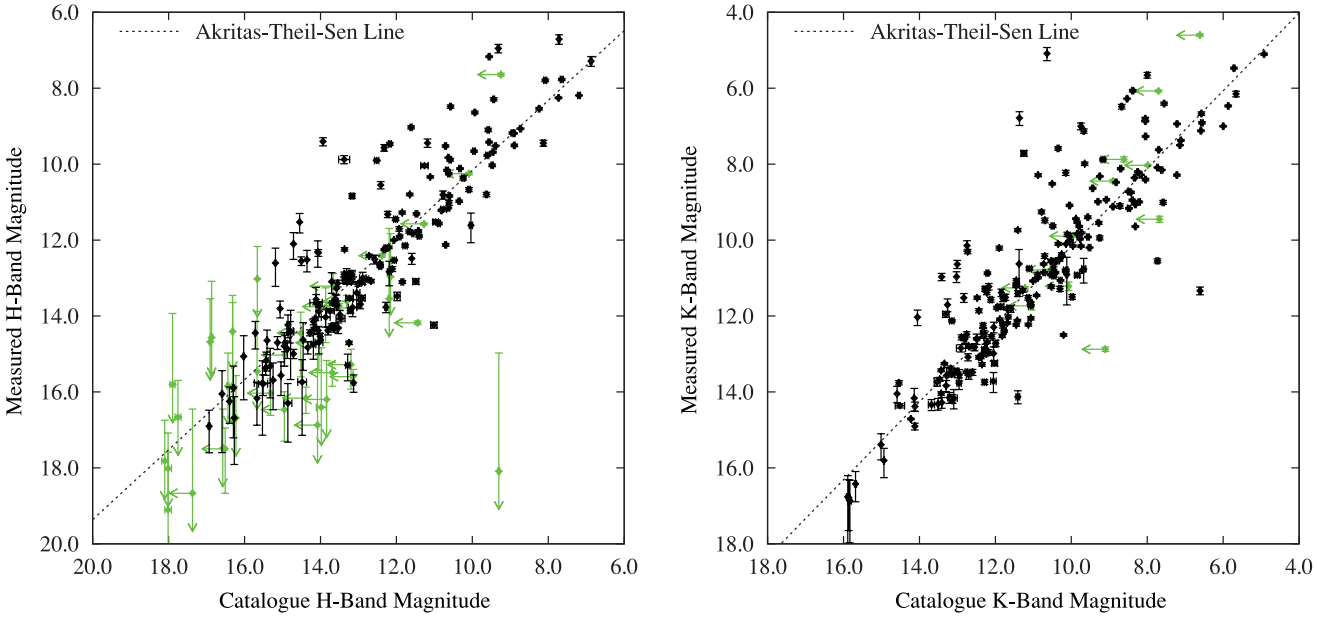

Figure 1. Measured versus catalogue magnitudes for both *H* and *K* bands. The catalogue magnitudes were taken from either UKIDSS or 2MASS depending on the object and the quality of the catalogue data. The detections are denoted by black diamonds and limits by green arrows. The dotted lines represent the ATS regressions. As expected, a strong correlation was found between the measured and catalogue magnitudes (see the text for more details).

used for analysis was decided on an object-by-object basis. Some objects are listed in both catalogues, others in only one and some do not have any near-IR magnitude data available. Where available, UKIDSS GPS magnitudes were preferred due to their improved sensitivity and resolution. However, due to its incomplete status, not all the objects we observed were covered by UKIDSS, and those that were do not always have data for all of *J*, *H* and *K* bands. In addition, the UKIDSS camera, Wide Field Camera (WFCAM; Casali et al. 2007) tends to saturate for the brighter objects. For objects with incomplete, low quality or saturated WFCAM data, 2MASS was used. Overall, from our 247 sources, 125 were compared to 2MASS photometry, 108 to UKIDSS and 14 had no magnitude data available in either catalogue. The data for each object are found in Table A2.

The magnitudes were also measured from the spectra using the FIGARO function ISTAT, which gives the mean and total flux and the rms. (σ) across a user-defined wavelength range. The ranges used to measure the total flux were 1.5365–1.7875 μm and 2.028–2.290 μm for *H* and *K*, respectively. These correspond to the wavelength ranges for the 2MASS magnitude measurements, as described in Cohen, Wheaton & Megeath (2003). UKIDSS magnitudes are calibrated to 2MASS (Hodgkin et al. 2009), so the same ranges were used to measure the spectral magnitude regardless of which catalogue magnitudes were used for comparison. The continuum noise (σ) was measured using 0.01 μm ranges around 1.6 μm and 2.2 μm for *H* and *K*, respectively. These ranges are clear of emission lines and of distortion from atmospheric features, both of which can cause an overestimation of σ. The fluxes were then converted into magnitudes, using the *H* and *K* zero-points 1.133×10^{-9} and 4.283×10^{-10} W m^{-2} μm^{-1} for 2MASS sources (Cohen et al. 2003), and 1.131×10^{-9} and 4.271×10^{-10} W m^{-2} μm^{-1} for UKIDSS sources (Hodgkin et al. 2009). The errors on the magnitudes given in Table A2 are 3σ errors. Some of the sources were not detected at *H*, in which case their *H*-band magnitudes could not be calculated. However, most spectra were bright enough at *H* that their magnitudes could be measured, and all were bright enough at *K*.

Fig. 1 shows a comparison of catalogue with measured magnitudes, for both *H* and *K* bands. The dotted lines represent Akritas–Thiel–Sen (ATS) regressions. The ATS regression and Kendall's τ were calculated using the CENKEN (Akritas, Murphy & LaValley 1995) function in the NADA library (Helsel 2005) from the R-project statistics package, and compared with other regression methods and correlation tests performed using the ASURV statistics package (Isobe, Feigelson & Nelson 1986; Isobe & Feigelson 1990; Lavalley, Isobe & Feigelson 1992). These statistical methods were used to take account of the many censored data present (see also Section 6.5). Based on a $y = a + bx$ fit, the ATS fit coefficients for *H* are $a_{\rm H} = 0.96$ and $b_{\rm H} = 0.92$. For *K*, the coefficients are $a_{\rm K} = -0.08$ and $b_{\rm K} = 1.02$. Kendall's τ values for *H* and *K* are 0.48 and 0.70, respectively, both with *p*-values $\simeq 0$; i.e. there is essentially no possibility that a correlation does not exist.

The lower τ and greater deviation in the fit from $m_{\rm obs} = m_{\rm cat}$ for *H*-band magnitudes are primarily due to the fact that many of the fainter objects have very noisy *H*-band spectra, and some were not detected at shorter wavelengths. This means that there are more limits, and the errors at the high end of the magnitude range are larger, both of which decrease the measured correlation coefficient and pull the regression line away from $m_{\rm obs} = m_{\rm cat}$. Nevertheless, the correlation is clearly there for both *H* and *K* bands, and the regression coefficients for the *K* band are very close to $m_{\rm obs} = m_{\rm cat}$. This shows that, for most objects, the photometry measured from the spectra is good despite the frequently poor weather conditions.

Those objects that deviate strongly from the $m_{\rm obs} = m_{\rm cat}$ were all taken in very poor weather conditions and/or with poor seeing. The conditions were highly time-variable for these badly affected observations. The much longer exposure times for the objects average out such variations whereas the shorter exposure times for the standards do not. The raw standard star data counts were noticeably very low for these observations in particular. The ratio of object to standard then becomes exaggerated. Since there is only one standard star spectrum per object, there was no way to mitigate against this. For consistency, all the fluxes were normalized to the catalogue

magnitudes. The correction factor, $f_{\rm obs}/f_{\rm corr} = 10^{(m_{\rm obs}-m_{\rm cat})/-2.5}$, was calculated using the standard equation for apparent magnitude, and is shown in Table A3.

4 CLASSIFICATION

The objects were primarily classified using the RMS follow-up observations. These criteria are described in detail in Lumsden et al. (in preparation). In summary, MYSOs conform to the colour cuts defined in Lumsden et al. (2002), are radio-quiet due to insufficient ionized gas, show strong millimetre CO emission as expected in a star formation region and appear as point sources in mid-IR images at 1 arcsec resolution. They show clustering in near-IR images in contrast to more evolved stars, which appear as isolated point sources. This left a sample of predominantly MYSOs, but also of some H II regions, proto-planetary nebulae (PPN), compact PN and embedded evolved stars. Near-IR spectroscopy was necessary to distinguish between the MYSOs and contaminants.

The spectra were classified according to the shape of their continuum and the presence or absence of emission and/or absorption features. All the spectra show telluric water absorption in the 1.8–2.0 μm range. Consequently, this range could not be used in the analysis and was taken out of the figures. The example spectra of the contaminants are shown in Fig. 2. Fig. 3 shows the example spectra of MYSOs. Each major emission line is present in at least one of the MYSO spectra shown in the example figures. The spectra of all objects observed will be available on the RMS data base.[4]

MYSOs are still embedded in their natal clouds, so their spectra show strong dust extinction in the form of a steep rising continuum, and occasionally excess dust emission at $\lambda \gtrsim 2.3$ μm. Almost all have emission lines, the most common being Brγ and H_2. Some also have *H*-band Brackett series, shocked [Fe II], fluorescent Fe II or CO bandhead emission. Both Brγ and He I can be seen in emission, absorption, or with a P-Cygni-type profile, though at this low resolution it was not possible to obtain expansion velocities for such profiles.

Massive YSOs were differentiated from low-mass YSOs by their luminosity; a loose cut of $L > 10^3$ $L_\odot$ was applied. Most of the RMS YSOs have luminosities characteristic of massive stars; 131/195 (∼70 per cent) of the RMS YSOs in this paper have $L > 5 \times 10^3$ $L_\odot$, which corresponds to $M > 8$ $M_\odot$ (Mottram et al. 2011b). However, their spectral properties are very different from those of typical main sequence stars (Hanson et al. 2005).

H II regions have comparatively flat continua, strong H I emission, and, often, He I emission. The H I emission conforms to case B of Baker & Menzel (1938) since it originates in an optically thin ionized region. It is worth noting that it was occasionally difficult to distinguish between MYSOs with strong H I emission and H II regions by their spectra alone. Generally, this was achieved using other data from the RMS survey follow-up or in the literature. In particular, radio observations and GLIMPSE images were used. In most cases, H II regions produce free–free radio emission owing to the large amount of ionized gas, whereas H I emission in MYSOs does not produce bright free–free emission. In addition, H II regions appear diffuse in mid-IR GLIMPSE images, so even radio-quiet 'weak' H II regions can usually be distinguished from MYSOs. Sometimes the suspected central star of an H II region has characteristics of a YSO. These were classified as 'YSO/HIIR'.

[4] See RMS data base http://www.ast.leeds.ac.uk/RMS/, Lumsden et al. (in preparation).

Evolved stars have much less dust extinction and therefore have comparatively blue continua, or continua that peak in the middle of the 1.5–2.5 μm range. They occasionally have the Brackett series in emission or absorption, and frequently have CO bandhead absorption. PPN are very red and can have strong CO absorption. Some of the PPN spectra closely resemble those of FU-Ori type objects, so it is possible that some of the objects we have classified as PPN are in fact FU-Ori type objects. The spectra of PN are flat or red and are often very similar to YSO or H II region spectra. In these cases, other data from the RMS survey follow-up and the literature were used to classify the object. The final class found within our sample were M-Giants. These have continua that peak in the middle of the 1.5–2.5 μm region, show molecular absorption lines owing to their cool atmospheres and have strong H_2O absorption.

Of the 247 objects whose spectra were taken, there were 180 YSOs, 15 YSOs within H II regions, 26 H II regions, 7 evolved stars, 5 PPN, 4 PN, 5 M-type supergiants and 5 evolved hot stars labelled as 'Other' in the table and on the RMS data base website due to unusual characteristics in their data. Spectra were found to be a valuable confirmation of classification in addition to our imaging data in 45 per cent of cases, and the only means of classifying the source in 5 per cent of cases.

5 EXTINCTION

Two estimates of extinction to each object were calculated using the Draine & Lee (1984)/Draine (1989) interstellar extinction model: one using $J - H$ colours and the other using $H - K$ colours. The MYSO colours were normalized to the intrinsic colours of a B0 star, taken from Koornneef (1983): $J - H = -0.12$ and $H - K = -0.05$. For these calculations, the catalogue magnitudes in Table A2 were used. The results are listed in Table A3 as 'A_V (*JH*)' and 'A_V (*HK*)' for calculations using the $J - H$ and $H - K$ colours, respectively. The equation for A_V is

$$A_V = \frac{m_1 - m_2 + c_{\rm int}}{0.55^{1.75}(\lambda_1^{-1.75} - \lambda_2^{-1.75})}, \quad (1)$$

where m_1 and m_2 are the magnitudes used to calculate the extinction (either *J*- and *H*-band magnitudes, or *H*- and *K*-band magnitudes), λ_1 and λ_2 are their reference wavelengths, $c_{\rm int}$ is the intrinsic $m_1 - m_2$ from Koornneef (1983) and 1.75 is the Draine & Lee (1984)/Draine (1989) reddening constant. The errors were calculated in quadrature as follows:

$$\delta A_V = \frac{\sqrt{\delta m_1^2 + \delta m_2^2}}{0.55^{1.75}(\lambda_1^{-1.75} - \lambda_2^{-1.75})}. \quad (2)$$

These are shown in Table A3. Where one or more magnitudes are unavailable, the extinctions cannot be calculated, and '–' is marked in the table. Where the 2MASS magnitude is a lower limit, the A_V given is also a lower limit. For 35 sources (27 of them YSOs), there were not enough magnitude data to calculate an extinction.

The left-hand panel of Fig. 4 shows A_V (*HK*) against A_V (*JH*) for the YSOs. The solid line represents A_V (*HK*) = A_V (*JH*), and the dotted line is the ATS regression line. Kendall's τ is 0.36, with a *p*-value of 3.0×10^{-11}, indicating a good correlation between the two. The equation for the fit is

$$A_V\,(HK) = 6.0 + 1.1 A_V\,(JH). \quad (3)$$

The regression line falls above the A_V (*HK*) = A_V (*JH*) line. This was explained by Porter, Drew & Lumsden (1998): the $H - K$ colours appear redder in young objects due to dust excess, and the $J - H$ colours appear bluer due to scattering at short wavelengths. This

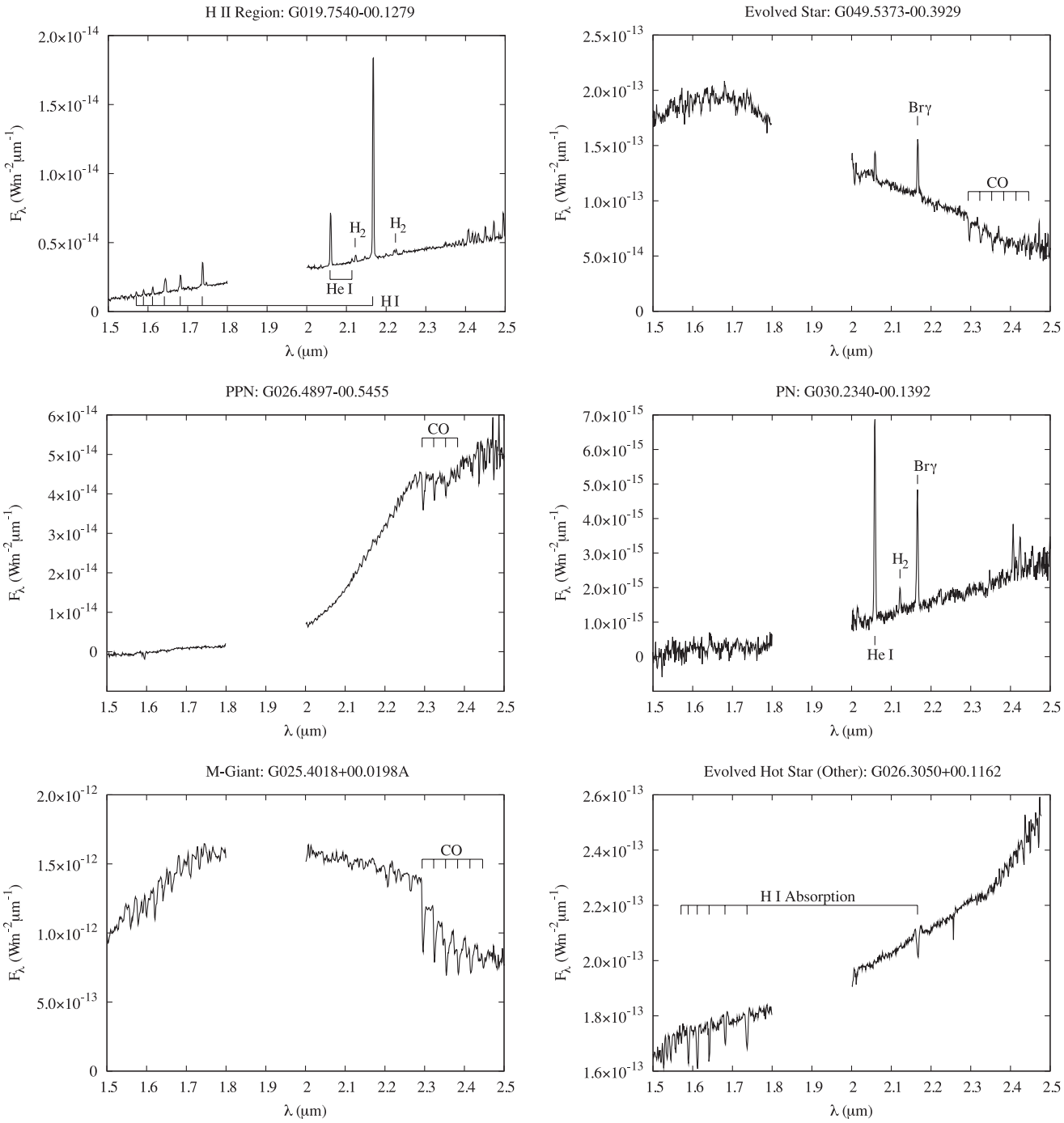

Figure 2. Example spectra of each class of contaminants found within the sample, i.e. the non-YSOs. From top-left to bottom-right: the H II region G019.7540−00.1279; the evolved star G049.5373−00.3929; the PPN G026.4897−00.5455; the PN G030.2340−00.1392; the M-Giant G025.4018+00.0198A and finally the hot star G026.3050+00.1162, labelled as 'Other' in the data base and tables. Note the similarity of the PN spectrum to that of the H II region. This object required the RMS follow-up campaign's mid-IR imaging data in order to be correctly classified.

artificially increases A_V (*HK*) and decreases A_V (*JH*), meaning the true value for extinction lies somewhere between the two. As the amount of dust increases, the effect becomes more pronounced and the regression line deviates further from the A_V (*HK*) = A_V (*JH*) line.

Fig. 5 shows a colour–colour diagram demonstrating this point. Some of the objects do fall very close to the extinction line, i.e. the line that runs parallel to the extinction vector and starts at the intrinsic $J - H$ and $H - K$ colours. However, most fall above this line, showing evidence of the dust excess emission and/or scattering described above.

For extinction correction, A_V (*HK*) was used where available, or A_V (*JH*) when A_V (*HK*) was not available, or was a lower limit. The number distribution of these extinctions is shown in the right-hand panel of Fig. 4. The median is $A_V = 42$, and the extinctions range from $A_V = 2.7$ to $A_V = 114$, demonstrating that this study covers the minimally obscured objects right through to very red, dusty sources.

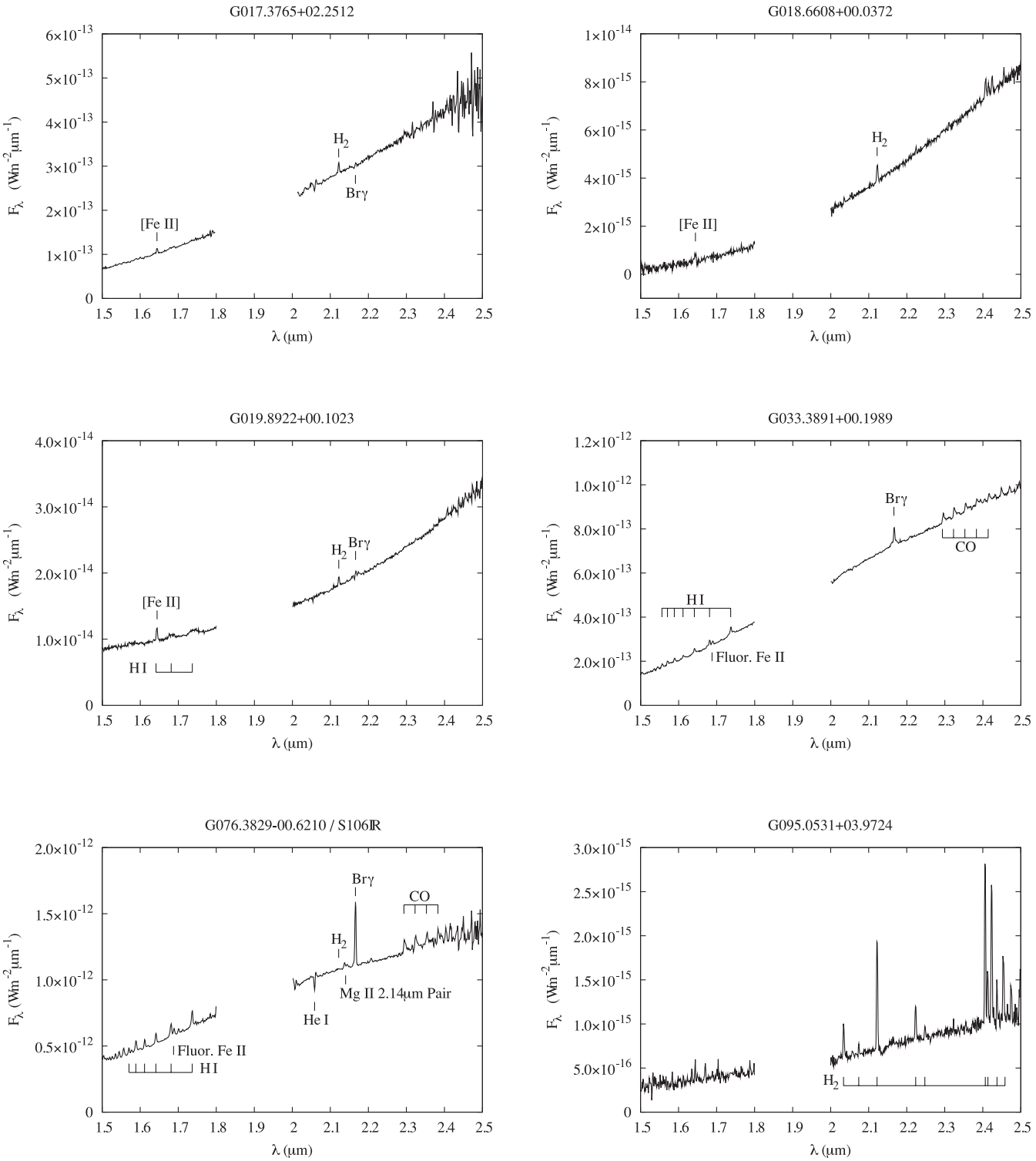

Figure 3. Example spectra of the MYSOs. All have the steep rising continuum and some emission lines; however, there is variation in which lines are present. This figure shows all the major emission lines seen in MYSOs, but is not intended to be representative in terms of the proportion of MYSOs that show each emission line.

6 YOUNG STELLAR OBJECTS

6.1 Spectral features

In addition to the strong dust extinction and corresponding steep rising continuum, most YSOs have emission lines in their spectra. However, not all of them show the same lines. One of the objectives of the RMS survey is to identify why there are differences. The main emission lines observed in YSOs in our sample were Brγ, Br 10, Br 11, Br 12, [Fe II] 1.64 μm line, H_2 2.1218 μm, H_2 2.2477 μm, fluorescent Fe II 1.6878 μm and CO bandhead. Some objects also exhibited the Pfund series, or other molecular H_2 lines.

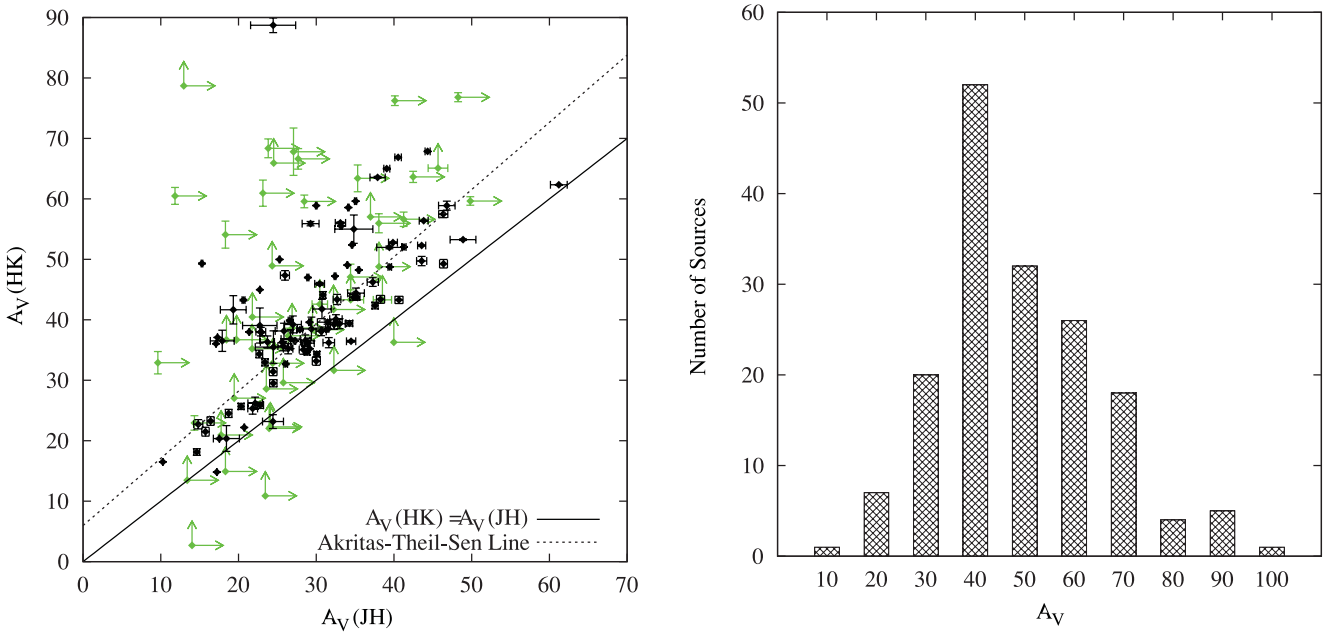

Figure 4. Left: comparison of extinction calculated using *J*- and *H*-band magnitudes (A_V (*JH*)) and *H*- and *K*-band magnitudes (A_V (*HK*)), for the YSOs. The detections are denoted by black diamonds and limits by green arrows. The solid line represents A_V (*HK*) = A_V (*JH*), and the dotted line is the ATS regression line. Right: number distribution of A_V for the YSOs, using A_V (*HK*) where available, or otherwise using A_V (*JH*).

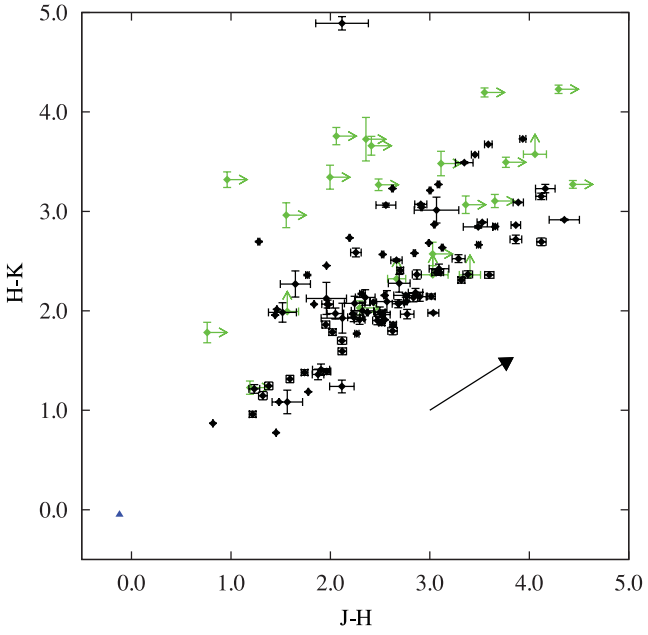

Figure 5. Colour–colour diagram showing YSO $J - H$ and $H - K$ colours for the RMS objects. The detections are denoted by black diamonds and limits by green arrows. The black arrow shows the extinction vector, of length $A_V = 10$, calculated using the Draine (1989) extinction law. The blue triangle shows the intrinsic colours of a B0 star, taken from Koornneef (1983): $J - H = -0.12$ and $H - K = -0.05$.

He I 2.0587 μm was seen in both emission and absorption. Both Brγ and He I were occasionally seen with P-Cygni-type profiles: 13 MYSOs had Brγ with a P-Cygni profile and 15 had He I with a P-Cygni profile, of which 8 had P-Cygni profiles for both Brγ and He I. These objects are listed in Table B3. However, the He I 2.11 μm doublet was not seen in the YSOs, only in H II regions. Detection frequencies are shown in Table 1.

Table 1. Detection frequency of spectral features in YSO spectra. All detections are at the 3σ level or better. The percentages are based on totals of 195 objects for the *K*-band, 188 for Br 10 and fluorescent Fe II, and 186 for the shorter wavelength *H*-band lines. This takes account of the fact that some of the objects were not detected for part or all of the *H*-band meaning determining the presence or absence of the lines in that region was impossible.

Emission feature	Number of sources	Frequency (per cent)
Brγ	147	75
Br 10	85	45
Br 11	69	37
Br 12 Unblended	35	19
Br 12/[Fe II] Blend	46	25
[Fe II] Unblended	20	11
H_2 2.1218 μm	109	56
H_2 2.2477 μm	18	9
Fluorescent Fe II	48	26
He I 2.0587 μm	30	15
Pfund Series	13	7
CO 2–0 Bandhead	34	17

6.2 Emission and absorption line fluxes

The fluxes of the YSO emission and absorption lines were measured using the Starlink package DIPSO. The continuum was fitted by a third-order polynomial function, and then subtracted. In many cases, the steepness of the continuum obscured the presence of emission lines that became visible when the continuum was subtracted. For all spectral features except the CO 2–0 bandhead, the line profiles were fitted with a Gaussian function, which DIPSO then integrated to find the total flux of the line. The majority of the spectral lines are unresolved so a Gaussian function is a good assumption.

Detections were defined as having $f_\lambda > 3\,\delta f_\lambda$, where f_λ is the line flux and δf_λ is the error. For the unresolved lines, DIPSO gave a good estimation of the error. Where the lines had broad wings or interference in the profile shape from noise, DIPSO could still fit the

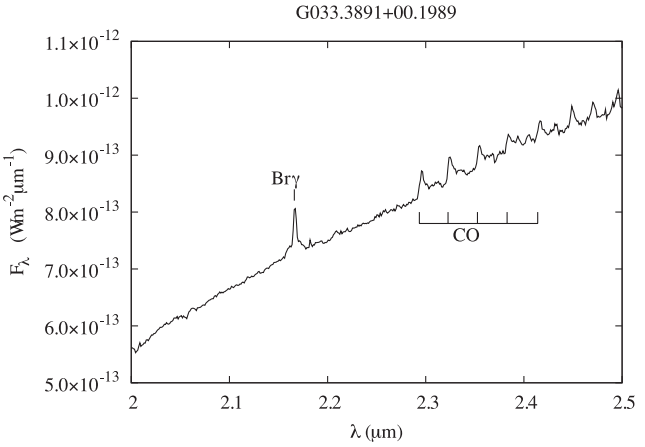

Figure 6. The *K*-band section of the spectrum of the YSO G033.3891+00.1989. This shows a very clear example of the saw-tooth profile of the CO bandhead. It also has Brγ emission.

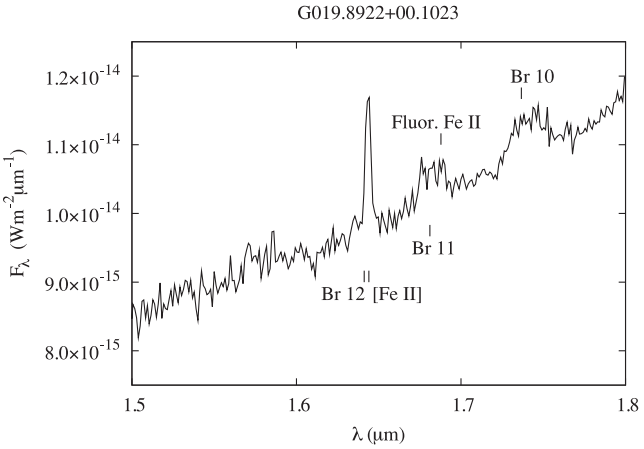

Figure 7. The *H*-band section of the spectrum of the YSO G019.8922+00.1023. This object has both the Brackett series and the [Fe II] 1.64402 μm line, as well as the fluorescent Fe II 1.6878 μm line. Note that the Br 12/[Fe II] line at ∼1.64 μm is much stronger than the other Brackett series lines.

line with a Gaussian, but could not accurately estimate the error. When this was the case, errors were calculated using the equation for a Gaussian with the height equal to the continuum rms noise, i.e.

$$\delta f_\lambda = h\left(\frac{W}{2\sqrt{2\ln 2}}\right), \quad (4)$$

where h is height and W is the full width at half-maximum (FWHM) of an unresolved peak at that wavelength.

The continuum rms noise was measured using FIGARO's ISTAT function, taking wavelength ranges with no spectral lines, close enough to the pertinent spectral line that extinction would not distort the result. The rms noise was measured for two ranges per line, one either side of the line, and the mean value of these was taken. The upper limits for non-detections were calculated using the same equation, with $h = 3 \times$ continuum rms.

The CO bandhead has a saw-tooth shaped profile (see Fig. 6), so different treatment was required. The equivalent width (EW) was measured from 2.289–2.313 μm, again using DIPSO. The mean continuum flux density was measured across the 2.2825–2.2875 μm range just to the blue end of the bandhead, using FIGARO's ISTAT function. The EWs were then converted into fluxes. This is consistent with the method used by Ishii et al. (2001). Detections were again defined as EW $> 3\,\delta$EW, where δEW is the error given by DIPSO. Limits were taken as $\mathrm{EW_{limit}} = 3\,\delta$EW.

The fluxes of the Brγ, Br 10, Br 11, Br 12/[Fe II] 1.64 μm line, H_2 2.1218 μm, H_2 2.2477 μm, fluorescent Fe II 1.6878 μm and He I 2.0587 μm lines are listed in Table B1, with the presence of the Pfund series denoted by 'P' in the final column. The EWs of the CO 2–0 bandhead are listed in Table B2. The errors in the tables are at the 1σ level. The fluxes and EWs in the tables are the raw values as measured directly from the spectra, and are not corrected for extinction or normalized to the catalogue magnitude (see Section 3).

Br 12 and [Fe II] 1.64402 μm are close to each other and form a blend when both are present (see Fig. 7). To determine whether the line seen at 1.64 μm is Br 12, [Fe II], or a blend, one has to compare this line with the rest of the Brackett series. For this reason, the fluxes of Br 12 and [Fe II] are listed in Table B1 in the same column. Unblended [Fe II] corresponds to the presence of a line at 1.64 μm when Br 10 and Br 11 are absent. When the rest of the Brackett series is present, the presence of [Fe II] can only be inferred if the relative strength of the 1.64 μm line compared to Br 11 is higher than expected. Assuming Baker & Menzel (1938) case-B recombination with the Storey & Hummer (1995) line ratios for $T_e = 7500$ K and $N_e = 10^6$ cm^{-3}, the 1.64 μm line was defined as a blend if $f(1.64\ \mu\mathrm{m}) > 0.788 \times f(\mathrm{Br\ 11})$. See Section 6.3 for a full discussion of the properties of H I lines.

This cut relies on the emission lines being optically thin. If the lines are not optically thin, the flux of the Br 12 line may fall above this limit but not have a contribution from [Fe II]. This means that there are probably some objects that are considered to have a blend of Br 12 and [Fe II] under this definition that actually only have Br 12. However, the low resolution of the spectra meant that deconvolving the lines was not possible, so this was considered to be the best available separation method for the purposes of this paper.

In nine of the YSO spectra, dust extinction rendered part or all of the *H* band too noisy to identify emission lines in this region with any confidence. This caused difficulties in the analysis of these spectra. However, given that there are 195 objects classified as YSO or YSO/HIIR, this represents only ∼5 per cent of the objects. Excluding these objects from the *H* band data analysis still leaves a large enough sample to make statistically sound conclusions.

6.3 H I emission

The detection rate of Brγ emission amongst the YSOs is 75 per cent, and many of these also have other H I lines. This detection frequency is lower than the 97 per cent found by Ishii et al. (2001) for intermediate-mass YSOs and Herbig Ae/Be stars, but comparable with the 71 per cent found by Carr (1990) for low-mass YSOs. Brγ was also seen with a P-Cygni profile in the spectra of 13 objects (see Table B3), indicating that for those objects, Brγ originated in an outflowing wind.

The left-hand panel of Fig. 8 shows a comparison of Brγ luminosity with bolometric luminosity (the latter from Mottram et al. 2011a). Correlation and regression tests were performed on the line versus bolometric luminosity data for the RMS objects only. The ATS regression is represented in the figure by the dotted line. The equation of the line is

$$L_{\mathrm{Br}\gamma} = 10^{-4.0} \times (L_{\mathrm{BOL}})^{0.85}. \quad (5)$$

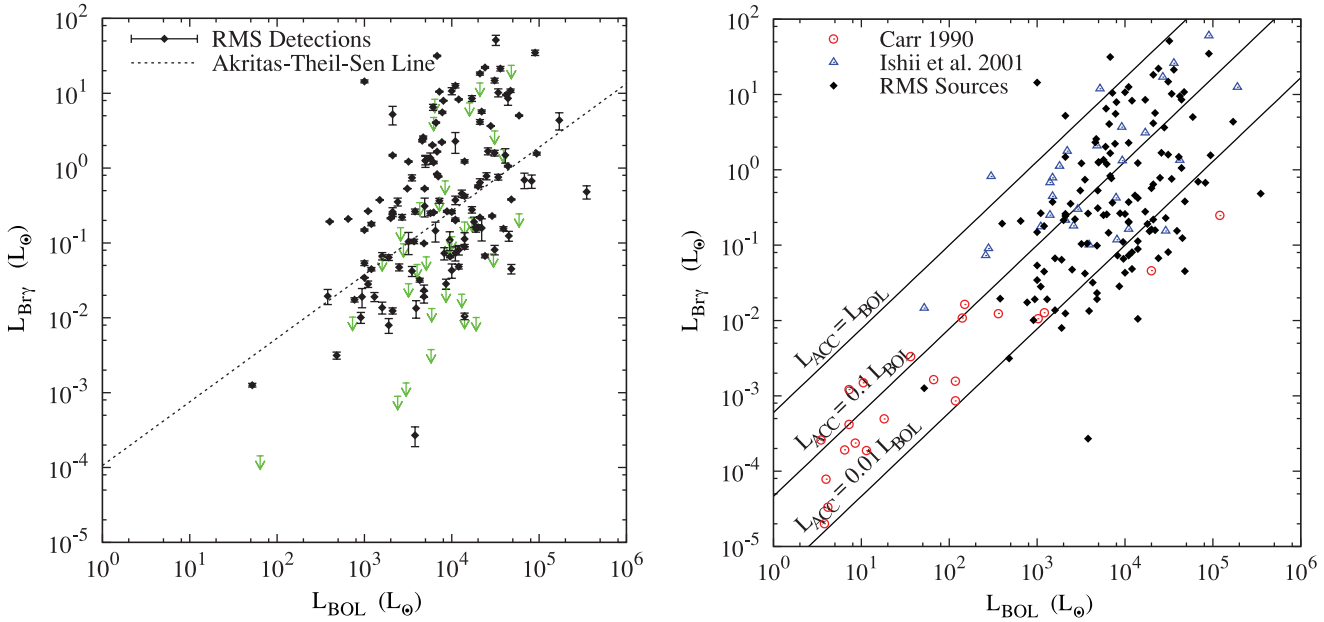

Figure 8. Left: Brγ luminosity against bolometric luminosity for RMS sources. The detections are denoted by black diamonds and limits by green arrows. The errors on detections are shown, but are frequently too small to be easily distinguishable on this scale. The dotted line represents the ATS regression. Right: comparison of RMS data (diamonds) with those of Carr (1990) (circles) and Ishii et al. (2001) (triangles). Only detections above the 3σ limit are shown. The solid lines represent the loci of $L_{\rm ACC} = L_{\rm BOL}$, $L_{\rm ACC} = 0.1\,L_{\rm BOL}$ and $L_{\rm ACC} = 0.01\,L_{\rm BOL}$ using the Calvet et al. (2004) relationship between $L_{\rm ACC}$ and $L_{\rm Br\gamma}$. In both plots, all the line luminosities have been corrected for extinction, and the RMS data have been corrected for the difference between measured and catalogue magnitudes.

Table 2. Summary of the results of the correlation tests for the emission line luminosities against $L_{\rm BOL}$. These fits were performed only on the RMS data; the low- and intermediate-mass stars were not included in the correlation and regression calculations.

Emission line	Kendall's τ	p-value
Brγ	0.26	6.1×10^{-7}
H_2	0.19	0.0003
CO Bandhead – all data	0.04	0.4
CO Bandhead – detections only	0.48	0.0006
Fluorescent Fe II – all data	0.07	0.2
Fluorescent Fe II – detections only	0.36	0.0003
He I – all data	0.05	0.4
He I 2.0587 μm – detections only	0.45	0.003

A summary of the results of the correlation tests for all the lines is shown in Table 2. The Kendall's τ coefficient for Brγ versus $L_{\rm BOL}$ shows that there is a strong correlation between the Brγ luminosity and the bolometric luminosity of the star. This correlation was also seen in the studies of low- and intermediate-mass YSOs and Herbig Ae/Be stars (Carr 1990; Ishii et al. 2001; Connelley & Greene 2010).

Brγ emission is known to be related to accretion in low-mass stars (Calvet et al. 2004), and has been scaled up to Herbig Ae/Be stars by Garcia-Lopez et al. (2006). The right-hand panel of Figure 8 compares detections in the RMS sources with those of Carr (1990) and Ishii et al. (2001). The solid lines represent the loci of $L_{\rm ACC} = L_{\rm BOL}$, $L_{\rm ACC} = 0.1\,L_{\rm BOL}$ and $L_{\rm ACC} = 0.01\,L_{\rm BOL}$ using the empirical relationship from Calvet et al. (2004):

$$\log_{10}(L_{\rm ACC}) = -0.7 + 0.9\left(\log_{10}\left(L_{\rm Br\gamma}\right) + 4\right). \quad (6)$$

The majority of the objects have $0.01\,L_{\rm BOL} < L_{\rm ACC} < L_{\rm BOL}$. This appears to be true for most RMS sources, implying that there is a common mechanism producing Brγ throughout the mass range covered by Carr (1990), Ishii et al. (2001) and the RMS sources. This trend is seen with other emission lines, suggesting that high-mass YSOs resemble scaled-up versions of low- or intermediate-mass YSOs.

One of the considerations when distinguishing MYSOs with Brackett series emission from H II regions is whether the recombination conforms to case B of Baker & Menzel (1938); recombination emission in typical compact H II regions conforms to case B, whereas this is not always true for MYSOs. Storey & Hummer (1995) tabulated the case-B line ratios for a range of temperatures and densities.

The temperature of the gas in which the Br series lines originate must lie between that of a UCHII region ($T_{\rm e} \sim 7500$ K) at the lower end, to an OB star ($T_{\rm e} \lesssim 30\,000$ K) at the upper end. Similarly, the density of a UCHII region imposes a lower limit on the density of $N_{\rm e} \gtrsim 10^4$ cm^{-3}. A realistic maximum density for the stellar wind would be $N_{\rm e} \lesssim 10^{11}$ cm^{-3}. For $T_{\rm e}$ and $N_{\rm e}$ in this range, the Storey & Hummer (1995) Br 10/Brγ ratio varies from 0.327 to 0.490, i.e. around a 30 per cent variation. Similarly, the Br 12/Br 11 ratio varies from 0.756 to 0.834, i.e. about 10 per cent.

We adopt the case-B values for MYSOs based on observational evidence (e.g. Porter et al. 1998). Though the values for $T_{\rm e}$ and $N_{\rm e}$ differ from those found for T-Tauri stars, the corresponding Br 12/Br 11 line ratios are comparable. For example, Hartigan et al. (1991) (and subsequently Muzerolle, Calvet, & Hartmann 1998) found values of $T_{\rm e} \sim 10\,000$ K and $N_{\rm e} = 10^{14}$ cm^{-3} when modelling production in infalling magnetospheric gas, whereas Bary et al. (2008) observed Paschen and Brackett series H I recombination line ratios consistent with temperatures $T_{\rm e} \leq 2000$ K and densities $10^9 < N_{\rm e} < 10^{10}$ cm^{-3}, inconsistent with production in accreting material. The Hartigan et al. (1991) and Bary et al. (2008) $T_{\rm e}$ and $N_{\rm e}$ values correspond to Storey & Hummer (1995) Br 12/Br 11 ratios

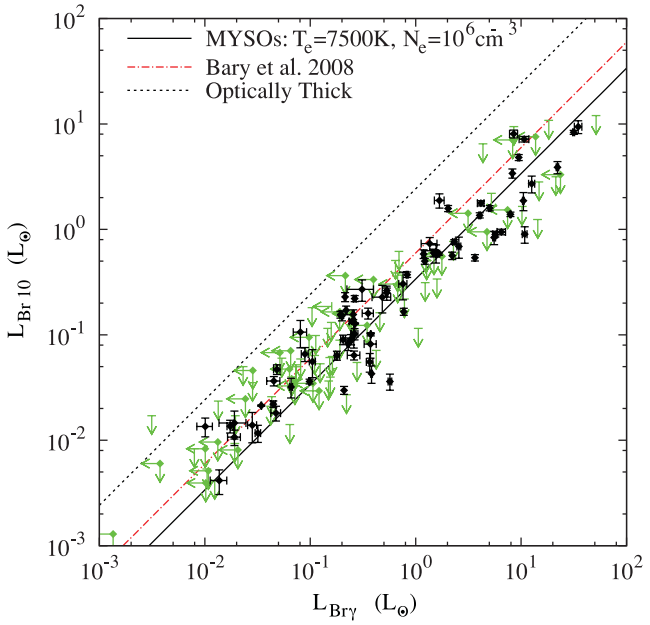

Figure 9. Br 10 luminosity against Brγ luminosity for RMS sources. The detections are denoted by black diamonds and limits by green arrows. The black solid line shows the case-B Storey & Hummer (1995) Br 10/Brγ ratio using values of T_e and N_e found from observations of MYSOs; the red dashed–dotted line represents the Br 10/Brγ ratio using T_e and N_e values for T-Tauri stars taken from Bary et al. (2008); and the black-dotted line represents the case in which Br 10 and Brγ are both optically thick (i.e. blackbody emission). The line luminosities have been corrected for extinction, and for the difference between measured and catalogue magnitudes.

of 0.757 and 0.764, respectively, which are not vastly different from the 0.788 ratio given by using the observational values for T_e and N_e, given a typical flux error for the 1.64 μm line of ∼10 per cent. However, while the Br 12/Br 11 ratio is very similar whichever set of T_e and N_e values are used, this is not the case for the Br 10/Brγ ratios. The observed T_e and N_e and the Hartigan et al. (1991) T_e and N_e produce line ratios of 0.338 and 0.301, respectively, whereas the Bary et al. (2008) ratio is 0.597.

Fig. 9 shows Br 10 luminosity against Brγ luminosity. Shown on the plot are three lines: one showing the Storey & Hummer (1995) Br 10/Brγ ratio using observed T_e and N_e values for MYSOs; one showing the Br 10/Brγ ratio for T-Tauri stars using T_e and N_e from Bary et al. (2008) and finally one showing the theoretical ratio for optically thick emission. The Hartigan et al. (1991) ratio for T-Tauri stars falls right next to the MYSO line, so is not shown on the plot.

Most of the MYSOs fall very close to, or on the $T_e = 7500$ K and $N_e = 10^6$ cm^{-3} line. However, for a minority of sources, the Br 10/Brγ ratio is much greater than that predicted by case-B recombination for the MYSO values of T_e and N_e – closer to the Bary et al. (2008) T-Tauri line. This could imply that for these YSOs Brγ is optically thick and therefore that the recombination does not conform to case B. This is in contrast to the optically thin H II regions in which recombination line ratios do follow the case-B values. Alternatively, the T_e and N_e values for these stars could be closer to those found by Bary et al. (2008) for T-Tauri stars than the previously observed values for MYSOs. Few of the objects have Br 10/Brγ ratios very close to the line for which both Br 10 and Brγ are assumed to be optically thick. This suggests that though Brγ may be optically thick for some sources, Br 10 is usually optically thin.

6.4 Shock emission: molecular H_2 and forbidden [Fe II]

The detection rate of the molecular H_2 2.1218 μm line is 56 per cent, and 9 per cent have additional molecular H_2 lines. This is a higher detection rate than found by Ishii et al. (2001) for intermediate-mass YSOs (34 per cent), and much higher than the rate found by Carr (1990) for low-mass YSOs (25 per cent). Ishii et al. (2001) interpret the presence of strong H_2 emission as emission produced by the shock where an outflow impacts the surrounding circumstellar material, indicating that at least 56 per cent of the YSOs in our sample have a strong outflow. There may be more YSOs with outflows in our sample, with either not enough circumstellar material to form a shock, or aligned at such an angle that we cannot see the light from the shock.

The left-hand panel of Fig. 10 shows H_2 luminosity against bolometric luminosity. The equation of the regression line is

$$L_{H_2} = 10^{-4.0} \times (L_{BOL})^{0.73}. \quad (7)$$

Kendall's τ value (see Table 2) shows that there is a correlation between the H_2 luminosity and the bolometric luminosity of the star.

The right-hand panel of Fig. 10 compares detections in the RMS sources with those of Carr (1990) and Ishii et al. (2001). The solid lines represent the loci of $L_{H_2} = 10^{-4}\ L_{BOL}$, $L_{H_2} = 10^{-5}\ L_{BOL}$ and $L_{H_2} = 10^{-6}\ L_{BOL}$. The Carr (1990) and Ishii et al. (2001) sources all have $10^{-6}\ L_{BOL} < L_{H_2} < 10^{-4}\ L_{BOL}$, as do most of the RMS sources. This implies a common production mechanism for H_2 for low-mass and high-mass YSOs, as with Brγ, adding further evidence to the idea that high-mass YSOs are very similar to low-mass YSOs.

[Fe II] 1.64402 μm emission is also shock excited (Lumsden, Puxley & Doherty 1994; Porter et al. 1998). As described in Section 6.1, its close proximity to Br 12 makes analysis of this line difficult. 20 objects (i.e. 11 per cent) were found to have [Fe II] emission without the rest of the Br series. An estimated 46 further objects (i.e. 25 per cent) have [Fe II] blended with Br 12. This figure is probably an upper limit, since the assumption that H I emission in YSOs conforms to case B of Baker & Menzel (1938) is probably not valid for all YSOs (see Section 6.3 and Fig. 9).

6.5 Accretion discs: CO bandhead and fluorescent Fe II emission

The production of CO bandhead emission requires high densities and temperatures which can only be found in a circumstellar disc (e.g. Carr 1989; Chandler, Carlstrom & Scoville 1995; Bik & Thi 2004; Davies et al. 2010; Wheelwright et al. 2010). Fluorescent Fe II 1.6878 μm emission in the MYSOs probably also originates in discs: it is known to originate in a disc in both AGN (e.g. Baldwin et al. 2004) and classical Be stars (e.g. Zorec et al. 2007), and has previously been observed in high-mass YSOs by Porter et al. (1998) and Lumsden et al. (2012), and in low-mass YSOs (though less frequently) by Hamann & Persson (1992).

The CO bandhead was seen in 17 per cent of the YSO spectra. This detection rate is lower than both the Carr (1989) rate for low-mass YSOs (20 per cent) and the Ishii et al. (2001) rate for intermediate-mass YSOs (22 per cent). Fe II emission was seen in 26 per cent of our sources with visible *H* band, usually in those objects with strong *H*-band H I emission. Seven objects were not visible at this wavelength, and more were very noisy so this detection rate should be considered as a lower limit. There is seldom overlap between the two lines – only six YSOs have both

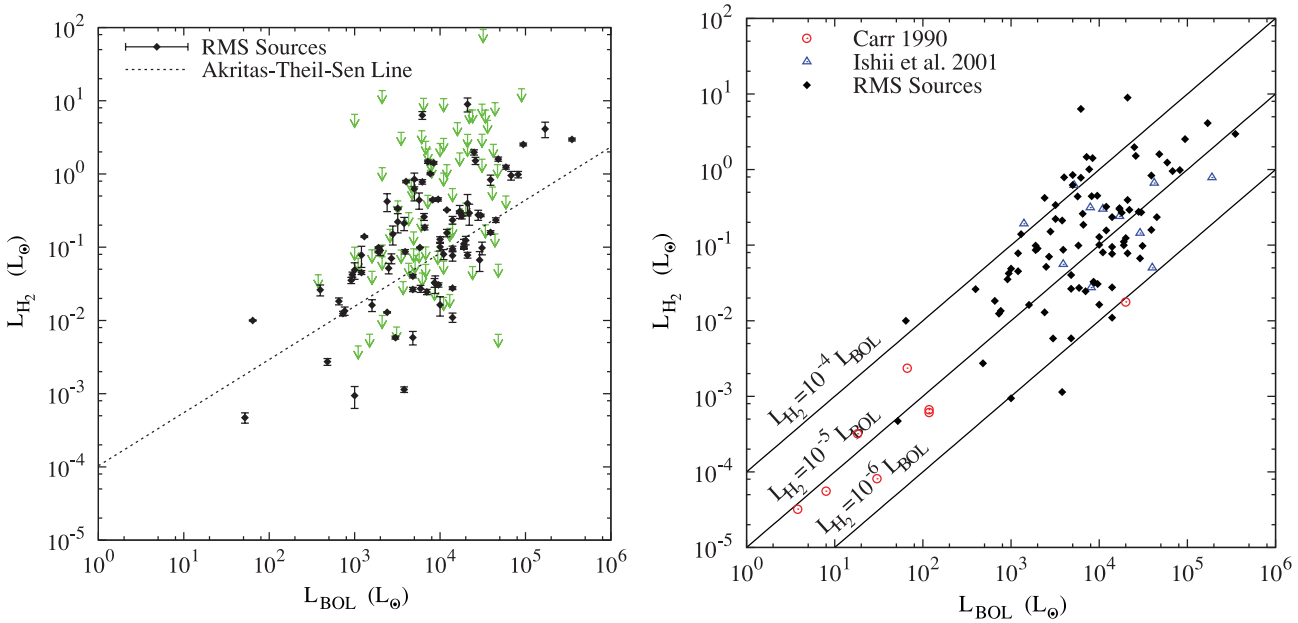

Figure 10. Left: H_2 luminosity against bolometric luminosity for RMS sources. The detections are denoted by black diamonds and limits by green arrows. The dotted line represents the ATS regression. The errors on detections are shown, but are frequently too small to be easily distinguishable on this scale. Right: comparison of RMS data (diamonds) with those of Carr (1990) (circles) and Ishii et al. (2001) (triangles). Only detections above the 3σ limit are shown. The solid lines represent the loci of $L_{H_2} = 10^{-4}\ L_{BOL}$, $L_{H_2} = 10^{-5}\ L_{BOL}$ and $L_{H_2} = 10^{-6}\ L_{BOL}$. In both plots, all the line luminosities have been corrected for extinction, and the RMS data have been corrected for the difference between measured and catalogue magnitudes.

fluorescent Fe II and CO bandhead emission. In total, 76 RMS objects (i.e. 39 per cent) have evidence of a circumstellar disc.

Connelley & Greene (2010) note in their paper on low-mass Class I YSOs that all objects with CO bandhead emission also show Brγ emission. This trend is seen, though not as strongly, in the high-mass RMS YSOs: 75 per cent of all YSOs have Brγ emission, and 85 per cent of YSOs with CO bandhead emission have Brγ. This is a higher Brγ detection rate for YSOs with CO bandhead. However, 5 out of 36 (i.e. 14 per cent) RMS objects with CO bandhead emission do not also have Brγ emission.

The left-hand panel of Fig. 11 shows CO 2–0 bandhead luminosity against bolometric luminosity. The lines represent the ATS regressions. Due to the number of censored data points (i.e. limits), a least-squares fit was not appropriate; the least-squares method either ignores the censored points or considers them with equal weight to the uncensored points, either of which gives a bias to the results of a fit. This is why regression was performed using the Akritas-Thiel-Sen (ATS) non-parametric algorithm rather than the usual least-squares method, and correlation tests were performed using Kendall's τ method (Akritas et al. 1995). These methods take into account the effect of censored data points on the correlation and regression, without giving them equal weight to the detections. For data with few censored points, the ATS line is comparable with the least-squares method, so can handle a wide variety of data sets. For consistency and to allow like-for-like comparison with the other lines, the ATS method was used for all regressions and correlation tests.

Initially, the fit and correlation tests were performed on all the data. The results show that there is no overall correlation between CO bandhead luminosity and bolometric luminosity (see Table 2). However, when non-detections are excluded, a correlation between the CO bandhead and bolometric luminosity is found. This difference is reflected in the regression lines. The equation for all the data including non-detections is

$$L_{CO} = 10^{-5.1} \times (L_{BOL})^{0.58}. \quad (8)$$

The equation for detections only is

$$L_{CO} = 10^{-4.1} \times (L_{BOL})^{0.83}. \quad (9)$$

The non-detections 'push' the line down to well below where it would be if only detections were taken into account. This demonstrates the effect that censored data points have on a large sample, and shows that it is important to include the censored points in the analysis when trying to understand the overall trends in the data set. This regression method was employed for all the data for consistency, even when the censored points have only a minimal effect on the results (e.g. Brγ emission).

For the CO bandhead emission, the reason for this difference may be that the ability to detect CO bandhead is unreliable. In some objects the broad CO bandhead emission may simply be obscured by the spectral noise, or it may be swamped in a steeply rising continuum caused by excess dust emission. This effect probably predominates for the sources with the higher limits in Fig. 11. It is known that CO bandhead emission is variable in some MYSOs (e.g. Biscaya et al. 1997; Clarke et al. 2006). If this is true for other MYSOs in our sample, we may not have observed the object when CO bandhead emission is present. There may be an inclination effect, though we have no way of testing this suggestion at this low resolution. Alternatively, some objects may be genuinely CO weak, particularly those objects with very low limits in Fig. 11. This may indicate the lack of a disc with suitable neutral material for these objects, suggestive of very low accretion rates.

The right-hand panel of Fig. 11 compares detections in the RMS sources with those of Carr (1989) and Ishii et al. (2001). The solid lines represent the loci of $L_{CO} = 10^{-3}\,L_{BOL}$, $L_{CO} = 10^{-4}\,L_{BOL}$ and $L_{CO} = 10^{-5}\,L_{BOL}$. Most sources from all three surveys have $10^{-5}\,L_{BOL} < L_{CO} < 10^{-3}\,L_{BOL}$. This shows that, once again, there is a trend through the low-, intermediate- and high-mass YSOs, implying a common mechanism throughout the mass range for sources in which CO is detected.

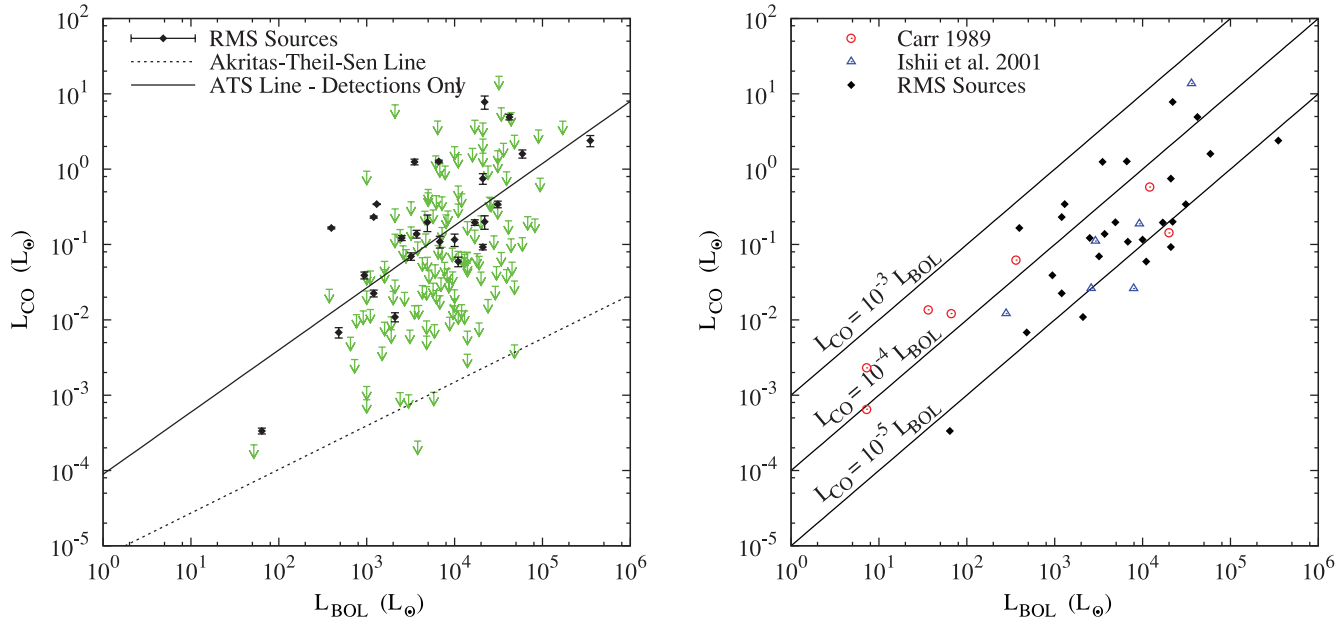

Figure 11. Left: CO 2–0 bandhead luminosity against bolometric luminosity for RMS sources. The detections are denoted by black diamonds and limits by green arrows. The lines represent the ATS regressions. Two lines are shown, one for regression with detections only (solid line), and one for all the data including non-detections (dotted line). The errors on detections are shown, but are frequently too small to be easily distinguishable on this scale. Right: comparison of RMS data (diamonds) with those of Carr (1989) (circles) and Ishii et al. (2001) (triangles). Only detections above the 3σ limit are shown. The solid lines represent the loci of $L_{\rm CO} = 10^{-3}\,L_{\rm BOL}$, $L_{\rm CO} = 10^{-4}\,L_{\rm BOL}$ and $L_{\rm CO} = 10^{-5}\,L_{\rm BOL}$. In both plots, all the line luminosities have been corrected for extinction, and the RMS data have been corrected for the difference between measured and catalogue magnitudes.

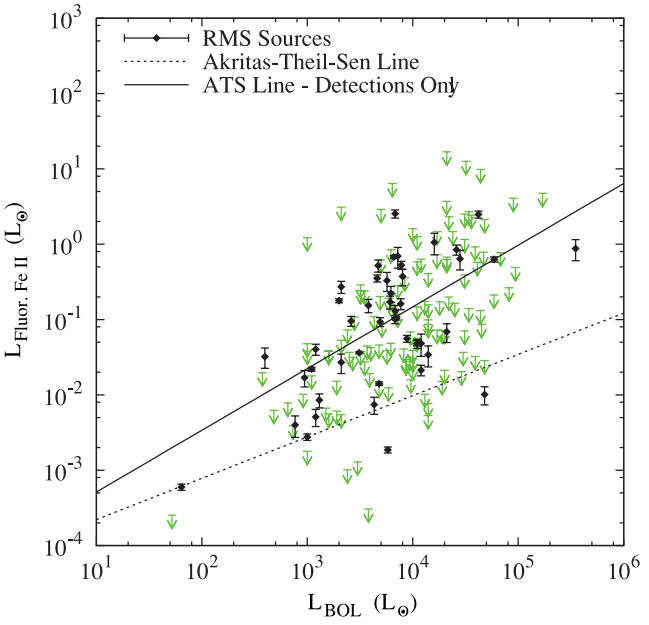

Figure 12. Fe II 1.6878 μm luminosity against bolometric luminosity for RMS sources. The detections are denoted by black diamonds and limits by green arrows. The lines represent the ATS regressions. Two lines are shown, one for regression with all the data including non-detections (dotted line), and one for regression with detections only (solid line). Line luminosities have been corrected for extinction and for the difference between measured and catalogue magnitudes.

Fluorescent Fe II 1.6878 μm emission is also thought to originate in a disc (Baldwin et al. 2004; Zorec et al. 2007). Fig. 12 shows fluorescent Fe II 1.6878 μm luminosity against bolometric luminosity. The lines represent the ATS regressions. Again, due to the large number of limits, two regressions were performed. No overall correlation was found, but there was a correlation between $L_{\rm Fe\,II}$ and $L_{\rm BOL}$ when non-detections were excluded (see Table 2). As for CO bandhead, this difference is reflected in the regression lines. The equation for all the data including non-detections is

$$L_{\rm Fe\,II} = 10^{-4.2} \times (L_{\rm BOL})^{0.54}. \quad (10)$$

The equation for detections only is

$$L_{\rm Fe\,II} = 10^{-4.1} \times (L_{\rm BOL})^{0.82}. \quad (11)$$

Spectral noise may have an effect, and is probably the cause of the higher upper limits in Fig. 12. However, we believe that the main effect differentiating between detections only and all data including non-detections is probably that there are genuine differences between sources. These differences will be discussed in more detail in a future paper.

6.6 He I

The He I 2.0587 μm line was seen in emission in 15 per cent of YSOs. Due to the requirement of hard ultraviolet (UV) photons to ionize helium, it was naively expected that there should be a threshold luminosity of $\sim 10^4$ $L_\odot$ or more. This is not seen in the data; the He I emission is seen across the whole luminosity range covered by the RMS data. This implies that either luminosity is not necessarily a good indicator of temperature for high-mass YSOs, or temperature does not drive He I production. Collisionally excited He I emission is frequently seen in low-mass T-Tauri stars, originating in a stellar wind (Edwards et al. 2006; Edwards 2007, 2009). The He I emission in the RMS sources with luminosity $L < 10^4$ $L_\odot$ is probably also collisionally excited, originating in a wind, rather than ionized as in H II regions. This may also be the emission mechanism for some (or all) of the stars with $L > 10^4$ $L_\odot$.

In addition, He I was seen in absorption in 5 spectra (e.g. G076.3829−00.6210/S106IR, see Fig. 3), or with a P-Cygni type

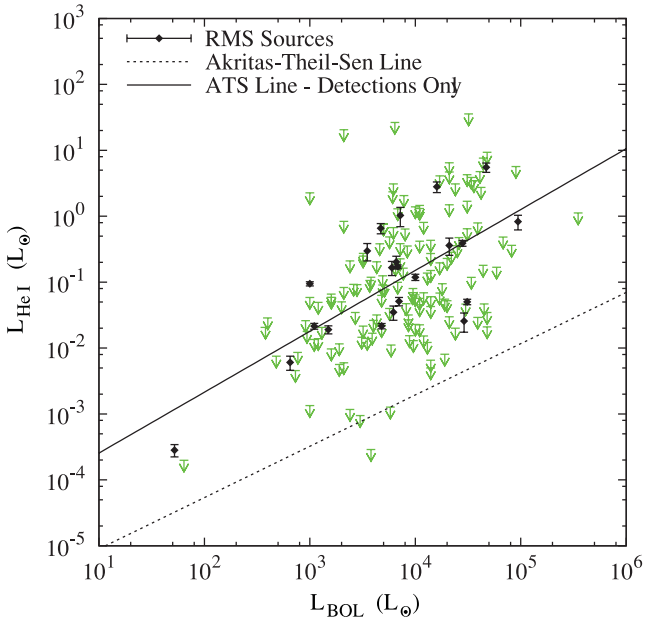

Figure 13. He I 2.0587 μm luminosity against bolometric luminosity for RMS sources. The detections are denoted by black diamonds and limits by green arrows. The lines represent the ATS regressions. Two lines are shown, one for regression with all the data including non-detections (dotted line), and one for regression with detections only (solid line). Line luminosities have been corrected for extinction and for the difference between measured and catalogue magnitudes.

profile in 15 spectra (see Table B3). Unfortunately, at this low resolution it was not possible to obtain expansion velocities for these lines. He I 2.0587 μm absorption has been studied in detail with high resolution spectroscopy for G076.3829−00.6210 by Drew, Bunn & Hoare (1993). They concluded that to be seen in absorption, this line requires high kinetic temperatures ($T \gtrsim 10^4$ K) and electron densities ($n_e \gtrsim 10^8$ cm^{-3}) in order for the transition to be preferentially populated from below rather than above. This suggests that the He I absorption in G076.3829−00.6210 is produced in an outflow originating very close to the star. It is likely that He I absorption in other high-mass YSOs also originates in an outflow.

Fig. 13 shows the He I 2.0587 μm luminosity against bolometric luminosity, for sources with He I in emission. He I absorption is not included in this plot. The lines represent the ATS regressions. Again, two regressions and correlation tests were performed, finding that a correlation between He I luminosity and bolometric luminosity is not an overall trend in the MYSO population, but does exist where He I is detected (see Table 2). The equation for all the data including non-detections is

$$L_{\mathrm{He\,I}} = 10^{-5.8} \times (L_{\mathrm{BOL}})^{0.78}. \quad (12)$$

The equation for detections only is

$$L_{\mathrm{He\,I}} = 10^{-4.5} \times (L_{\mathrm{BOL}})^{0.92}. \quad (13)$$

In this case, spectral noise is less likely to be a causal factor for the differences in the analysis; the spectrum at 2.0587 μm is not as noisy as at ∼2.3 μm or the *H* band. It is possible that the low resolution of the spectra means that self-absorption could prevent us from detecting He I if the line is sufficiently narrow. At higher resolutions we may see He I in more objects when the profile could be resolved. However, it is more likely that the results of these correlation tests reflect real differences between the sources.

7 CONCLUSIONS

Near-IR spectroscopic data were obtained for 247 objects selected from the RMS survey. The spectra were classified, finding 180 YSOs, 15 YSOs within H II regions, 26 H II regions, 7 evolved stars, 5 PPN, 4 PN, 5 M-type supergiants and 5 evolved hot stars. Spectra were found to be a valuable confirmation of classification in addition to our imaging data in 45 per cent of cases, and the only means of classifying the source in 5 per cent. The properties of the YSOs are as follows.

(i) The YSOs have luminosities ranging from 52 to 3.5×10^5 L$_\odot$, and extinctions ranging from $A_V = 2.7$ to $A_V = 114$.

(ii) Most YSOs were found to have emission lines, though not all had the same lines. The detection rates of Brγ, H_2, CO bandhead, [Fe II] 1.64 μm, fluorescent Fe II 1.6878 μm and He I 2.0587 μm were 75, 56, 17, 11, 26 and 15 per cent, respectively. He I 2.0587 μm was seen in absorption in five spectra. Brγ and He I 2.0587 μm were seen with P-Cygni type profiles in 13 and 15 objects, respectively, of which 8 objects had both lines with P-Cygni profiles. This indicates the presence of an outflowing wind.

(iii) In total, 39 per cent of the YSOs were found to have either fluorescent Fe II 1.6878 μm or CO bandhead emission (or both), both of which are evidence of a circumstellar disc. 56 per cent had H_2 emission, indicating the presence of an outflow.

(iv) The Brγ, H_2 and CO bandhead data were compared with low-mass YSOs from Carr (1989, 1990) and intermediate-mass YSOs from Ishii et al. (2001). The Brγ detection rate was lower than that for the intermediate-mass YSOs, but comparable with the detection rate for low-mass YSOs. The H_2 detection rate was higher than the detection rates for both the low- and intermediate-mass YSOs. Conversely, the CO bandhead detection rate was lower for the RMS YSOs than for both the low- and intermediate-mass YSOs. The differences in detection rates between the three data sets may be due to differences in obscuration and evolution. We will discuss these differences in more detail in Cooper et al. (in preparation).

(v) Strong correlations were found between $L_{\mathrm{Br}\gamma}$ and L_{BOL} and between $L_{\mathrm{H_2}}$ and L_{BOL}.

(vi) For CO bandhead, no overall correlation was found with L_{BOL}. However, when non-detections were excluded, there was a correlation. This may be due to the difficulty in distinguishing broad emission lines from a steeply rising continuum, variability in the emission, or because some objects genuinely do not have CO bandhead emission (perhaps indicating an evolutionary sequence).

(vii) The same effect was seen for both Fe II 1.6878 μm and He I 2.0587 μm emission: no overall correlation with L_{BOL} was found but there were correlations found when only detections above 3σ were considered. For Fe II, spectral noise is likely to be an issue for some sources, but we believe the major contribution is that there are real differences between the sources. For He I, spectral noise is unlikely to be the issue: the continuum at around ∼2.06 μm is not as noisy as at ∼ 2.3 μm or in the *H* band. However, self-absorption might cause the emission line not to be seen at this low resolution. Again, it may also be explained by genuine differences between the sources.

(viii) The line luminosity data for Brγ, H_2 and CO bandhead detections were compared with the low-mass YSOs from Carr (1989, 1990) and intermediate-mass YSOs from Ishii et al. (2001). For all three lines, a trend was seen across the whole mass range, from luminosities spanning five orders of magnitude. This suggests that the production mechanism for each line is the same for low-, intermediate- and high-mass stars, i.e. high-mass YSOs appear to resemble scaled-up versions of low-mass YSOs. This is consistent

with current theories in which all stars form in a similar fashion, e.g. Krumholz et al. (2009).

ACKNOWLEDGMENTS

This publication makes use of data products from the Two Micron All Sky Survey, which is a joint project of the University of Massachusetts and the Infrared Processing and Analysis Center/California Institute of Technology, funded by the National Aeronautics and Space Administration and the National Science Foundation. We also make use of data obtained at the United Kingdom Infrared Telescope, which is operated by the Joint Astronomy Centre on behalf of the Science and Technology Facilities Council of the United Kingdom, and the SIMBAD data base, operated at CDS, Strasbourg, France.

REFERENCES

Akritas M. G., Murphy S. A., LaValley M. P., 1995, J. Am. Stat. Assoc., 90, 170
Baker J. G., Menzel D. H., 1938, ApJ, 88, 52
Baldwin J. A., Ferland G. J., Korista K. T., Hamann F., LaCluyzé A., 2004, ApJ, 615, 610
Bary J. S., Matt S. P., Skrutskie M. F., Wilson J. C., Peterson D. E., Nelson M. J., 2008, ApJ, 687, 376
Beuther H., Walsh A., Schilke P., Sridharan T. K., Menten K. M., Wyrowski F., 2002, A&A, 390, 289
Bik A., Thi W. F., 2004, A&A, 427, L13
Biscaya A. M., Rieke G. H., Narayanan G., Luhman K. L., Young E. T., 1997, ApJ, 491, 359
Bunn J. C., Hoare M. G., Drew J. E., 1995, MNRAS, 272, 346
Calvet N., Muzerolle J., Briceño C., Hernández J., Hartmann L., Saucedo J. L., Gordon K. D., 2004, AJ, 128, 1294
Carr J. S., 1989, ApJ, 345, 522
Carr J. S., 1990, AJ, 100, 1244
Casali M. et al., 2007, A&A, 467, 777
Chandler C. J., Carlstrom J. E., Scoville N. Z., 1995, ApJ, 446, 793
Clarke A. J., Lumsden S. L., Oudmaijer R. D., Busfield A. L., Hoare M. G., Moore T. J. T., Sheret T. L., Urquhart J. S., 2006, A&A, 457, 183
Cohen M., Wheaton W. A., Megeath S. T., 2003, AJ, 126, 1090
Connelley M. S., Greene T. P., 2010, AJ, 140, 1214
Davies B., Lumsden S. L., Hoare M. G., Oudmaijer R. D., de Wit W.-J., 2010, MNRAS, 402, 1504
Davies B., Hoare M. G., Lumsden S. L., Hosokawa T., Oudmaijer R. D., Urquhart J. S., Mottram J. C., Stead J., 2011, MNRAS, 416, 972
Draine B. T., 1989, Infrared Spectrosc. Astron., 290, 93
Draine B. T., Lee H. M., 1984, ApJ, 285, 89
Drew J. E., Bunn J. C., Hoare M. G., 1993, MNRAS, 265, 12
Edwards S., 2007, in Bouvier J., Appenzeller I., eds, Proc. IAU Symp., 243, Star-Disk Interaction in Young Stars. Cambridge Univ. Press, Cambridge, p. 171
Edwards S., 2009, in Stempels E., ed., AIP Conf. Ser. Vol. 1094, Proc. 15th Cambridge Workshop on Cool Stars, Stellar Systems, and the Sun. Am. Inst. Phys., New York, p. 29
Edwards S., Fischer W., Hillenbrand L., Kwan J., 2006, ApJ, 646, 319
Egan M. P., Price S. D., Kraemer K. E., 2003, BAAS, 35, 1301
Garcia Lopez R., Natta A., Testi L., Habart E., 2006, A&A, 459, 837
Hamann F., Persson S. E., 1992, ApJS, 82, 247
Hambly N. C. et al., 2008, MNRAS, 384, 637
Hanson M. M., Kudritzki R.-P., Kenworthy M. A., Puls J., Tokunaga A. T., 2005, ApJS, 161, 154
Hartigan P., Kenyon S. J., Hartmann L., Strom S. E., Edwards S., Welty A. D., Stauffer J., 1991, ApJ, 382, 617
Helsel D. R., 2005, Non-detects and Data Analysis: Statistics for Censored Environmental Data. John Wiley and Sons, Hoboken, NJ
Hewett P. C., Warren S. J., Leggett S. K., Hodgkin S. T., 2006, MNRAS, 367, 454
Hoare M. G., Franco J., 2007, in Hartquist T. W., Pittard J. M., Falle S. A. E. G., eds, Diffuse Matter from Star Forming Regions to Active Galaxies. Series A&SSP, 61
Hoare M. G., Lumsden S. L., Oudmaijer R. D., Busfield A. L., King T. L., Moore T. L. J., 2004, in Clemens D., Shah R., Brainerd T., eds, ASP Conf. Ser., Vol. 317, Milky Way Surveys: The Structure and Evolution of our Galaxy. Astron. Soc. Pac., San Francisco, p. 156
Hoare M. G. et al., 2005, in Cesaroni R., Felli M., Churchwell E., Walmsley M., eds, IAU Symp 227, Massive Star Birth: A Crossroads of Astrophysics. Cambridge Univ. Press, Cambridge , p. 370
Hodgkin S. T., Irwin M. J., Hewett P. C., Warren S. J., 2009, MNRAS, 394, 675
Irwin M. J., 2008, ESO Instrument Calibration Workshop 2007. Springer-Verlag, Berlin, Heidelberg, p. 541
Ishii M., Nagata T., Sato S., Yao Y., Jiang Z., Nakaya H., 2001, AJ, 121, 3191
Isobe T., Feigelson E. D., 1990, BAAS, 22, 917
Isobe T., Feigelson E. D., Nelson P. I., 1986, ApJ, 306, 490
Koornneef J., 1983, A&A, 128, 84
Krumholz M. R., Klein R. I., McKee C. F., Offner S. S. R., Cunningham A. J., 2009, Sci, 323, 754
Lavalley M. P., Isobe T., Feigelson E. D., 1992, BAAS, 24, 839
Lawrence A. et al., 2007, MNRAS, 379, 1599
Lumsden S. L., Puxley P. J., Doherty R. M., 1994, MNRAS, 268, 821
Lumsden S. L., Hoare M. G., Oudmaijer R. D., Richards D., 2002, MNRAS, 336, 621
Lumsden S. L., Wheelwright H. E., Hoare M. G., Oudmaijer R. D., Drew J. E., 2012, MNRAS, 424, 1088
Molinari S., Brand J., Cesaroni R., Palla F., 1996, A&A, 308, 573
Mottram J. C., Hoare M. G., Lumsden S. L., Oudmaijer R. D., Urquhart J. S., Sheret T. L., Clarke A. J., Allsopp J., 2007, A&A, 476, 1019
Mottram J. C., Hoare M. G., Lumsden S. L., Oudmaijer R. D., Urquhart J. S., Meade M. R., Moore T. J. T., Stead J. J., 2010, A&A, 510, A89
Mottram J. C. et al., 2011a, A&A, 525, A149
Mottram J. C. et al., 2011b, ApJ, 730, L33
Muzerolle J., Calvet N., Hartmann L., 1998, ApJ, 492, 743
Porter J. M., Drew J. E., Lumsden S. L., 1998, A&A, 332, 999
Schmidt-Kaler T., 1982, in Hellwege K.-H., ed., Landolt-Börnstein, Group VI, Vol. 2. Springer, Heidelberg, p. 451
Shepherd D. S., Churchwell E., 1996, ApJ, 472, 225
Shu F. H., Adams F. C., Lizano S., 1987, ARA&A, 25, 23
Skrutskie M. F. et al., 2006, AJ, 131, 1163
Sridharan T. K., Beuther H., Schilke P., Menten K. M., Wyrowski F., 2002, ApJ, 566, 931
Storey P. J., Hummer D. G., 1995, MNRAS, 272, 41
Urquhart J. S., Busfield A. L., Hoare M. G., Lumsden S. L., Clarke A. J., Moore T. J. T., Mottram J. C., Oudmaijer R. D., 2007a, A&A, 461, 11
Urquhart J. S. et al., 2007b, A&A, 474, 891
Urquhart J. S. et al., 2008a, in Beuther H., Linz H., Henning T., eds, ASP Conf. Ser. Vol. 387, Massive Star Formation: Observations Confront Theory. Astron. Soc. Pac., San Francisco, p. 381
Urquhart J. S. et al., 2008b, A&A, 487, 253
Urquhart J. S. et al., 2009a, A&A, 501, 539
Urquhart J. S. et al., 2009b, A&A, 507, 795
Urquhart J. S. et al., 2011a, MNRAS, 418, 1689
Urquhart J. S. et al., 2011b, MNRAS, 410, 1237
Urquhart J. S. et al., 2012, MNRAS, 420, 1656
Wheelwright H. E., Oudmaijer R. D., de Wit W. J., Hoare M. G., Lumsden S. L., Urquhart J. S., 2010, MNRAS, 408, 1840
Zorec J., Arias M. L., Cidale L., Ringuelet A. E., 2007, A&A, 470, 239

APPENDIX A: TARGET OBJECT DATA TABLES

APPENDIX B: EMISSION LINE FLUXES AND EQUIVALENT WIDTHS

Table A1. Table of all spectra, showing RA, Dec., observing date, position angle (PA), total exposure time (Exp. Time), classification, distance, luminosity and radio data. The PA was chosen individually for each object from any images that were available. For the earlier objects, these were 2MASS images, but for the later runs GLIMPSE images were used. The aim was to centre on the target object, but to align the slit to catch any extended emission, outflow, or other interesting nearby objects in the slit at the same time. Some objects were observed multiple times with different PAs to get spectra of all the interesting features in the region (see Section 2). The exposure times were chosen based on the magnitudes of the target object (shown in Table A2). The classification process is described in Section 4, and the distance, luminosity and radio data were taken from other RMS publications, listed in Section 1. *The final spectrum of G025.6498+01.0491 is a composite of two spectra, taken on 2007-06-26 and 2007-06-30.

Name	RA (J2000)	Dec. (J2000)	Date	PA (°)	Exp. time (s)	NIR classification	Distance (kpc)	Luminosity ($L_{\odot}$)	Rad. freq. (GHz)	Rad. flux (mJy)
G010.8411−02.5919	18:19:12.21	−20:47:29.70	2004-04-15	13	720	YSO	1.8	2.2×10^4	8.6	3.6
G010.8856+00.1221	18:09:07.97	−19:27:23.70	2008-08-15	0	60	YSO	13.5	9.0×10^4	5	<1.0
G011.9019+00.7265	18:08:58.77	−18:16:29.70	2008-08-16	−90	60	YSO	3.1	2.1×10^3	5	<0.7
G016.7122+01.3119 – 1	18:16:26.38	−13:46:24.40	2004-08-05	80	90	YSO	2.0	1.6×10^3	5	<0.6
G016.7122+01.3119 – 2	18:16:27.54	−13:46:21.40	2004-08-05	80	90	YSO	2.0	1.6×10^3	5	<0.6
G016.7981+00.1264	18:20:55.30	−14:15:30.70	2007-07-11	−78	60	YSO	2.0	2.6×10^3	5	<0.6
G017.0332+00.7476A	18:19:07.33	−13:45:23.20	2007-06-22	0	240	YSO	2.0	1.6×10^3	5	<0.8
G017.3765+02.2512	18:14:21.05	−12:44:33.20	2004-08-06	70	90	YSO	1.2	912	5	<0.7
G018.3412+01.7681	18:17:58.11	−12:07:24.80	2003-04-30	−90	60	YSO	2.0	1.1×10^4	8.6	<0.4
G018.3706−00.3818	18:25:48.37	−13:06:29.10	2007-07-13	54	60	YSO	4.1	4.9×10^3	5	<1.2
G018.6608+00.0372	18:24:50.23	−12:39:22.30	2007-06-22	−90	240	YSO	10.9	2.0×10^4	5	<1.0
G019.7540−00.1279	18:27:31.59	−11:45:55.10	2007-06-23	−90	120	HIIR	8.0	4.4×10^4	8.6	<0.4
G019.8922+00.1023	18:26:57.29	−11:32:09.10	2007-07-11	−90	780	YSO	12.6	8.2×10^4	5	<1.1
G019.9224−00.2577	18:28:18.96	−11:40:36.90	2007-06-22	−68	240	YSO	4.6	3.2×10^3	5	<1.1
G020.5143+00.4936	18:26:43.24	−10:48:18.20	2008-08-16	−86.5	840	YSO	2.3/13.6	$360/1.3 \times 10^4$	5	<0.6
G021.3853−00.2537	18:31:03.99	−10:22:44.70	2007-06-23	67	240	HIIR	5.5	3.2×10^4	5	106.6
G021.5624−00.0329	18:30:36.06	−10:07:11.00	2008-08-16	−90	60	YSO	7.9	1.6×10^4	5	<1.0
G023.3891+00.1851	18:33:14.32	−08:23:57.40	2007-06-26	−90	40	YSO	3.2	2.1×10^4	5	<1.0
G023.4394−00.2394	18:34:51.69	−08:33:01.00	2008-06-28	−45	60	HIIR	5.6	2.0×10^4	5	<1.1
G023.4984−00.0373	18:34:14.28	−08:24:15.00	2008-06-24	−90	40	Evolved Star	–	–	5	<1.0
G023.6566−00.1273	18:34:51.56	−08:18:21.40	2007-06-26	−90	60	YSO	3.2	6.2×10^3	5	<1.0
G024.6343−00.3233	18:37:22.71	−07:31:41.70	2007-06-21	40	60	YSO	3.3	5.7×10^3	5	<0.7
G025.4018+00.0198A	18:37:34.48	−06:41:21.10	2008-08-07	−90	5	M Star	7.7	6.5×10^3	5	<1.6
G025.6498+01.0491*	18:34:20.90	−05:59:42.60	–	0	240	YSO	3.1	2.1×10^4	8.6	3.8
G025.7161+00.0486	18:38:02.83	−06:23:47.90	2007-06-26	−34.01	120	YSO/HIIR	9.4	7.3×10^4	5	15.8
G025.8015−00.1570 – 1	18:38:56.37	−06:24:53.50	2007-07-11	0	60	YSO/HIIR	5.6	2.8×10^4	5	29.2
G025.8015−00.1570 – 2	18:38:56.38	−06:24:52.63	2007-07-11	0	60	YSO	5.6	2.8×10^4	5	29.2
G026.2020+00.2262	18:38:18.52	−05:52:57.50	2008-06-28	−90	40	YSO	7.6	3.1×10^4	5	<1.1
G026.3050+00.1162	18:38:53.55	−05:50:30.60	2008-06-28	0	40	Other	–	–	5	<1.0
G026.3176−00.0134	18:39:23.01	−05:53:19.90	2007-06-21	−90	60	Other	–	–	5	19.5
G026.3819+01.4057 – 1	18:34:25.82	−05:10:52.80	2004-05-13	−39.1	60	YSO	2.3	1.4×10^4	5	<0.6
G026.3819+01.4057 – 2	18:34:25.68	−05:10:50.30	2004-05-13	−39.1	60	YSO	2.3	1.4×10^4	5	<0.6
G026.4207+01.6858	18:33:30.55	−05:01:02.10	2004-08-06	0	1350	YSO	2.3	1.2×10^4	5	<0.6
G026.4488+01.7425A	18:33:21.19	−04:58:05.90	2004-08-06	0	90	Other	2.3	5.2×10^3	5	<0.7
G026.4488+01.7425B	18:33:21.21	−04:58:01.40	2004-08-06	0	90	HIIR	2.3	6.7×10^3	5	5.2
G026.4897−00.5455	18:41:35.93	−05:58:50.80	2007-07-11	0	60	PPN	4.4	6.2×10^3	5	<0.6
G026.4958+00.7105 – 1	18:37:07.29	−05:24:01.30	2007-06-23	6	240	YSO	11.9	2.0×10^4	5	<0.6
G026.4958+00.7105 – 2	18:37:07.31	−05:23:58.30	2007-06-23	6	240	YSO	11.9	2.0×10^4	5	<0.6
G026.5972−00.0241	18:39:55.89	−05:38:45.04	2007-06-23	0	240	YSO/HIIR	1.9	2.4×10^3	8.6	<0.4
G027.2220+00.1361 – 1	18:40:30.75	−05:01:03.96	2008-07-25	−65	240	Evolved Star	7.6	1.0×10^4	5	<0.7
G027.2220+00.1361 – 2	18:40:30.83	−05:01:04.52	2008-07-25	−65	240	YSO	7.6	1.0×10^4	5	<0.7
G027.7954−00.2772	18:43:02.29	−04:41:49.10	2007-07-11	30	60	YSO	3.1	2.1×10^3	5	<1.0
G028.2325+00.0394	18:42:42.50	−04:09:46.00	2008-07-25	21	120	YSO	6.2	3.3×10^3	5	<1.5
G028.3046−00.3871A	18:44:22.00	−04:17:39.50	2007-06-26	45	60	YSO	5.2	1.0×10^4	5	<1.4
G028.3373+00.1189	18:42:37.12	−04:02:02.20	2008-07-22	−90	960	YSO	5.0	1.3×10^4	5	<1.2
G028.7799+03.4978	18:31:23.97	−02:05:29.50	2004-04-28	0	14	Other	–	–	5	1.3

Table A1 – *continued*

Name	RA (J2000)	Dec. (J2000)	Date	PA (°)	Exp. time (s)	NIR classification	Distance (kpc)	Luminosity ($L_{\odot}$)	Rad. freq. (GHz)	Rad. flux (mJy)
G028.8621+00.0657	18:43:46.45	−03:35:31.30	2007-06-22	−60	120	YSO	6.2	1.0×10^5	5	<1.2
G030.1468+01.4075	18:41:20.60	−01:50:07.60	2004-08-09	90	150	PPN	–	–	5	<0.9
G030.1981−00.1691	18:47:03.07	−02:30:36.20	2007-06-26	41	60	YSO	7.4	3.4×10^4	5	<0.8
G030.2340−00.1392	18:47:00.42	−02:27:52.30	2007-06-26	−73	40	PN	7.4	1.4×10^4	5	349.9
G030.2971+00.0549	18:46:25.77	−02:19:13.80	2007-06-23	36.99	240	YSO	7.4	7.8×10^3	5	<1.0
G030.4117−00.2277	18:47:39.01	−02:20:52.30	2008-07-24	−67.9	60	YSO	7.4	4.7×10^3	5	<1.1
G030.5942−00.1273	18:47:37.55	−02:08:19.80	2007-07-04	40	40	YSO	5.7	6.0×10^3	5	<1.0
G030.8185+00.2729	18:46:36.62	−01:45:21.70	2007-07-15	−5	60	YSO	5.7	1.1×10^4	8.6	<0.4
G030.9726−00.1410	18:48:22.06	−01:48:29.80	2008-07-25	−75.3	120	YSO	5.7	2.8×10^3	5	<0.7
G030.9727+00.5620	18:45:51.70	−01:29:13.10	2008-07-22	−59	240	YSO	11.9	2.1×10^4	5	<0.7
G030.9959−00.0771	18:48:10.67	−01:45:25.60	2007-06-24	−90	240	YSO	5.7	5.9×10^3	5	<1.2
G031.1677+00.1259	18:47:46.26	−01:30:46.20	2008-07-24	−4	60	PPN	–	–	5	<1.4
G031.6617+00.3667	18:47:48.90	−00:57:48.00	2008-07-24	−33	60	PN	12.7	5.3×10^4	5	<0.5
G032.0451+00.0589	18:49:36.56	−00:45:45.50	2007-06-24	−90	4080	YSO	5.7	2.8×10^4	5	<1.1
G032.0518−00.0902	18:50:09.23	−00:49:28.90	2008-07-25	−45	120	YSO	4.5	4.0×10^3	5	<1.1
G032.1514+00.1317	18:49:32.50	−00:38:05.40	2004-04-28	−29.7	60	HIIR	5.7	5.0×10^4	5	264.4
G032.4727+00.2041	18:49:52.55	−00:18:56.90	2007-06-30	0	60	YSO/HIIR	11.0	4.7×10^4	8.6	<0.4
G032.8205−00.3300	18:52:24.47	−00:14:57.80	2008-07-24	−86.8	1080	YSO	5.1	1.4×10^4	5	<0.7
G032.9957+00.0415	18:51:24.46	+00:04:33.70	2007-06-26	17	1140	YSO	8.9	3.2×10^4	8.6	<0.4
G033.3891+00.1989	18:51:33.82	+00:29:51.10	2007-07-04	27.99	15	YSO	5.1	1.0×10^4	5	<1.0
G034.0126−00.2832	18:54:25.06	+00:49:56.60	2007-07-04	0	300	YSO	13.3	3.6×10^4	5	<0.7
G034.0500−00.2977	18:54:32.31	+00:51:32.60	2007-07-04	18	40	YSO	13.3	2.4×10^4	5	<0.8
G034.4035+00.2282	18:53:18.37	+01:24:54.64	2007-06-24	−31.5	120	YSO	3.1	9.3×10^3	5	9.7
G034.6243−00.1300	18:54:59.25	+01:26:47.30	2008-07-22	−39.41	120	YSO/HIIR	1.6/12.4	$956/5.7 \times 10^4$	5	6.8
G034.7569+00.0247	18:54:40.73	+01:38:06.60	2007-06-24	45	240	YSO	5.0	9.4×10^3	8.6	<0.4
G034.8211+00.3519	18:53:37.89	+01:50:30.60	2007-07-04	−36	15	YSO	3.1	6.4×10^3	5	<0.7
G035.1979−00.7427	18:58:13.11	+01:40:39.90	2004-04-29	15.6	1260	YSO	2.2	3.1×10^4	5	6
G036.8780−00.4728 – 1	19:00:19.83	+03:17:42.90	2008-07-26	−90	120	YSO	3.6	5.0×10^3	5	5.7
G036.8780−00.4728 – 2	19:00:19.84	+03:17:43.40	2008-07-27	−10	120	YSO	3.6	5.0×10^3	5	5.7
G036.9194+00.4825A	18:56:59.79	+03:46:04.00	2007-06-24	51	5280	YSO	12.7	1.0×10^4	5	<0.6
G037.5536+00.2008	18:59:09.96	+04:12:15.60	2007-06-24	−70.01	480	YSO	6.7	3.9×10^4	8.6	<0.4
G039.4943−00.9933	19:06:59.71	+05:22:53.30	2008-07-24	26.6	60	YSO	3.6	8.0×10^3	5	<0.6
G039.8821−00.3457	19:05:24.12	+06:01:25.90	2007-06-25	6	240	HIIR	9.1	5.1×10^4	5	355
G040.0809+01.5117	18:59:07.15	+07:02:58.90	2004-08-22	−52.01	120	M Star	–	–	5	<0.6
G040.4247+00.6989A	19:02:39.54	+06:59:08.10	2008-07-26	0	240	Evolved star	12.0	9.9×10^3	5	5.2
G040.5451+02.5961A	18:56:04.56	+07:57:26.15	2004-08-06	35	90	HIIR	2.3	1.6×10^4	5	464.8
G042.0341+00.1905A	19:07:28.19	+08:10:53.30	2008-07-22	−31.1	1380	YSO	11.4	3.1×10^4	5	<0.6
G042.0977+00.3521	19:07:00.52	+08:18:45.60	2008-07-24	39.79	2880	YSO	11.4	6.8×10^4	5	<0.6
G042.1099−00.4466	19:09:53.58	+07:57:14.50	2008-07-24	5.3	3000	YSO/HIIR	8.5	4.1×10^4	8.6	14.8
G043.1635−00.0697A	19:10:30.28	+09:03:45.40	2008-07-27	64.89	120	YSO	11.7	1.1×10^4	5	<10.2
G043.5216−00.6476	19:13:15.44	+09:06:49.20	2006-09-16	90	60	YSO	8.2	3.8×10^3	5	<0.6
G043.9956−00.0111	19:11:51.64	+09:49:40.50	2008-07-24	45	60	YSO	7.5	2.6×10^4	5	<0.6
G044.3103+00.0416	19:12:15.71	+10:07:53.50	2008-07-26	−90	2160	YSO/HIIR	7.5	2.9×10^4	5	6.4
G045.1894−00.4387	19:15:38.98	+10:41:14.40	2008-07-22	0	60	YSO	6.0	7.2×10^3	–	–
G045.4543+00.0600 – 1	19:14:21.28	+11:09:15.54	2004-06-16	6.2	60	HIIR	7.3	–	5	417.6
G045.4543+00.0600 – 2	19:14:21.28	+11:09:16.76	2004-06-16	6.2	60	HIIR	7.3	–	5	417.6
G045.4641+00.0284	19:14:29.09	+11:08:49.90	2008-07-27	−90	6240	YSO	7.3	1.2×10^4	5	<3.5
G048.6085+00.0258D	19:20:30.60	+13:55:38.10	2008-07-20	−46	40	M Star	10.3	1.1×10^5	5	61
G048.9897−00.2992A	19:22:26.64	+14:06:45.60	2003-10-26	0	120	YSO	5.1	9.5×10^3	5	<1.3
G048.9897−00.2992B	19:22:26.13	+14:06:39.70	2003-10-26	0	120	HIIR	5.1	2.4×10^4	5	11.5
G049.0431−01.0787	19:25:22.25	+13:47:19.70	2003-08-02	−43.5	60	YSO	2.9	2.7×10^3	5	<0.7
G049.4227−00.3715	19:23:32.65	+14:27:28.60	2008-07-20	0	540	YSO	5.1	2.1×10^4	5	<18.1

Table A1 – *continued*

Name	RA (J2000)	Dec. (J2000)	Date	PA (°)	Exp. time (s)	NIR classification	Distance (kpc)	Luminosity ($L_\odot$)	Rad. freq. (GHz)	Rad. flux (mJy)
G049.4883−00.3545A	19:23:35.87	+14:31:28.60	2008-07-22	−49	120	HIIR	5.1	5.1×10^3	5	<13.1
G049.4883−00.3545B	19:23:36.79	+14:31:16.70	2008-07-22	−49	120	YSO	5.1	5.1×10^3	5	<13.1
G049.4970−00.4718	19:24:03.16	+14:28:34.30	2003-08-04	−58	60	HIIR	5.1	6.4×10^3	5	<6.8
G049.5373−00.3929	19:23:50.46	+14:32:57.50	2008-07-20	−90	20	Evolved star	5.1	2.1×10^5	5	<7.8
G050.0721+00.5591	19:21:24.79	+15:28:04.60	2008-07-24	−37	3360	YSO	11.2	1.8×10^4	5	<0.6
G050.2213−00.6063	19:25:57.82	+15:02:59.50	2003-06-11	35	60	YSO	3.3	4.3×10^3	5	<0.6
G050.2844−00.3925A	19:25:17.79	+15:12:24.50	2004-06-16	65.7	1740	YSO	9.9	2.1×10^4	5	<0.9
G050.4802+00.7058	19:21:40.43	+15:53:54.50	2003-05-07	−90	60	PN	–	–	5	5.4
G052.2025+00.7217A	19:24:59.86	+17:25:18.10	2004-06-16	58.1	60	YSO	10.2	1.6×10^4	5	<0.7
G052.2078+00.6890	19:25:08.56	+17:24:47.40	2008-07-20	−49	3600	YSO	10.2	1.9×10^4	5	<0.7
G052.5405−00.9272	19:31:45.04	+16:55:59.20	2005-07-12	90	180	YSO	4.9	1.4×10^4	5	<0.6
G052.9217+00.4142	19:27:35.01	+17:54:38.00	2003-08-04	40	60	YSO	5.7	3.2×10^3	5	<0.6
G052.9221−00.4892	19:30:54.61	+17:28:41.80	2005-07-10	26	60	HIIR	5.1	7.2×10^3	5	<0.6
G053.1417+00.0705	19:29:17.59	+17:56:23.30	2003-06-11	12	60	YSO	1.6	3.3×10^3	5	<0.7
G053.5343−00.7943	19:33:16.39	+17:52:05.00	2004-06-16	−42.7	42	YSO	4.7	6.2×10^3	5	<0.6
G055.1581−00.2991A	19:34:45.99	+19:31:37.90	2006-09-08	33	120	YSO	4.9	1.4×10^4	5	10.4
G055.3704+00.1858	19:33:24.25	+19:56:55.70	2008-07-07	−90	10	M Star	3.1	9.6×10^3	5	<0.7
G056.3694−00.6333	19:38:31.56	+20:25:19.50	2006-09-15	−10	60	YSO	6.4	6.5×10^3	5	<0.6
G056.4120−00.0277	19:36:21.53	+20:45:18.00	2008-07-07	−90	40	YSO	10.0	1.7×10^4	5	<0.7
G057.5474−00.2717A	19:39:39.61	+21:37:31.80	2005-07-16	−67	60	HIIR	9.1	3.1×10^4	5	<1.0
G059.3614−00.2068	19:43:17.96	+23:14:01.60	2003-06-01	45	60	YSO	2.2	941	8.6	<0.4
G059.6403−00.1812A	19:43:48.54	+23:29:17.90	2003-05-31	−90	60	YSO	2.2	1.5×10^3	5	<0.8
G059.7831+00.0648	19:43:11.22	+23:44:04.00	2003-06-01	60	60	YSO	2.2	8.4×10^3	8.6	1
G059.8329+00.6729	19:40:59.59	+24:04:45.18	2006-09-16	60	120	YSO	4.2	1.9×10^3	5	<0.7
G060.5750−00.1861	19:45:52.48	+24:17:42.20	2006-09-15	−30	480	YSO	0.2/8.2	$20/3.6 \times 10^4$	5	<0.4
G063.1140+00.3416	19:49:32.10	+26:45:15.10	2005-07-16	0	60	YSO	5.6	6.1×10^3	5	<0.7
G065.7798−02.6121	20:07:06.57	+27:28:53.20	2005-07-29	−13	60	YSO	0.3	52	5	<0.7
G068.2040+00.2387	20:01:59.96	+31:03:10.30	2003-08-04	−59	60	YSO	10.1	1.4×10^4	5	<0.9
G069.5395−00.9754	20:10:09.06	+31:31:35.80	2004-07-06	−75.1	120	HIIR	1.2/4.7	$6.5 \times 10^3/9.4 \times 10^4$	–	146.8
G070.3329+01.5864 – 1	20:01:55.08	+33:34:20.10	2003-08-04	0	60	HIIR	7.0	9.1×10^4	5	126.7
G070.3329+01.5864 – 2	20:01:55.09	+33:34:19.10	2003-08-04	0	60	HIIR	7.0	9.1×10^4	5	126.7
G070.6740+01.1919	20:04:23.65	+33:39:04.30	2006-10-01	45	14	Other	1.7	2.6×10^3	5	387.8
G071.8944+01.3107	20:07:04.79	+34:44:42.70	2003-08-04	72	60	YSO	1.7	3.5×10^3	8.6	<0.4
G072.2479+00.2617B	20:12:17.41	+34:28:12.10	2007-06-23	45.99	3840	YSO	13.1	1.1×10^4	5	<0.9
G073.0633+01.7958	20:08:10.09	+35:59:24.10	2003-10-26	45	60	YSO	1.7	2.4×10^3	5	<1.0
G073.6525+00.1944	20:16:21.96	+35:36:06.30	2003-08-16	0	1980	YSO	13.1	3.5×10^5	5	<0.7
G073.6952−00.9996	20:21:18.89	+34:57:50.90	2003-06-11	−37	42	YSO	8.5	2.2×10^4	5	<1.0
G075.6014+01.6394	20:15:48.16	+38:01:31.30	2007-06-22	0	4200	YSO	13.2	3.9×10^4	5	<1.0
G075.7666+00.3424 – 1	20:21:41.57	+37:26:06.20	2008-07-22	16.5	60	YSO	1.7	4.8×10^4	5	<2.4
G075.7666+00.3424 – 2	20:21:39.42	+37:25:15.00	2008-07-24	71.9	60	YSO	1.7	4.8×10^4	5	<2.4
G076.0902+00.1412	20:23:27.30	+37:34:54.00	2004-07-16	0	60	YSO	1.7	1.0×10^3	5	<1.1
G076.1877+00.0974	20:23:55.15	+37:38:10.70	2008-07-22	45	120	HIIR	1.7	1.0×10^4	5	396.7
G076.3829−00.6210	20:27:26.77	+37:22:47.80	2003-06-11	−12	7	YSO/HIIR	1.7	5.9×10^4	–	14.9
G077.3455+04.4309	20:08:38.46	+41:00:40.70	2005-07-29	57	60	M Star	–	–	5	<0.6
G077.4052−01.2136	20:32:54.10	+37:51:29.70	2004-07-02	70	120	YSO	1.7	654	5	<1.1
G077.4622+01.7600 – 1	20:20:39.34	+39:37:55.30	2004-07-08	0	60	YSO	1.7	8.2×10^3	5	24.9
G077.4622+01.7600 – 2	20:20:39.07	+39:37:58.60	2004-05-13	15	60	YSO	1.7	8.2×10^3	5	24.9
G077.8999+01.7678	20:21:55.02	+39:59:45.50	2003-08-20	−3	60	YSO	1.7	1.1×10^3	5	<1.0
G077.9550+00.0058	20:29:31.76	+39:01:20.80	2007-06-26	0	60	HIIR	1.7	2.2×10^3	–	–
G078.1224+03.6320	20:14:25.86	+41:13:36.40	2003-08-18	−57.51	60	YSO	1.7	5.8×10^3	8.6	<0.4
G078.4373+02.6584B	20:19:38.49	+40:56:33.70	2003-08-16	74.7	2160	YSO	1.7	1.0×10^4	–	82.2
G078.4705−00.1830	20:31:53.35	+39:19:37.60	2007-06-22	0	240	YSO/HIIR	10.6	4.4×10^4	5	<1.2

Table A1 – *continued*

Name	RA (J2000)	Dec. (J2000)	Date	PA (°)	Exp. time (s)	NIR classification	Distance (kpc)	Luminosity ($L_\odot$)	Rad. freq. (GHz)	Rad. flux (mJy)
G078.4754+01.0421	20:26:44.44	+40:02:57.80	2004-07-08	−50	60	YSO	1.7	3.5×10^3	5	<1.1
G078.7641+01.6862	20:24:51.67	+40:39:25.30	2007-06-24	45	1200	YSO	12.4	5.9×10^4	5	<0.7
G078.8867+00.7087	20:29:24.87	+40:11:19.40	2003-06-12	63	259	YSO	1.7	4.8×10^4	5	<0.4
G078.9761+00.3567	20:31:11.26	+40:03:07.60	2008-07-22	−49.6	40	YSO	1.7	8.8×10^3	8.6	7.6
G079.1272+02.2782	20:23:23.83	+41:17:39.30	2007-07-04	18	60	YSO	1.7	2.7×10^3	8.6	1.4
G079.3202+01.3131	20:28:10.25	+40:53:37.60	2008-07-22	−90	120	HIIR	8.6	4.8×10^4	5	6.1
G079.3248+01.2901	20:28:16.15	+40:52:58.00	2008-07-30	18.19	120	HIIR	8.6	5.1×10^4	5	<1.7
G080.0467+00.3101	20:34:43.26	+40:53:13.60	2004-07-08	90	60	YSO	1.7	1.3×10^3	5	<1.2
G080.1909+00.5353	20:34:13.26	+41:08:14.10	2004-08-05	−37	90	YSO	1.7	1.0×10^3	5	<1.2
G080.8282+00.5670A	20:36:07.53	+41:40:09.10	2004-08-05	68	90	YSO	1.7	4.3×10^3	8.6	1.8
G080.8645+00.4197	20:36:52.17	+41:36:24.70	2004-07-02	23	120	YSO/HIIR	1.7	2.4×10^4	5	50.8
G081.5168+00.1926	20:39:57.77	+41:59:14.60	2004-07-08	−19	120	YSO	1.7	730	5	<1.1
G081.7131+00.5792	20:38:57.19	+42:22:41.00	2004-07-16	37.6	42	YSO	1.7	6.8×10^3	5	<15.8
G081.7624+00.5916	20:39:03.72	+42:25:29.60	2004-08-06	−45	120	YSO	1.7	1.0×10^3	5	<5.3
G082.5682+00.4040A	20:42:33.76	+42:56:51.40	2004-07-16	−90	60	YSO	1.7	6.2×10^3	5	<1.0
G083.7071+03.2817	20:33:36.51	+45:35:44.10	2007-06-26	−45	40	YSO	1.7	5.7×10^3	5	<1.2
G084.3065+01.8933	20:41:58.52	+45:14:00.40	2008-07-21	0	60	YSO	13.1	1.2×10^4	5	<1.1
G084.6490+02.1267	20:42:07.73	+45:38:47.70	2007-06-26	0	120	HIIR	13.1	2.2×10^4	5	2.1
G085.4102+00.0032A	20:54:14.36	+44:54:04.60	2008-07-24	−68	4560	YSO	6.8	3.1×10^4	5	<1.0
G089.6368+00.1732	21:09:45.76	+48:10:58.10	2007-06-26	50	60	YSO	8.0	2.4×10^4	5	<0.9
G090.2095+02.0405	21:03:41.76	+49:51:47.10	2007-07-04	0	9	YSO	9.0	4.4×10^4	5	<1.0
G094.3228−00.1671	21:31:45.04	+51:15:37.02	2007-07-04	−34.01	60	YSO	6.1	1.1×10^4	5	<1.0
G094.4637−00.8043	21:35:09.16	+50:53:09.20	2004-07-03	−52.5	60	YSO	6.1	3.2×10^4	5	<1.0
G095.0026−01.5779	21:40:57.42	+50:39:58.30	2004-08-06	90	120	YSO	3.6	3.0×10^3	5	<0.6
G095.0531+03.9724	21:15:55.64	+54:43:31.00	2007-06-23	−90	1440	YSO	10.7	1.9×10^4	5	<1.0
G096.3597+01.2982	21:35:05.02	+53:43:00.40	2008-07-22	−5.31	120	YSO	8.8	2.0×10^4	5	<1.0
G096.4353+01.3233A – 1	21:35:21.25	+53:47:12.47	2007-07-03	28.99	60	YSO	8.8	1.9×10^4	5	<0.6
G096.4353+01.3233A – 2	21:35:21.16	+53:47:10.64	2007-07-03	28.99	600	YSO/HIIR	8.8	1.9×10^4	5	<0.6
G097.5268+03.1837C	21:32:10.69	+55:53:35.40	2007-06-27	46.99	120	YSO	8.7	3.4×10^4	5	<1.1
G097.9978+01.4688	21:42:43.19	+54:55:51.90	2004-08-23	90	60	YSO	8.0	6.6×10^3	5	<1.9
G098.8555+02.9344	21:40:28.98	+56:35:55.70	2004-08-23	54.99	120	YSO	0.5	64	5	<1.0
G100.1620+01.6647	21:53:38.81	+56:27:50.00	2007-07-04	45	120	YSO	7.5	1.7×10^4	5	<1.0
G100.1685+02.0266	21:52:02.77	+56:44:59.80	2007-07-04	0	60	YSO	7.5	4.5×10^4	5	<0.7
G100.2124+01.8829	21:52:57.15	+56:39:54.30	2007-06-26	0	60	YSO	7.5	1.7×10^4	5	<0.9
G100.3779−03.5784	22:16:10.35	+52:21:34.70	2003-06-12	0	60	YSO	4.9	3.0×10^4	5	<1.0
G102.3533+03.6360	21:57:25.19	+59:21:56.70	2004-08-05	26.6	17	YSO	10.6	1.7×10^5	5	<0.8
G103.8034+00.4062	22:20:46.18	+57:34:17.30	2008-07-24	0	120	YSO	7.3	7.2×10^3	5	<1.0
G103.8744+01.8558	22:15:09.09	+58:49:07.80	2007-06-25	64.99	60	YSO	2.6	1.3×10^4	8.6	3.7
G105.5072+00.2294	22:32:23.82	+58:18:59.60	2002-12-15	0	60	YSO	2.9	3.9×10^3	5	<1.0
G107.6823−02.2423A	22:55:29.83	+57:09:25.00	2003-08-20	66.4	60	YSO	6.1	7.0×10^3	5	<0.8
G108.2118−01.2887	22:55:59.77	+58:14:42.40	2002-12-16	19.99	60	HIIR	5.9	2.5×10^4	5	3.4
G108.7575−00.9863	22:58:47.41	+58:45:02.12	2004-07-02	34.9	60	YSO	5.5	9.0×10^4	5	<2.5
G110.8038−02.5649	23:17:52.26	+58:05:11.10	2004-08-23	−32	60	YSO	3.7	1.2×10^3	5	<1.0
G111.2348−01.2385	23:17:21.02	+59:28:48.00	2002-12-16	−90	660	YSO	2.4	1.2×10^4	8.6	<0.4
G133.8512−01.9272	02:17:57.82	+59:05:52.00	2002-12-15	−90	60	Evolved Star	–	–	5	<0.9
G139.9091+00.1969A	03:07:24.52	+58:30:43.30	2003-08-15	2.6	42	YSO	4.3	2.1×10^4	–	20
G141.9996+01.8202	03:27:38.77	+58:47:00.10	2003-08-23	2.6	3	YSO	1.4	4.6×10^3	5	<0.7
G142.2446+01.4299	03:27:31.37	+58:19:21.80	2002-12-16	−90	60	YSO/HIIR	5.7	2.9×10^4	5	7.4
G144.6678−00.7136	03:33:10.02	+55:10:55.00	2002-12-15	−90	60	YSO	2.8	765	5	<1.0
G145.1975+02.9870 – 1	03:52:27.33	+57:48:31.80	2006-09-15	−69.3	60	YSO	8.9	8.6×10^3	5	<0.9
G145.1975+02.9870 – 2	03:52:28.02	+57:48:29.70	2006-09-15	−69.3	60	YSO	8.9	8.6×10^3	5	<0.9
G148.1201+00.2928	03:56:15.36	+53:52:13.10	2003-08-18	−68.8	42	YSO	4.3	7.2×10^3	5	<1.0

Table A1 – *continued*

Name	RA (J2000)	Dec. (J2000)	Date	PA (°)	Exp. time (s)	NIR classification	Distance (kpc)	Luminosity ($L_{\odot}$)	Rad. freq. (GHz)	Rad. flux (mJy)
G150.6862−00.6887	04:04:49.62	+51:26:57.20	2002-12-15	−90	60	YSO	2.8	396	5	<1.0
G151.6120−00.4575	04:10:11.86	+50:59:54.50	2003-08-17	0	17	YSO	8.9	4.2×10^4	5	<1.0
G152.3371−00.2899	04:14:15.92	+50:37:32.00	2002-12-15	−90	60	HIIR	4.7	2.4×10^3	5	<1.0
G154.3472+02.6099	04:36:21.02	+51:12:55.00	2002-12-15	−90	60	HIIR	6.1	5.3×10^4	5	113
G166.8141−03.1986	04:56:55.25	+37:57:14.60	2002-12-16	0	60	HIIR	2.0	1.2×10^3	5	4.4
G168.0627+00.8221	05:17:13.69	+39:22:19.40	2002-12-16	0	60	YSO	2.0	1.2×10^3	5	<1.0
G169.6459−00.0687	05:18:10.80	+37:33:58.20	2002-12-16	0	60	YSO/HIIR	2.0	1.0×10^3	5	<1.1
G173.4815+02.4459	05:39:13.30	+35:45:53.90	2006-09-25	80.6	180	YSO	1.6	4.8×10^3	8.6	<0.4
G173.4839+02.4317	05:39:09.92	+35:45:17.20	2005-02-11	32	60	YSO	1.6	4.8×10^3	8.6	<0.4
G173.6328+02.8064	05:41:07.04	+35:49:34.80	2005-02-14	−52.01	42	YSO	1.6	4.8×10^3	5	<0.7
G173.6339+02.8218	05:41:11.02	+35:50:01.80	2006-09-15	−69.3	14	YSO	1.6	3.2×10^3	5	<0.7
G173.7215+02.6924	05:40:52.36	+35:41:29.40	2005-01-15	−82	60	YSO/HIIR	1.6	3.1×10^3	5	<0.8
G177.7291−00.3358	05:38:47.16	+30:41:18.10	2003-10-28	−71.01	42	YSO	2.0	3.7×10^3	5	<1.0
G178.7540+01.1609	05:47:12.53	+30:36:13.30	2003-10-28	72.99	60	YSO	2.0	1.1×10^3	5	<1.0
G179.0380+04.3003	06:00:33.40	+31:56:44.50	2006-09-23	52	120	YSO	1.1	481	5	<0.6
G183.4530−01.7774	05:46:51.53	+25:03:47.60	2002-12-15	−90	60	YSO	2.0	375	5	<1.0
G184.8704−01.7329	05:50:13.90	+23:52:17.70	2002–12-15	−90	51	YSO	2.0	2.0×10^3	5	<1.0
G184.9551−00.8559	05:53:43.56	+24:14:44.70	2006-09-15	−36.3	84	PPN	–	–	5	<0.9
G188.8120+01.0686	06:09:17.91	+21:50:49.90	2005-02-14	90	120	YSO	2.0	1.0×10^3	5	<0.9
G188.9479+00.8871	06:08:53.41	+21:38:28.10	2005-01-20	−55	60	YSO	2.0	9.4×10^3	5	<1.1
G188.9696−01.9380	05:58:24.44	+20:13:57.60	2002-12-15	−90	60	YSO	2.0	1.9×10^3	5	<0.9
G189.0065+01.1263	06:09:55.17	+21:42:17.80	2005-01-21	90	60	PPN	2.0	604	5	<1.0
G189.0307+00.7821	06:08:40.52	+21:31:00.40	2005-01-18	9.99	42	YSO	2.0	2.0×10^4	5	0.7
G189.0323+00.8092	06:08:46.74	+21:31:44.20	2005-01-18	90	17	YSO	2.0	7.8×10^3	5	<1.0
G192.6005−00.0479	06:12:54.01	+17:59:23.10	2005-01-21	75	420	YSO	2.5	5.4×10^4	5	<1.0
G192.9089−00.6259	06:11:23.74	+17:26:28.60	2005-02-15	−50	240	YSO	2.0	3.8×10^3	5	<1.0
G194.9349−01.2224	06:13:16.14	+15:22:43.30	2005-01-21	19.99	60	YSO	2.0	2.5×10^3	5	<1.0
G196.1620−01.2546	06:15:34.71	+14:17:03.20	2002-12-15	−90	60	YSO	2.1	2.1×10^3	5	<1.0
G196.4542−01.6777	06:14:37.06	+13:49:36.50	2003-10-28	90	60	YSO	5.3	9.4×10^4	5	<1.1
G200.0789−01.6323	06:21:47.63	+10:39:21.40	2002-12-16	−90	60	YSO/HIIR	7.9	1.4×10^4	5	1.9
G203.3166+02.0564	06:41:10.16	+09:29:33.70	2006-09-15	−28.5	10	YSO	0.8	2.1×10^3	5	<0.9
G207.2654−01.8080 – 1	06:34:37.74	+04:12:44.20	2002-12-16	80	60	YSO	1.6	6.8×10^3	–	–
G207.2654−01.8080 – 2	06:34:37.41	+04:12:42.50	2002-12-16	80	60	YSO	1.6	6.8×10^3	–	–
G211.8957−01.2025	06:45:16.01	+00:22:25.00	2002-12-16	−63	60	YSO	6.4	9.6×10^3	5	<0.8
G212.0641−00.7395	06:47:13.36	+00:26:06.60	2006-09-19	59.7	126	YSO	6.4	2.5×10^4	5	<0.9
G212.2344−03.5038	06:37:41.60	−00:58:37.70	2004-04-29	−90	42	YSO	6.7	4.5×10^3	5	<0.9
G212.2468−01.1034 – 1	06:46:15.75	+00:06:23.50	2002-12-16	−90	60	Evolved star	–	–	5	<0.9
G212.2468−01.1034 – 2	06:46:15.27	+00:06:23.30	2002-12-16	−90	60	Evolved star	–	–	5	<0.9
G212.9626+01.2954	06:56:06.32	+00:33:47.80	2005-01-27	54.99	60	YSO	5.7	2.4×10^3	5	<0.6
G213.0763−02.2174	06:43:48.44	−01:08:19.80	2004-04-29	−90	60	PN	–	–	5	616.2
G213.9180+00.3786	06:54:35.14	−00:42:17.80	2004-04-30	13.2	60	YSO	5.3	2.1×10^3	5	<0.8
G215.8902−02.0094	06:49:40.24	−03:32:52.40	2002-12-16	−90	60	YSO	8.3	4.9×10^3	5	<0.9
G217.6047−02.6170	06:50:37.41	−05:21:00.90	2004-12-24	−31	120	YSO	9.2	7.7×10^3	5	<0.9
G224.6075−01.0063	07:09:20.55	−10:50:28.20	2005-02-22	51	60	YSO	1.6	1.6×10^3	–	–
G232.6207+00.9959	07:32:09.90	−16:58:14.10	2005-02-23	−50	60	YSO	1.7	1.1×10^4	8.6	1.3

Table A2. Table showing catalogue and measured magnitudes for all spectra. For the catalogue magnitudes, the most appropriate of 2MASS Point Source Catalogue or UKIDSS Galactic Plane Survey are shown. These are the magnitudes used for calculating extinction etc. and in Fig. 1 for comparing measured magnitudes with catalogue magnitudes (see Section 3). '–' is shown when there are no catalogue magnitudes available at that wavelength. Where '–' is marked in the error field for the catalogue magnitudes, the magnitude shown is a lower limit (i.e. an upper limit on the flux for non-detections or confused fields). Note that this only happens for 2MASS PSC magnitudes; UKIDSS GPS have a different quality flagging system, as described on the WFCAM Science Archive website. The measured magnitudes were calculated from flux measurements in the spectra (see Section 3). '–' is marked in the upper error field of the *H* band measured magnitude to indicate where the *H* band flux is so low that the flux error bar goes below zero, which makes the magnitude error incalculable. Several of the objects are invisible at *H* in the spectrum. In these cases, '–' is marked in the measured *H* band magnitude fields.

Name	Catalogue	Catalogue magnitudes			Measured magnitudes					
		J band	*H* band	*K* band	*H* band	*H* L. Error	*H* U. Error	*K* band	*K* L. Error	*K* U. Error
G010.8411−02.5919	2MASS PSC	>16.3	13.2 ± 0.1	9.67 ± 0.05	13.8	0.2	0.2	10.8	0.3	0.4
G010.8856+00.1221	UKIDSS GPS	18.67 ± 0.10	13.190 ± 0.002	9.769 ± 0.000	13.09	0.06	0.07	9.97	0.02	0.02
G011.9019+00.7265	UKIDSS GPS	16.46 ± 0.01	13.932 ± 0.003	11.365 ± 0.001	9.4	0.1	0.1	6.8	0.2	0.2
G016.7122+01.3119 – 1	2MASS PSC	13.44 ± 0.06	10.67 ± 0.04	8.70 ± 0.03	10.16	0.03	0.03	8.12	0.03	0.03
G016.7122+01.3119 – 2	2MASS PSC	>16.5	14.5 ± 0.1	11.14 ± 0.04	16	1	1	11.52	0.06	0.06
G016.7981+00.1264	UKIDSS GPS	16.171 ± 0.009	13.168 ± 0.001	9.957 ± 0.000	13.0	0.1	0.1	10.15	0.03	0.03
G017.0332+00.7476A	UKIDSS GPS	–	–	14.93 ± 0.01	19	3	–	15.8	0.3	0.4
G017.3765+02.2512	2MASS PSC	13.8 ± 0.1	11.26 ± 0.10	9.17 ± 0.05	10.04	0.04	0.05	7.88	0.03	0.04
G018.3412+01.7681	2MASS PSC	>15.3	12.91 ± 0.09	9.25 ± 0.03	13.53	0.07	0.07	9.94	0.05	0.05
G018.3706−00.3818	UKIDSS GPS	14.614 ± 0.003	11.925 ± 0.001	9.848 ± 0.000	11.70	0.06	0.06	9.53	0.03	0.03
G018.6608+00.0372	UKIDSS GPS	–	–	12.756 ± 0.003	15.6	0.4	0.6	12.48	0.07	0.07
G019.7540−00.1279	UKIDSS GPS	17.00 ± 0.02	14.457 ± 0.005	12.101 ± 0.002	14.6	0.5	0.8	12.54	0.05	0.05
G019.8922+00.1023	UKIDSS GPS	13.895 ± 0.002	12.433 ± 0.001	10.417 ± 0.001	12.62	0.04	0.04	10.86	0.03	0.03
G019.9224−00.2577	UKIDSS GPS	18.07 ± 0.06	15.41 ± 0.01	12.896 ± 0.003	14.6	0.3	0.4	12.56	0.06	0.07
G020.5143+00.4936	UKIDSS GPS	13.607 ± 0.001	12.152 ± 0.001	11.377 ± 0.001	13	1	–	10.6	0.4	0.6
G021.3853−00.2537	UKIDSS GPS	–	–	13.298 ± 0.004	16	1	1	13.8	0.1	0.2
G021.5624−00.0329	UKIDSS GPS	–	–	10.641 ± 0.001	9.2	0.1	0.1	5.1	0.2	0.2
G023.3891+00.1851	2MASS PSC	15.77 ± 0.09	11.61 ± 0.03	8.38 ± 0.03	9.03	0.04	0.04	6.07	0.03	0.04
G023.4394−00.2394	UKIDSS GPS	–	14.950 ± 0.005	11.695 ± 0.001	14.8	0.4	0.5	11.80	0.03	0.03
G023.4984−00.0373	2MASS PSC	11.40 ± 0.02	9.56 ± 0.03	8.53 ± 0.02	7.17	0.02	0.02	6.278	0.009	0.009
G023.6566−00.1273	UKIDSS GPS	–	14.070 ± 0.003	9.648 ± 0.000	12.3	0.3	0.4	7.99	0.04	0.04
G024.6343−00.3233	2MASS PSC	>15.8	13.31 ± 0.05	10.04 ± 0.03	12.9	0.2	0.2	9.9	0.1	0.1
G025.4018+00.0198A	2MASS PSC	9.35 ± 0.03	6.88 ± 0.03	5.66 ± 0.02	7.3	0.1	0.1	6.15	0.07	0.08
G025.6498+01.0491*	UKIDSS GPS	–	–	12.321 ± 0.002	17	1	–	12.4	0.1	0.1
G025.7161+00.0486	UKIDSS GPS	16.97 ± 0.02	–	–	14.3	0.1	0.2	12.42	0.04	0.05
G025.8015−00.1570 – 1	UKIDSS GPS	16.49 ± 0.01	13.647 ± 0.002	11.067 ± 0.001	14.3	0.1	0.1	12.06	0.04	0.05
G025.8015−00.1570 – 2	–	–	–	–	14.7	0.1	0.1	12.00	0.03	0.04
G026.2020+00.2262	2MASS PSC	14.21 ± 0.04	10.61 ± 0.03	8.25 ± 0.02	11.02	0.06	0.06	8.20	0.03	0.02
G026.3050+00.1162	2MASS PSC	10.69 ± 0.03	9.39 ± 0.03	8.17 ± 0.03	9.52	0.02	0.02	8.28	0.01	0.01
G026.3176−00.0134	2MASS PSC	13.19 ± 0.03	10.09 ± 0.03	8.39 ± 0.02	10.67	0.05	0.06	8.95	0.03	0.03
G026.3819+01.4057 – 1	UKIDSS GPS	16.176 ± 0.008	13.802 ± 0.002	11.819 ± 0.001	14.4	0.1	0.1	12.52	0.04	0.04
G026.3819+01.4057 – 2	UKIDSS GPS	14.161 ± 0.002	12.200 ± 0.001	9.745 ± 0.000	12.19	0.03	0.03	10.16	0.03	0.03
G026.4207+01.6858	UKIDSS GPS	16.165 ± 0.008	13.248 ± 0.001	10.207 ± 0.000	14.71	0.04	0.05	12.50	0.03	0.03
G026.4488+01.7425A	UKIDSS GPS	10.899 ± 0.000	11.107 ± 0.000	10.139 ± 0.000	10.34	0.03	0.03	10.10	0.01	0.02
G026.4488+01.7425B	UKIDSS GPS	14.910 ± 0.003	13.709 ± 0.002	12.234 ± 0.002	14.27	0.06	0.07	12.99	0.05	0.05
G026.4897−00.5455	UKIDSS GPS	–	–	10.402 ± 0.001	16	2	–	10.55	0.07	0.08
G026.4958+00.7105 – 1	UKIDSS GPS	–	–	15.01 ± 0.02	–	–	–	15.4	0.3	0.4
G026.4958+00.7105 – 2	UKIDSS GPS	–	–	15.89 ± 0.04	21	4	–	17	1	1
G026.5972−00.0241	UKIDSS GPS	18.42 ± 0.08	–	15.83 ± 0.04	20	2	–	17	1	1
G027.2220+00.1361 – 1	UKIDSS GPS	14.749 ± 0.004	14.180 ± 0.005	14.54 ± 0.02	14.15	0.08	0.08	13.76	0.05	0.06
G027.2220+00.1361 – 2	–	–	–	–	19	1	–	16	1	1
G027.7954−00.2772	UKIDSS GPS	–	16.44 ± 0.03	10.890 ± 0.001	15.8	0.9	–	10.91	0.06	0.07
G028.2325+00.0394	UKIDSS GPS	–	–	12.306 ± 0.002	17	1	1	12.53	0.06	0.06
G028.3046−00.3871A	UKIDSS GPS	16.599 ± 0.009	14.054 ± 0.003	11.898 ± 0.001	12.34	0.09	0.09	10.21	0.05	0.05
G028.3373+00.1189	UKIDSS GPS	–	15.664 ± 0.009	12.748 ± 0.002	13.0	0.9	–	10.1	0.1	0.1

Table A2 – *continued*

Name	Catalogue	Catalogue magnitudes			Measured magnitudes					
		J band	*H* band	*K* band	*H* band	*H* L. Error	*H* U. Error	*K* band	*K* L. Error	*K* U. Error
G028.7799+03.4978	2MASS PSC	8.74 ± 0.02	7.19 ± 0.04	6.00 ± 0.02	8.19	0.01	0.01	7.00	0.01	0.01
G028.8621+00.0657	UKIDSS GPS	–	–	13.411 ± 0.004	17.5	0.9	–	14.3	0.1	0.2
G030.1468+01.4075	UKIDSS GPS	–	17.75 ± 0.08	12.433 ± 0.002	16.7	1.0	–	11.86	0.05	0.06
G030.1981−00.1691	2MASS PSC	>17.0	12.57 ± 0.03	9.30 ± 0.03	12.5	0.1	0.1	8.99	0.03	0.03
G030.2340−00.1392	UKIDSS GPS	18.21 ± 0.04	16.23 ± 0.01	13.288 ± 0.003	17	1	–	13.6	0.2	0.3
G030.2971+00.0549	UKIDSS GPS	–	–	15.87 ± 0.04	–	–	–	16.8	0.5	0.9
G030.4117−00.2277	UKIDSS GPS	15.804 ± 0.007	13.611 ± 0.002	10.877 ± 0.001	13.5	0.1	0.1	10.99	0.03	0.03
G030.5942−00.1273	2MASS PSC	13.24 ± 0.04	10.62 ± 0.03	8.82 ± 0.03	10.25	0.03	0.03	8.48	0.02	0.02
G030.8185+00.2729	UKIDSS GPS	–	14.335 ± 0.004	10.528 ± 0.001	14.8	0.1	0.2	11.22	0.05	0.05
G030.9726−00.1410	2MASS PSC	>17.9	14.9 ± 0.1	12.29 ± 0.05	16	1	1	13.74	0.06	0.06
G030.9727+00.5620	UKIDSS GPS	20.0 ± 0.3	17.90 ± 0.07	13.004 ± 0.002	16	2	–	10.6	0.1	0.1
G030.9959−00.0771	2MASS PSC	>17.4	>15.3	13.54 ± 0.08	16.0	0.4	0.6	13.7	0.1	0.1
G031.1677+00.1259	UKIDSS GPS	13.018 ± 0.001	11.596 ± 0.001	10.697 ± 0.001	12.5	0.1	0.2	9.48	0.06	0.07
G031.6617+00.3667	2MASS PSC	>17.3	>15.0	13.21 ± 0.05	16.5	0.5	0.8	14.2	0.1	0.2
G032.0451+00.0589	–	–	–	–	–	–	–	15.0	0.2	0.2
G032.0518−00.0902	UKIDSS GPS	16.48 ± 0.02	14.711 ± 0.007	12.352 ± 0.002	15.0	0.1	0.1	13.28	0.05	0.05
G032.1514+00.1317	UKIDSS GPS	13.585 ± 0.002	12.065 ± 0.001	11.009 ± 0.001	12.00	0.02	0.02	11.08	0.02	0.02
G032.4727+00.2041	UKIDSS GPS	17.23 ± 0.02	13.577 ± 0.002	10.729 ± 0.001	13.3	0.2	0.2	10.63	0.03	0.03
G032.8205−00.3300	2MASS PSC	>16.9	>14.0	11.77 ± 0.05	14.7	0.4	0.7	12.40	0.03	0.03
G032.9957+00.0415	UKIDSS GPS	–	16.02 ± 0.02	10.702 ± 0.001	15	1	1	10.42	0.06	0.06
G033.3891+00.1989	2MASS PSC	12.96 ± 0.04	9.58 ± 0.03	7.22 ± 0.02	9.10	0.04	0.04	6.94	0.02	0.02
G034.0126−00.2832	2MASS PSC	11.51 ± 0.03	9.56 ± 0.03	7.70 ± 0.02	9.42	0.02	0.02	7.62	0.02	0.02
G034.0500−00.2977	UKIDSS GPS	–	11.650 ± 0.000	–	10.80	0.03	0.04	9.44	0.02	0.02
G034.4035+00.2282	–	–	–	–	17.2	0.2	0.3	13.76	0.07	0.08
G034.6243−00.1300	UKIDSS GPS	–	16.87 ± 0.03	13.023 ± 0.003	15	1	–	11.0	0.1	0.2
G034.7569+00.0247	UKIDSS GPS	–	–	15.68 ± 0.03	–	–	–	16.4	0.3	0.5
G034.8211+00.3519	2MASS PSC	13.43 ± 0.04	9.30 ± 0.03	6.61 ± 0.03	18	3	–	11.3	0.1	0.1
G035.1979−00.7427	2MASS PSC	>17.2	13.57 ± 0.05	10.46 ± 0.04	13.7	0.1	0.1	10.78	0.08	0.08
G036.8780−00.4728 – 1	UKIDSS GPS	–	18.01 ± 0.09	13.133 ± 0.003	19	2	–	14.22	0.07	0.08
G036.8780−00.4728 – 2	UKIDSS GPS	–	18.01 ± 0.09	13.133 ± 0.003	18.0	0.9	–	14.2	0.1	0.1
G036.9194+00.4825A	2MASS PSC	>18.2	>16.5	14.5 ± 0.1	17	1	1	14.36	0.05	0.06
G037.5536+00.2008	2MASS PSC	>18.4	>17.4	13.04 ± 0.05	19	2	–	13.46	0.08	0.09
G039.4943−00.9933	UKIDSS GPS	–	14.035 ± 0.003	10.255 ± 0.000	13.7	0.1	0.1	10.38	0.04	0.05
G039.8821−00.3457	UKIDSS GPS	–	18.6 ± 0.1	14.121 ± 0.007	–	–	–	14.91	0.09	0.09
G040.0809+01.5117	UKIDSS GPS	15.897 ± 0.007	13.615 ± 0.002	12.044 ± 0.001	13.64	0.08	0.08	12.3	0.1	0.2
G040.4247+00.6989A	UKIDSS GPS	15.532 ± 0.007	14.134 ± 0.003	13.428 ± 0.004	14.07	0.05	0.05	13.43	0.04	0.04
G040.5451+02.5961A	–	–	–	–	14.7	0.2	0.2	12.18	0.05	0.05
G042.0341+00.1905A	UKIDSS GPS	17.81 ± 0.04	14.355 ± 0.004	10.785 ± 0.001	12.5	0.2	0.3	9.26	0.05	0.05
G042.0977+00.3521	UKIDSS GPS	19.13 ± 0.10	16.57 ± 0.02	13.510 ± 0.003	17	1	–	14.3	0.1	0.2
G042.1099−00.4466	UKIDSS GPS	19.6 ± 0.2	15.248 ± 0.007	12.332 ± 0.002	15.7	0.5	0.8	13.02	0.05	0.05
G043.1635−00.0697A	UKIDSS GPS	15.451 ± 0.004	13.674 ± 0.002	12.488 ± 0.002	13.66	0.05	0.05	12.60	0.03	0.03
G043.5216−00.6476	UKIDSS GPS	16.312 ± 0.009	13.547 ± 0.002	11.452 ± 0.001	13.14	0.09	0.09	11.20	0.05	0.05
G043.9956−00.0111	UKIDSS GPS	16.295 ± 0.009	13.170 ± 0.001	10.534 ± 0.001	12.9	0.1	0.1	10.55	0.04	0.04
G044.3103+00.0416	UKIDSS GPS	18.48 ± 0.06	15.447 ± 0.007	13.467 ± 0.003	15.4	0.2	0.2	13.67	0.05	0.05
G045.1894−00.4387	UKIDSS GPS	18.14 ± 0.04	14.550 ± 0.003	10.876 ± 0.001	11.5	0.2	0.3	8.29	0.04	0.04
G045.4543+00.0600 – 1	UKIDSS GPS	–	–	12.265 ± 0.002	14.9	0.2	0.3	12.8	0.1	0.1
G045.4543+00.0600 – 2	–	–	–	–	16	1	1	12.8	0.1	0.1
G045.4641+00.0284	UKIDSS GPS	–	–	14.226 ± 0.009	18.2	0.2	0.2	14.71	0.02	0.02
G048.6085+00.0258D	2MASS PSC	12.13 ± 0.03	9.32 ± 0.03	8.00 ± 0.03	7.0	0.1	0.1	5.66	0.07	0.08
G048.9897−00.2992A	UKIDSS GPS	16.412 ± 0.008	15.133 ± 0.005	12.436 ± 0.002	14.7	0.2	0.2	13.09	0.05	0.05
G048.9897−00.2992B	–	–	–	–	15.4	0.3	0.4	15.1	0.4	0.6

Table A2 – *continued*

Name	Catalogue	Catalogue magnitudes			Measured magnitudes					
		J band	*H* band	*K* band	*H* band	*H* L. Error	*H* U. Error	*K* band	*K* L. Error	*K* U. Error
G049.0431−01.0787	–	–	–	–	15.8	0.2	0.3	12.75	0.06	0.07
G049.4227−00.3715	2MASS PSC	13.44 ± 0.10	10.04 ± 0.04	>7.7	11.6	0.3	0.5	9.45	0.08	0.08
G049.4883−00.3545A	UKIDSS GPS	17.01 ± 0.02	14.709 ± 0.004	12.731 ± 0.002	12.1	0.3	0.4	10.30	0.06	0.06
G049.4883−00.3545B	UKIDSS GPS	–	16.91 ± 0.02	14.053 ± 0.005	15	1	–	12.0	0.2	0.2
G049.4970−00.4718	UKIDSS GPS	14.620 ± 0.002	13.367 ± 0.001	12.481 ± 0.002	12.24	0.04	0.05	11.52	0.04	0.04
G049.5373−00.3929	2MASS PSC	9.54 ± 0.03	8.13 ± 0.04	7.58 ± 0.03	9.45	0.07	0.08	9.01	0.05	0.05
G050.0721+00.5591	UKIDSS GPS	17.19 ± 0.02	14.873 ± 0.005	12.702 ± 0.002	14.9	0.2	0.3	12.80	0.05	0.05
G050.2213−00.6063	2MASS PSC	>13.7	>11.4	9.84 ± 0.07	14.18	0.05	0.05	10.92	0.05	0.05
G050.2844−00.3925A	UKIDSS GPS	18.39 ± 0.05	14.502 ± 0.003	11.411 ± 0.001	12.6	0.1	0.1	9.74	0.04	0.04
G050.4802+00.7058	–	–	–	–	13.22	0.09	0.10	11.35	0.04	0.04
G052.2025+00.7217A	UKIDSS GPS	16.46 ± 0.01	13.377 ± 0.001	10.106 ± 0.000	12.90	0.06	0.06	9.85	0.06	0.06
G052.2078+00.6890	2MASS PSC	>15.3	>13.7	12.21 ± 0.04	13.2	0.3	0.5	10.87	0.04	0.04
G052.5405−00.9272	2MASS PSC	>16.6	>14.5	11.85 ± 0.05	14	1	1	11.4	0.1	0.1
G052.9217+00.4142	UKIDSS GPS	19.06 ± 0.09	15.715 ± 0.009	12.225 ± 0.001	14.4	0.3	0.4	11.38	0.05	0.06
G052.9221−00.4892	2MASS PSC	>15.9	14.1 ± 0.2	>11.2	13.6	0.4	0.6	11.26	0.03	0.03
G053.1417+00.0705	UKIDSS GPS	–	–	12.720 ± 0.002	18	1	–	13.08	0.09	0.10
G053.5343−00.7943	2MASS PSC	13.80 ± 0.03	10.70 ± 0.02	8.31 ± 0.02	12.13	0.04	0.04	9.64	0.02	0.02
G055.1581−00.2991A	UKIDSS GPS	18.59 ± 0.05	15.063 ± 0.005	12.174 ± 0.001	13.8	0.2	0.2	11.23	0.08	0.09
G055.3704+00.1858	2MASS PSC	11.33 ± 0.03	7.72 ± 0.02	>6.6	6.7	0.1	0.1	4.60	0.03	0.03
G056.3694−00.6333	UKIDSS GPS	–	15.322 ± 0.007	12.496 ± 0.002	15.3	0.5	0.8	12.6	0.1	0.1
G056.4120−00.0277	2MASS PSC	12.45 ± 0.02	9.93 ± 0.02	8.05 ± 0.02	8.64	0.04	0.04	6.81	0.04	0.04
G057.5474−00.2717A	UKIDSS GPS	16.52 ± 0.01	13.526 ± 0.002	11.131 ± 0.001	14.3	0.1	0.1	12.23	0.04	0.04
G059.3614−00.2068	UKIDSS GPS	14.074 ± 0.002	11.847 ± 0.001	9.879 ± 0.000	11.28	0.04	0.04	9.44	0.02	0.02
G059.6403−00.1812A	UKIDSS GPS	15.323 ± 0.004	13.488 ± 0.001	11.422 ± 0.001	14.0	0.1	0.1	12.12	0.03	0.03
G059.7831+00.0648	UKIDSS GPS	–	16.32 ± 0.01	11.662 ± 0.001	16	2	–	12.02	0.05	0.05
G059.8329+00.6729	UKIDSS GPS	19.1 ± 0.1	16.29 ± 0.02	14.138 ± 0.007	16	1	1	14.2	0.3	0.3
G060.5750−00.1861	2MASS PSC	15.51 ± 0.10	13.9 ± 0.1	11.59 ± 0.06	14.0	0.2	0.3	11.81	0.09	0.09
G063.1140+00.3416	2MASS PSC	>16.9	13.17 ± 0.05	9.67 ± 0.02	10.84	0.05	0.06	7.13	0.06	0.06
G065.7798−02.6121	2MASS PSC	>14.8	12.52 ± 0.06	10.49 ± 0.04	9.91	0.01	0.01	9.63	0.04	0.04
G068.2040+00.2387	UKIDSS GPS	17.60 ± 0.02	14.113 ± 0.002	11.448 ± 0.001	13.6	0.1	0.1	11.20	0.02	0.03
G069.5395−00.9754	–	–	–	–	18	1	–	16	1	4
G070.3329+01.5864 – 1	2MASS PSC	>15.0	13.28 ± 0.06	11.41 ± 0.05	15.3	0.3	0.4	14.1	0.2	0.2
G070.3329+01.5864 – 2	2MASS PSC	>15.0	13.28 ± 0.06	11.41 ± 0.05	13.0	0.2	0.2	11.41	0.07	0.08
G070.6740+01.1919	2MASS PSC	10.33 ± 0.03	8.24 ± 0.02	6.56 ± 0.03	8.54	0.03	0.03	6.91	0.03	0.03
G071.8944+01.3107	2MASS PSC	>18.2	14.80 ± 0.08	11.74 ± 0.04	14.4	0.2	0.3	11.51	0.08	0.08
G072.2479+00.2617B	UKIDSS GPS	17.86 ± 0.03	15.429 ± 0.009	13.343 ± 0.003	15.2	0.2	0.3	13.25	0.03	0.03
G073.0633+01.7958	2MASS PSC	>15.4	>13.3	12.12 ± 0.04	13.6	0.2	0.2	11.57	0.06	0.06
G073.6525+00.1944	2MASS PSC	13.94 ± 0.03	11.47 ± 0.04	9.57 ± 0.02	11.31	0.03	0.03	9.40	0.04	0.04
G073.6952−00.9996	2MASS PSC	12.89 ± 0.04	10.63 ± 0.04	8.05 ± 0.02	11.16	0.02	0.02	8.41	0.03	0.03
G075.6014+01.6394	2MASS PSC	16.1 ± 0.1	14.01 ± 0.05	12.77 ± 0.04	14.54	0.09	0.09	13.48	0.03	0.03
G075.7666+00.3424 – 1	UKIDSS GPS	14.960 ± 0.003	12.412 ± 0.001	10.501 ± 0.001	10.6	0.1	0.1	8.52	0.03	0.03
G075.7666+00.3424 – 2	UKIDSS GPS	–	14.855 ± 0.005	11.448 ± 0.001	14.2	0.3	0.3	11.06	0.05	0.05
G076.0902+00.1412	UKIDSS GPS	–	16.40 ± 0.02	12.310 ± 0.001	16.2	0.4	0.6	12.45	0.07	0.08
G076.1877+00.0974	UKIDSS GPS	–	15.67 ± 0.01	12.832 ± 0.002	15	2	–	11.5	0.1	0.1
G076.3829−00.6210	2MASS PSC	10.36 ± 0.03	7.73 ± 0.02	5.87 ± 0.02	8.25	0.02	0.02	6.47	0.02	0.02
G077.3455+04.4309	UKIDSS GPS	12.438 ± 0.001	11.180 ± 0.000	10.145 ± 0.000	9.4	0.1	0.1	8.23	0.06	0.07
G077.4052−01.2136	2MASS PSC	>17.1	15.5 ± 0.1	12.55 ± 0.04	15.8	0.2	0.3	12.82	0.09	0.10
G077.4622+01.7600 – 1	UKIDSS GPS	–	–	10.914 ± 0.001	13.09	0.08	0.09	11.46	0.03	0.03
G077.4622+01.7600 – 2	2MASS PSC	>12.9	11.02 ± 0.09	>9.1	14.24	0.07	0.08	12.88	0.06	0.06
G077.8999+01.7678	UKIDSS GPS	16.258 ± 0.008	13.213 ± 0.001	10.345 ± 0.000	13.07	0.03	0.03	10.10	0.04	0.04
G077.9550+00.0058	UKIDSS GPS	14.731 ± 0.003	13.007 ± 0.001	11.882 ± 0.001	13.15	0.06	0.06	12.09	0.03	0.04

Table A2 – *continued*

Name	Catalogue	Catalogue magnitudes			Measured magnitudes					
		J band	*H* band	*K* band	*H* band	*H* L. Error	*H* U. Error	*K* band	*K* L. Error	*K* U. Error
G078.1224+03.6320	UKIDSS GPS	14.614 ± 0.002	13.130 ± 0.001	12.047 ± 0.001	15.8	0.2	0.3	13.0	0.2	0.2
G078.4373+02.6584B	UKIDSS GPS	–	14.936 ± 0.004	11.281 ± 0.001	14.7	0.2	0.2	11.33	0.05	0.05
G078.4705−00.1830	UKIDSS GPS	19.8 ± 0.1	16.27 ± 0.01	13.426 ± 0.003	17	1	1	14.04	0.05	0.05
G078.4754+01.0421	2MASS PSC	>17.2	12.95 ± 0.04	8.72 ± 0.02	13.7	0.1	0.1	9.10	0.06	0.06
G078.7641+01.6862	UKIDSS GPS	–	16.93 ± 0.03	14.118 ± 0.005	16.9	0.4	0.7	14.4	0.1	0.1
G078.8867+00.7087	2MASS PSC	>14.3	10.77 ± 0.04	6.58 ± 0.02	10.8	0.1	0.1	6.67	0.04	0.05
G078.9761+00.3567	2MASS PSC	11.40 ± 0.03	9.44 ± 0.02	8.05 ± 0.02	8.29	0.04	0.04	6.87	0.01	0.01
G079.1272+02.2782	UKIDSS GPS	15.708 ± 0.005	12.718 ± 0.001	10.036 ± 0.000	12.42	0.04	0.04	10.02	0.04	0.04
G079.3202+01.3131	UKIDSS GPS	–	16.31 ± 0.01	13.260 ± 0.002	14.4	0.8	–	11.7	0.2	0.2
G079.3248+01.2901	UKIDSS GPS	19.4 ± 0.1	16.59 ± 0.02	14.589 ± 0.006	16	1	2	14.0	0.2	0.2
G080.0467+00.3101	2MASS PSC	14.44 ± 0.04	11.42 ± 0.02	9.28 ± 0.02	11.76	0.03	0.03	9.55	0.04	0.04
G080.1909+00.5353	2MASS PSC	13.88 ± 0.04	10.82 ± 0.02	8.43 ± 0.02	11.22	0.03	0.03	8.74	0.03	0.03
G080.8282+00.5670A	2MASS PSC	>15.3	12.02 ± 0.05	>8.9	11.45	0.04	0.04	8.45	0.04	0.04
G080.8645+00.4197	2MASS PSC	>18.5	>16.3	12.70 ± 0.06	–	–	–	13.5	0.1	0.1
G081.5168+00.1926	2MASS PSC	>18.3	>14.9	12.28 ± 0.05	15.0	0.2	0.3	11.29	0.06	0.06
G081.7131+00.5792	2MASS PSC	13.18 ± 0.03	10.35 ± 0.03	8.21 ± 0.03	10.98	0.03	0.03	9.00	0.02	0.02
G081.7624+00.5916	UKIDSS GPS	–	18.10 ± 0.08	11.809 ± 0.001	18	1	–	12.25	0.07	0.07
G082.5682+00.4040A	2MASS PSC	10.85 ± 0.03	8.73 ± 0.03	7.14 ± 0.02	9.07	0.02	0.02	7.50	0.01	0.01
G083.7071+03.2817	2MASS PSC	12.25 ± 0.04	9.96 ± 0.04	8.05 ± 0.03	9.66	0.03	0.03	7.27	0.02	0.02
G084.3065+01.8933	2MASS PSC	15.09 ± 0.07	12.23 ± 0.03	10.05 ± 0.02	11.32	0.08	0.08	9.09	0.03	0.03
G084.6490+02.1267	2MASS PSC	16.01 ± 0.10	14.19 ± 0.07	12.95 ± 0.04	14.8	0.3	0.4	13.6	0.1	0.2
G085.4102+00.0032A	2MASS PSC	>17.9	15.5 ± 0.2	11.80 ± 0.05	16	1	1	11.53	0.08	0.09
G089.6368+00.1732	UKIDSS GPS	17.98 ± 0.03	14.041 ± 0.002	10.312 ± 0.000	13.9	0.1	0.1	10.51	0.04	0.04
G090.2095+02.0405	2MASS PSC	14.16 ± 0.05	12.19 ± 0.03	10.12 ± 0.02	14	2	–	10.9	0.5	0.8
G094.3228−00.1671	UKIDSS GPS	16.329 ± 0.009	13.705 ± 0.002	10.475 ± 0.001	13.1	0.2	0.3	10.61	0.05	0.05
G094.4637−00.8043	UKIDSS GPS	17.29 ± 0.02	–	11.451 ± 0.001	14.68	0.08	0.09	12.23	0.04	0.04
G095.0026−01.5779	2MASS PSC	>15.2	>13.7	12.9 ± 0.1	15.5	0.3	0.4	12.8	0.1	0.1
G095.0531+03.9724	2MASS PSC	>15.5	>14.4	13.68 ± 0.08	16.2	0.3	0.4	14.3	0.1	0.2
G096.3597+01.2982	UKIDSS GPS	17.45 ± 0.02	15.186 ± 0.005	13.415 ± 0.003	12.6	0.4	0.6	10.97	0.09	0.10
G096.4353+01.3233A – 1	–	–	–	–	12.43	0.06	0.06	10.85	0.02	0.02
G096.4353+01.3233A – 2	–	–	–	–	14.1	0.2	0.2	11.95	0.06	0.06
G097.5268+03.1837C	2MASS PSC	14.95 ± 0.06	12.43 ± 0.04	10.46 ± 0.02	12.69	0.03	0.03	10.59	0.02	0.02
G097.9978+01.4688	2MASS PSC	13.90 ± 0.05	11.67 ± 0.04	9.73 ± 0.03	11.78	0.04	0.04	9.81	0.02	0.02
G098.8555+02.9344	2MASS PSC	16.3 ± 0.1	14.79 ± 0.09	12.80 ± 0.05	14	1	1	12.6	0.1	0.1
G100.1620+01.6647	2MASS PSC	16.1 ± 0.2	14.0 ± 0.1	12.05 ± 0.07	16	2	–	13.7	0.2	0.3
G100.1685+02.0266	2MASS PSC	14.61 ± 0.07	13.05 ± 0.09	>11.1	13.4	0.3	0.4	11.7	0.1	0.1
G100.2124+01.8829	2MASS PSC	>13.6	12.89 ± 0.08	11.11 ± 0.06	13.0	0.2	0.2	10.75	0.04	0.04
G100.3779−03.5784	2MASS PSC	15.9 ± 0.1	12.91 ± 0.07	>10.5	13.11	0.04	0.04	10.79	0.03	0.02
G102.3533+03.6360	2MASS PSC	12.33 ± 0.02	9.63 ± 0.02	7.22 ± 0.02	10.80	0.06	0.06	8.29	0.03	0.03
G103.8034+00.4062	UKIDSS GPS	18.58 ± 0.06	15.673 ± 0.009	12.602 ± 0.002	16.2	0.4	0.7	13.48	0.08	0.08
G103.8744+01.8558	2MASS PSC	>17.4	>13.8	11.87 ± 0.09	16	1	–	11.76	0.07	0.07
G105.5072+00.2294	UKIDSS GPS	–	14.060 ± 0.002	11.687 ± 0.001	14.4	0.1	0.1	12.18	0.03	0.03
G107.6823−02.2423A	2MASS PSC	>13.0	11.77 ± 0.06	10.54 ± 0.04	12.15	0.04	0.04	10.91	0.02	0.03
G108.2118−01.2887	2MASS PSC	12.82 ± 0.05	11.40 ± 0.05	10.29 ± 0.04	11.90	0.03	0.03	11.06	0.02	0.02
G108.7575−00.9863	–	–	–	–	15.8	0.4	0.6	10.69	0.08	0.09
G110.8038−02.5649	2MASS PSC	14.60 ± 0.05	11.92 ± 0.04	9.84 ± 0.02	11.91	0.03	0.03	9.83	0.02	0.02
G111.2348−01.2385	2MASS PSC	>14.1	>11.3	9.56 ± 0.03	11.57	0.03	0.03	9.92	0.02	0.02
G133.8512−01.9272	2MASS PSC	10.72 ± 0.03	9.48 ± 0.03	8.31 ± 0.02	10.03	0.04	0.04	9.06	0.01	0.01
G139.9091+00.1969A	2MASS PSC	12.76 ± 0.04	10.88 ± 0.04	9.52 ± 0.04	11.56	0.03	0.04	10.20	0.01	0.01
G141.9996+01.8202	2MASS PSC	10.95 ± 0.02	8.08 ± 0.04	5.72 ± 0.02	7.79	0.03	0.03	5.47	0.02	0.02
G142.2446+01.4299	UKIDSS GPS	–	–	12.384 ± 0.001	17	1	1	13.07	0.05	0.05

Table A2 – *continued*

Name	Catalogue	Catalogue magnitudes			Measured magnitudes					
		J band	*H* band	*K* band	*H* band	*H* L. Error	*H* U. Error	*K* band	*K* L. Error	*K* U. Error
G144.6678−00.7136	2MASS PSC	13.16 ± 0.03	11.57 ± 0.03	10.25 ± 0.03	11.83	0.02	0.02	10.44	0.02	0.02
G145.1975+02.9870 – 1	2MASS PSC	15.6 ± 0.1	14.0 ± 0.1	12.96 ± 0.06	14.7	0.2	0.3	13.8	0.1	0.2
G145.1975+02.9870 – 2	2MASS PSC	15.28 ± 0.07	13.37 ± 0.05	11.96 ± 0.03	13.06	0.07	0.08	11.79	0.04	0.04
G148.1201+00.2928	2MASS PSC	16.5 ± 0.2	13.5 ± 0.1	10.46 ± 0.05	14.06	0.07	0.07	10.94	0.04	0.04
G150.6862−00.6887	2MASS PSC	11.70 ± 0.03	10.32 ± 0.03	9.08 ± 0.02	10.12	0.02	0.02	8.94	0.03	0.03
G151.6120−00.4575	2MASS PSC	10.92 ± 0.02	8.90 ± 0.03	7.12 ± 0.02	9.19	0.01	0.01	7.37	0.02	0.02
G152.3371−00.2899	2MASS PSC	>12.8	>12.4	13.15 ± 0.06	12.41	0.05	0.05	12.13	0.03	0.03
G154.3472+02.6099	2MASS PSC	13.40 ± 0.06	12.06 ± 0.06	11.07 ± 0.06	12.53	0.02	0.02	11.73	0.03	0.03
G166.8141−03.1986	UKIDSS GPS	15.564 ± 0.005	14.162 ± 0.003	13.179 ± 0.003	14.34	0.04	0.04	13.39	0.07	0.07
G168.0627+00.8221	UKIDSS GPS	13.551 ± 0.001	12.106 ± 0.001	10.149 ± 0.000	12.76	0.06	0.07	10.81	0.04	0.04
G169.6459−00.0687	UKIDSS GPS	13.486 ± 0.001	12.667 ± 0.001	11.798 ± 0.001	13.08	0.04	0.04	12.21	0.03	0.03
G173.4815+02.4459	UKIDSS GPS	18.91 ± 0.05	15.040 ± 0.003	12.177 ± 0.001	15.6	0.4	0.5	12.96	0.07	0.07
G173.4839+02.4317	2MASS PSC	12.37 ± 0.03	10.63 ± 0.02	9.25 ± 0.02	9.83	0.02	0.02	8.32	0.01	0.02
G173.6328+02.8064	2MASS PSC	12.43 ± 0.04	>10.1	>8.0	10.25	0.03	0.03	8.03	0.02	0.02
G173.6339+02.8218	2MASS PSC	12.21 ± 0.03	8.90 ± 0.02	6.59 ± 0.02	9.51	0.03	0.03	7.12	0.02	0.02
G173.7215+02.6924	2MASS PSC	10.68 ± 0.03	9.46 ± 0.02	8.50 ± 0.02	9.69	0.03	0.03	8.72	0.02	0.02
G177.7291−00.3358	2MASS PSC	11.28 ± 0.03	>9.2	>7.7	7.64	0.04	0.04	6.07	0.02	0.03
G178.7540+01.1609	2MASS PSC	11.91 ± 0.03	10.58 ± 0.03	9.44 ± 0.03	9.89	0.04	0.04	8.64	0.02	0.03
G179.0380+04.3003	2MASS PSC	14.74 ± 0.05	11.84 ± 0.04	9.70 ± 0.03	13.10	0.04	0.04	10.80	0.02	0.02
G183.4530−01.7774	2MASS PSC	>14.1	12.27 ± 0.03	>10.1	13.8	0.1	0.1	11.2	0.1	0.1
G184.8704−01.7329	2MASS PSC	10.18 ± 0.04	8.95 ± 0.04	7.73 ± 0.02	9.18	0.03	0.03	8.09	0.01	0.01
G184.9551−00.8559	2MASS PSC	12.55 ± 0.03	10.24 ± 0.04	8.33 ± 0.02	10.37	0.05	0.05	8.36	0.01	0.01
G188.8120+01.0686	2MASS PSC	>15.6	>13.5	12.33 ± 0.04	13.74	0.07	0.08	12.25	0.06	0.07
G188.9479+00.8871	2MASS PSC	15.26 ± 0.09	12.17 ± 0.04	9.75 ± 0.03	9.47	0.04	0.04	7.00	0.08	0.09
G188.9696−01.9380	2MASS PSC	15.56 ± 0.08	13.21 ± 0.06	11.08 ± 0.05	13.86	0.06	0.07	11.65	0.04	0.04
G189.0065+01.1263	2MASS PSC	13.12 ± 0.03	10.58 ± 0.02	8.67 ± 0.02	8.49	0.04	0.05	6.48	0.06	0.06
G189.0307+00.7821	2MASS PSC	16.2 ± 0.1	12.19 ± 0.05	>8.6	12.8	0.3	0.4	7.88	0.06	0.07
G189.0323+00.8092	2MASS PSC	14.83 ± 0.05	10.71 ± 0.03	7.56 ± 0.02	9.52	0.03	0.03	6.41	0.04	0.04
G192.6005−00.0479	–	–	–	–	15.0	0.4	0.7	10.94	0.06	0.06
G192.9089−00.6259	2MASS PSC	>15.9	>13.9	13.31 ± 0.08	13.8	0.5	0.9	11.96	0.08	0.08
G194.9349−01.2224	2MASS PSC	15.61 ± 0.06	12.32 ± 0.03	9.79 ± 0.03	12.25	0.03	0.03	9.64	0.03	0.03
G196.1620−01.2546	2MASS PSC	>16.7	>14.1	11.99 ± 0.06	17	2	–	12.72	0.08	0.09
G196.4542−01.6777	2MASS PSC	>14.6	13.62 ± 0.07	10.30 ± 0.03	14.3	0.1	0.1	11.29	0.06	0.07
G200.0789−01.6323	2MASS PSC	>14.4	>13.2	13.10 ± 0.09	15.3	0.4	0.6	14.2	0.2	0.3
G203.3166+02.0564	2MASS PSC	11.51 ± 0.04	7.64 ± 0.04	4.92 ± 0.02	7.77	0.03	0.03	5.11	0.03	0.03
G207.2654−01.8080 – 1	2MASS PSC	>13.5	11.49 ± 0.08	7.73 ± 0.04	13.09	0.07	0.08	10.55	0.05	0.05
G207.2654−01.8080 – 2	2MASS PSC	12.10 ± 0.03	9.61 ± 0.04	7.62 ± 0.03	9.77	0.03	0.02	8.16	0.01	0.02
G211.8957−01.2025	2MASS PSC	>14.6	>13.1	12.02 ± 0.08	15.6	0.2	0.2	13.24	0.06	0.07
G212.0641−00.7395	2MASS PSC	14.30 ± 0.08	11.98 ± 0.08	9.98 ± 0.04	13.5	0.1	0.1	11.50	0.06	0.06
G212.2344−03.5038	2MASS PSC	12.72 ± 0.04	10.60 ± 0.03	8.90 ± 0.02	10.84	0.03	0.03	9.12	0.01	0.01
G212.2468−01.1034 – 1	2MASS PSC	14.38 ± 0.08	13.2 ± 0.1	12.29 ± 0.07	13.53	0.05	0.06	12.88	0.05	0.05
G212.2468−01.1034 – 2	2MASS PSC	14.38 ± 0.07	13.7 ± 0.1	13.16 ± 0.08	13.86	0.06	0.06	13.54	0.06	0.06
G212.9626+01.2954	2MASS PSC	14.37 ± 0.07	12.32 ± 0.05	10.35 ± 0.03	9.57	0.08	0.09	7.59	0.05	0.05
G213.0763−02.2174	2MASS PSC	11.94 ± 0.06	10.97 ± 0.07	10.15 ± 0.06	11.52	0.05	0.05	10.79	0.02	0.03
G213.9180+00.3786	2MASS PSC	14.95 ± 0.08	12.28 ± 0.04	>10.0	12.21	0.01	0.01	9.90	0.02	0.02
G215.8902−02.0094	2MASS PSC	15.03 ± 0.08	12.79 ± 0.06	10.71 ± 0.03	13.03	0.04	0.04	10.86	0.03	0.03
G217.6047−02.6170	UKIDSS GPS	16.26 ± 0.01	14.278 ± 0.003	12.216 ± 0.001	14.44	0.08	0.08	12.68	0.04	0.04
G224.6075−01.0063	2MASS PSC	15.3 ± 0.1	13.4 ± 0.1	11.25 ± 0.07	9.9	0.1	0.1	7.72	0.07	0.07
G232.6207+00.9959	2MASS PSC	13.45 ± 0.08	10.76 ± 0.08	8.48 ± 0.04	11.19	0.03	0.04	9.17	0.02	0.02

Table A3. A_V and f_{obs}/f_{corr} for all objects. A_V was calculated twice for each object using the Draine & Lee (1984) model, once with J and H band magnitudes ('A_V (JH)' in the table) and once with H and K band magnitudes ('A_V (HK)' in the table). Where the required magnitudes were not available, '–' is shown. f_{obs}/f_{corr} is the correction factor used to correct for the difference between the observed and catalogue magnitudes. '–' is shown in that column when no catalogue magnitudes are available for comparison. See Sections 3 and 5.

Name	A_V (JH)	A_V (HK)	f_{obs}/f_{corr}	Name	A_V (JH)	A_V (HK)	f_{obs}/f_{corr}	Name	A_V (JH)	A_V (HK)	f_{obs}/f_{corr}
G010.8411−02.5919	>35	63 ± 2	0.37	G030.5942−00.1273	30.0 ± 0.5	33.2 ± 0.7	1.4	G050.2844−00.3925A	43.8 ± 0.6	56.39 ± 0.06	4.7
G010.8856+00.1221	61 ± 1	62.33 ± 0.04	0.83	G030.8185+00.2729	–	69.26 ± 0.07	0.53	G050.4802+00.7058	–	–	–
G011.9019+00.7265	28.9 ± 0.1	46.99 ± 0.05	68	G030.9726−00.1410	>34	47 ± 2	0.26	G052.2025+00.7217A	35.1 ± 0.1	59.62 ± 0.03	1.3
G016.7122+01.3119 – 1	31.6 ± 0.7	36.2 ± 0.8	1.7	G030.9727+00.5620	24 ± 3	89 ± 1	8.9	G052.2078+00.6890	>19	>27	3.4
G016.7122+01.3119 – 2	>23	61 ± 2	0.70	G030.9959−00.0771	>24	>33	0.83	G052.5405−00.9272	>24	>49	1.5
G016.7981+00.1264	34.13 ± 0.10	58.56 ± 0.03	0.83	G031.1677+00.1259	16.85 ± 0.02	17.03 ± 0.02	3.1	G052.9217+00.4142	37.9 ± 1.0	63.6 ± 0.2	2.2
G017.0332+00.7476A	–	–	0.45	G031.6617+00.3667	>27	>32	0.42	G052.9221−00.4892	>21	>53	0.97
G017.3765+02.2512	29 ± 2	38 ± 2	3.3	G032.0451+00.0589	–	–	–	G053.1417+00.0705	–	–	0.72
G018.3412+01.7681	>28	67 ± 2	0.53	G032.0518−00.0902	20.6 ± 0.2	43.3 ± 0.1	0.43	G053.5343−00.7943	35.2 ± 0.4	43.8 ± 0.5	0.29
G018.3706−00.3818	30.71 ± 0.03	38.18 ± 0.01	1.3	G032.1514+00.1317	17.92 ± 0.02	19.86 ± 0.02	0.94	G055.1581−00.2991A	39.9 ± 0.6	52.77 ± 0.08	2.4
G018.6608+00.0372	–	–	1.3	G032.4727+00.2041	41.3 ± 0.3	52.04 ± 0.04	1.1	G055.3704+00.1858	40.8 ± 0.4	>21	6.4
G019.7540−00.1279	29.1 ± 0.2	43.2 ± 0.1	0.67	G032.8205−00.3300	>32	>42	0.56	G056.3694−00.6333	–	51.6 ± 0.1	0.90
G019.8922+00.1023	17.30 ± 0.02	37.09 ± 0.02	0.67	G032.9957+00.0415	–	96.4 ± 0.3	1.3	G056.4120−00.0277	28.8 ± 0.3	34.7 ± 0.5	3.2
G019.9224−00.2577	30.4 ± 0.6	45.9 ± 0.2	1.4	G033.3891+00.1989	38.3 ± 0.5	43.4 ± 0.7	1.3	G057.5474−00.2717A	34.0 ± 0.1	43.90 ± 0.03	0.36
G020.5143+00.4936	17.21 ± 0.02	14.82 ± 0.02	2.0	G034.0126−00.2832	22.7 ± 0.4	34.3 ± 0.6	1.1	G059.3614−00.2068	25.65 ± 0.02	36.24 ± 0.01	1.5
G021.3853−00.2537	–	–	0.61	G034.0500−00.2977	–	–	–	G059.6403−00.1812A	21.38 ± 0.04	37.99 ± 0.03	0.52
G021.5624−00.0329	–	–	166	G034.4035+00.2282	–	–	–	G059.7831+00.0648	–	84.4 ± 0.3	0.72
G023.3891+00.1851	47 ± 1	58.9 ± 0.7	8.4	G034.6243−00.1300	–	69.9 ± 0.5	6.6	G059.8329+00.6729	31 ± 1	39.6 ± 0.3	0.98
G023.4394−00.2394	–	59.34 ± 0.10	0.90	G034.7569+00.0247	–	–	0.51	G060.5750−00.1861	19 ± 2	42 ± 2	0.82
G023.4984−00.0373	21.4 ± 0.4	19.3 ± 0.6	8.0	G034.8211+00.3519	46.4 ± 0.5	49.3 ± 0.7	0.013	G063.1140+00.3416	>42	63.6 ± 0.9	10
G023.6566−00.1273	–	80.29 ± 0.06	4.6	G035.1979−00.7427	>41	57 ± 1	0.74	G065.7798−02.6121	>26	37 ± 1	2.2
G024.6343−00.3233	>28	60 ± 1	1.1	G036.8780−00.4728 – 1	–	89 ± 2	0.37	G068.2040+00.2387	39.5 ± 0.2	48.74 ± 0.04	1.3
G025.4018+00.0198A	28.4 ± 0.4	22.7 ± 0.6	0.64	G036.8780−00.4728 – 2	–	89 ± 2	0.38	G069.5395−00.9754	–	–	–
G025.6498+01.0491	–	–	0.91	G036.9194+00.4825A	>20	>37	1.2	G070.3329+01.5864 – 1	>20	35 ± 1	0.082
G025.7161+00.0486	–	–	–	G037.5536+00.2008	>13	>79	0.68	G070.3329+01.5864 – 2	>20	35 ± 1	1.0
G025.8015−00.1570 – 1	32.4 ± 0.1	47.22 ± 0.04	0.40	G039.4943−00.9933	–	68.77 ± 0.05	0.90	G070.6740+01.1919	24.2 ± 0.4	31.0 ± 0.7	0.72
G025.8015−00.1570 – 2	–	–	–	G039.8821−00.3457	–	81 ± 3	0.48	G071.8944+01.3107	>38	56 ± 2	1.2
G026.2020+00.2262	40.6 ± 0.5	43.3 ± 0.6	1.0	G040.0809+01.5117	26.26 ± 0.07	29.10 ± 0.04	0.79	G072.2479+00.2617B	27.9 ± 0.4	38.4 ± 0.2	1.1
G026.3050+00.1162	15.5 ± 0.4	22.8 ± 0.7	0.90	G040.4247+00.6989A	16.60 ± 0.09	13.57 ± 0.10	1.0	G073.0633+01.7958	>24	>22	1.7
G026.3176−00.0134	35.2 ± 0.5	31.3 ± 0.7	0.60	G040.5451+02.5961A	–	–	–	G073.6525+00.1944	28.3 ± 0.5	35.1 ± 0.8	1.2
G026.3819+01.4057 – 1	27.26 ± 0.09	36.50 ± 0.04	0.52	G042.0341+00.1905A	39.1 ± 0.4	65.00 ± 0.07	4.1	G073.6952−00.9996	26.0 ± 0.6	47.3 ± 0.8	0.72
G026.3819+01.4057 – 2	22.75 ± 0.02	44.98 ± 0.01	0.68	G042.0977+00.3521	29 ± 1	55.9 ± 0.4	0.48	G075.6014+01.6394	24 ± 1	23 ± 1	0.52
G026.4207+01.6858	33.19 ± 0.09	55.50 ± 0.02	0.12	G042.1099−00.4466	49 ± 2	53.2 ± 0.1	0.53	G075.7666+00.3424 – 1	29.17 ± 0.04	35.22 ± 0.02	6.2
G026.4488+01.7425A	–	18.28 ± 0.01	1.0	G043.1635−00.0697A	20.74 ± 0.05	22.19 ± 0.04	0.91	G075.7666+00.3424 – 2	–	62.08 ± 0.09	1.4
G026.4488+01.7425B	14.45 ± 0.04	27.37 ± 0.04	0.50	G043.5216−00.6476	31.5 ± 0.1	38.51 ± 0.03	1.3	G076.0902+00.1412	–	74.2 ± 0.3	0.88
G026.4897−00.5455	–	–	0.87	G043.9956−00.0111	35.5 ± 0.1	48.23 ± 0.02	0.98	G076.1877+00.0974	–	51.8 ± 0.2	3.3
G026.4958+00.7105 – 1	–	–	0.70	G044.3103+00.0416	34.5 ± 0.6	36.4 ± 0.1	0.83	G076.3829−00.6210	30.1 ± 0.4	34.3 ± 0.4	0.58
G026.4958+00.7105 – 2	–	–	0.45	G045.1894−00.4387	40.5 ± 0.4	66.88 ± 0.06	11	G077.3455+04.4309	15.061 ± 0.009	19.48 ± 0.01	5.9
G026.5972−00.0241	–	–	0.39	G045.4543+00.0600 – 1	–	–	0.58	G077.4052−01.2136	>18	54 ± 2	0.78
G027.2220+00.1361 – 1	7.54 ± 0.07	–	2.1	G045.4543+00.0600 – 2	–	–	–	G077.4622+01.7600 – 1	–	–	0.61
G027.2220+00.1361 – 2	–	–	–	G045.4641+00.0284	–	–	0.64	G077.4622+01.7600 – 2	>22	>35	0.031
G027.7954−00.2772	–	100.5 ± 0.5	0.98	G048.6085+00.0258D	32.1 ± 0.4	24.6 ± 0.7	8.6	G077.8999+01.7678	34.60 ± 0.08	52.40 ± 0.02	1.3
G028.2325+00.0394	–	–	0.81	G048.9897−00.2992A	15.3 ± 0.1	49.31 ± 0.09	0.55	G077.9550+00.0058	20.16 ± 0.03	21.09 ± 0.03	0.83
G028.3046−00.3871A	29.1 ± 0.1	39.60 ± 0.05	4.7	G048.9897−00.2992B	–	–	–	G078.1224+03.6320	17.54 ± 0.03	20.35 ± 0.03	0.42
G028.3373+00.1189	–	53.3 ± 0.2	11	G049.0431−01.0787	–	–	–	G078.4373+02.6584B	–	66.53 ± 0.08	0.96
G028.7799+03.4978	18.2 ± 0.5	22.3 ± 0.8	0.40	G049.4227−00.3715	39 ± 1	>43	0.20	G078.4705−00.1830	39 ± 2	52.0 ± 0.2	0.57
G028.8621+00.0657	–	–	0.45	G049.4883−00.3545A	26.5 ± 0.2	36.43 ± 0.07	9.4	G078.4754+01.0421	>48	76.8 ± 0.7	0.70
G030.1468+01.4075	–	96 ± 1	1.7	G049.4883−00.3545B	–	52.1 ± 0.4	6.4	G078.7641+01.6862	–	51.4 ± 0.5	0.78
G030.1981−00.1691	>50	59.6 ± 0.7	1.3	G049.4970−00.4718	15.01 ± 0.03	16.81 ± 0.04	2.4	G078.8867+00.7087	>40	76.2 ± 0.8	0.92
G030.2340−00.1392	23.0 ± 0.5	53.7 ± 0.2	0.77	G049.5373−00.3929	16.7 ± 0.5	10.7 ± 0.8	0.27	G078.9761+00.3567	22.8 ± 0.4	25.9 ± 0.5	3.0
G030.2971+00.0549	–	–	0.43	G050.0721+00.5591	26.6 ± 0.2	39.88 ± 0.09	0.91	G079.1272+02.2782	34.00 ± 0.06	49.05 ± 0.02	1.0
G030.4117−00.2277	25.28 ± 0.08	49.99 ± 0.04	0.90	G050.2213−00.6063	>26	>30	0.37	G079.3202+01.3131	–	55.7 ± 0.2	4.2

Table A3 – *continued*

Name	A_V (*JH*)	A_V (*HK*)	f_{obs}/f_{corr}	Name	A_V (*JH*)	A_V (*HK*)	f_{obs}/f_{corr}
G079.3248+01.2901	32 ± 1	36.9 ± 0.3	1.6	G150.6862−00.6887	16.4 ± 0.5	23.3 ± 0.7	1.1
G080.0467+00.3101	34.3 ± 0.4	39.4 ± 0.4	0.78	G151.6120−00.4575	23.4 ± 0.4	33.0 ± 0.6	0.79
G080.1909+00.5353	34.8 ± 0.5	43.7 ± 0.5	0.75	G152.3371−00.2899	>5.9	–	2.6
G080.8282+00.5670A	>37	>57	1.5	G154.3472+02.6099	16.0 ± 0.9	19 ± 1	0.54
G080.8645+00.4197	>25	>66	0.46	G166.8141−03.1986	16.63 ± 0.06	18.55 ± 0.07	0.83
G081.5168+00.1926	>38	>49	2.5	G168.0627+00.8221	17.10 ± 0.02	36.04 ± 0.01	0.54
G081.7131+00.5792	32.3 ± 0.5	39.2 ± 0.8	0.49	G169.6459−00.0687	10.26 ± 0.02	16.50 ± 0.03	0.69
G081.7624+00.5916	–	114 ± 1	0.67	G173.4815+02.4459	43.6 ± 0.5	52.30 ± 0.06	0.49
G082.5682+00.4040A	24.5 ± 0.5	29.5 ± 0.6	0.72	G173.4839+02.4317	20.3 ± 0.4	25.7 ± 0.5	2.4
G083.7071+03.2817	26.4 ± 0.6	35.2 ± 0.8	2.0	G173.6328+02.8064	>27	>39	0.96
G084.3065+01.8933	32.5 ± 0.8	40.1 ± 0.7	2.4	G173.6339+02.8218	37.6 ± 0.4	42.4 ± 0.5	0.61
G084.6490+02.1267	21 ± 1	23 ± 1	0.58	G173.7215+02.6924	14.6 ± 0.4	18.1 ± 0.5	0.81
G085.4102+00.0032A	>27	68 ± 4	1.3	G177.7291−00.3358	>24	>29	4.5
G089.6368+00.1732	44.3 ± 0.3	67.86 ± 0.04	0.83	G178.7540+01.1609	15.8 ± 0.5	21.5 ± 0.7	2.1
G090.2095+02.0405	22.9 ± 0.6	38.0 ± 0.7	0.48	G179.0380+04.3003	33.0 ± 0.7	39.4 ± 0.8	0.36
G094.3228−00.1671	30.00 ± 0.10	58.89 ± 0.03	0.89	G183.4530−01.7774	>22	>40	0.35
G094.4637−00.8043	–	–	0.49	G184.8704−01.7329	14.8 ± 0.6	22.7 ± 0.8	0.72
G095.0026−01.5779	>18	>15	1.1	G184.9551−00.8559	26.5 ± 0.6	35.2 ± 0.8	0.98
G095.0531+03.9724	>13	>13	0.55	G188.8120+01.0686	>24	>22	1.1
G096.3597+01.2982	26.1 ± 0.2	32.7 ± 0.1	9.5	G188.9479+00.8871	35 ± 1	44.4 ± 0.8	13
G096.4353+01.3233A – 1	–	–	–	G188.9696−01.9380	27 ± 1	39 ± 1	0.59
G096.4353+01.3233A – 2	–	–	–	G189.0065+01.1263	29.1 ± 0.4	35.0 ± 0.5	7.5
G097.5268+03.1837C	28.9 ± 0.8	36.1 ± 0.8	0.89	G189.0307+00.7821	46 ± 1	>65	2.0
G097.9978+01.4688	25.7 ± 0.7	35.7 ± 0.8	0.93	G189.0323+00.8092	46.3 ± 0.6	57.5 ± 0.6	2.9
G098.8555+02.9344	18 ± 2	37 ± 2	1.2	G192.6005−00.0479	–	–	–
G100.1620+01.6647	24 ± 2	35 ± 3	0.22	G192.9089−00.6259	>23	>11	3.5
G100.1685+02.0266	18 ± 1	>37	0.53	G194.9349−01.2224	37.3 ± 0.7	46.2 ± 0.7	1.1
G100.2124+01.8829	>10	33 ± 2	1.4	G196.1620−01.2546	>30	>38	0.51
G100.3779−03.5784	34 ± 2	>43	0.80	G196.4542−01.6777	>12	60 ± 1	0.40
G102.3533+03.6360	30.8 ± 0.4	44.1 ± 0.5	0.37	G200.0789−01.6323	>14	>3	0.37
G103.8034+00.4062	33.1 ± 0.7	56.0 ± 0.2	0.44	G203.3166+02.0564	43.6 ± 0.7	49.7 ± 0.8	0.85
G103.8744+01.8558	>40	>36	1.1	G207.2654−01.8080 – 1	>24	68 ± 2	0.075
G105.5072+00.2294	–	43.51 ± 0.04	0.63	G207.2654−01.8080 – 2	28.6 ± 0.6	36.6 ± 0.9	0.61
G107.6823−02.2423A	>14	23 ± 1	0.71	G211.8957−01.2025	>18	>21	0.32
G108.2118−01.2887	16.8 ± 0.8	21 ± 1	0.49	G212.0641−00.7395	27 ± 1	37 ± 2	0.25
G108.7575−00.9863	–	–	–	G212.2344−03.5038	24.5 ± 0.5	31.4 ± 0.7	0.82
G110.8038−02.5649	30.6 ± 0.7	38.1 ± 0.7	1.0	G212.2468−01.1034 – 1	14 ± 1	18 ± 2	0.58
G111.2348−01.2385	>32	>32	0.72	G212.2468−01.1034 – 2	8 ± 1	11 ± 2	0.70
G133.8512−01.9272	14.9 ± 0.4	21.8 ± 0.7	0.50	G212.9626+01.2954	23.7 ± 0.9	36 ± 1	13
G139.9091+00.1969A	21.8 ± 0.6	25.3 ± 1.0	0.54	G213.0763−02.2174	12 ± 1	16 ± 2	0.55
G141.9996+01.8202	32.7 ± 0.5	43.4 ± 0.8	1.3	G213.9180+00.3786	30.5 ± 1.0	>43	1.1
G142.2446+01.4299	–	–	0.53	G215.8902−02.0094	26 ± 1	38 ± 1	0.88
G144.6678−00.7136	18.7 ± 0.4	24.5 ± 0.7	0.84	G217.6047−02.6170	22.9 ± 0.1	37.93 ± 0.07	0.65
G145.1975+02.9870 – 1	18 ± 2	20 ± 2	0.47	G224.6075−01.0063	23 ± 2	39 ± 3	26
G145.1975+02.9870 – 2	22.1 ± 0.9	26 ± 1	1.2	G232.6207+00.9959	31 ± 1	42 ± 2	0.53
G148.1201+00.2928	35 ± 2	55 ± 2	0.64				

Table B1. YSO and YSO/HIIR emission line fluxes for Brγ, Br 10, Br 11, Br 12/[Fe II] 1.64402 μm blend, H_2 2.1218 μm, H_2 2.2477 μm, fluorescent Fe II 1.6878 μmand He I 2.0587 μm. Fluxes are in W m^{-2} μm^{-1}, and a negative value indicates absorption. '–' is marked to indicate that a measurement was not possible due to a negative *H* band flux (i.e. where the object was invisible at *H*). The presence or absence of the Pfund series is shown in the 'Pfund' column: 'P' for present, '–' for absent.

Name	Brγ	Br 10	Br 11	Br 12/[Fe II]	H_2 2.1218 μm	H_2 2.2477 μm	Fluorescent Fe II	He I 2.0587 μm	Pfund?
G010.8411−02.5919	$2.9 \pm 0.9 \times 10^{-18}$	$<2.4 \times 10^{-18}$	$<3.5 \times 10^{-18}$	$<3.3 \times 10^{-18}$	$4 \pm 1 \times 10^{-18}$	$<5.7 \times 10^{-18}$	$<3.6 \times 10^{-18}$	$<5.2 \times 10^{-18}$	–
G010.8856+00.1221	$2.8 \pm 0.2 \times 10^{-17}$	$8 \pm 1 \times 10^{-18}$	$4 \pm 1 \times 10^{-18}$	$<3.1 \times 10^{-18}$	$<9.6 \times 10^{-18}$	$<8.2 \times 10^{-18}$	$<3.3 \times 10^{-18}$	$<4.6 \times 10^{-18}$	–
G011.9019+00.7265	$1.2 \pm 0.2 \times 10^{-15}$	$2.9 \pm 0.3 \times 10^{-16}$	$3.0 \pm 0.5 \times 10^{-16}$	$3.4 \pm 0.3 \times 10^{-16}$	$<4.1 \times 10^{-16}$	$<8.5 \times 10^{-16}$	$1.2 \pm 0.3 \times 10^{-16}$	$<3.7 \times 10^{-16}$	–
G016.7122+01.3119 – 1	$<4.2 \times 10^{-17}$	$<3.2 \times 10^{-17}$	$-1.1 \pm 0.2 \times 10^{-17}$	$-1.5 \pm 0.1 \times 10^{-17}$	$<2.8 \times 10^{-17}$	$<2.8 \times 10^{-17}$	$<2.5 \times 10^{-17}$	$<4.4 \times 10^{-17}$	–
G016.7122+01.3119 – 2	$2.3 \pm 0.3 \times 10^{-18}$	$<1.4 \times 10^{-18}$	$<1.2 \times 10^{-18}$	$<1.2 \times 10^{-18}$	$<2.7 \times 10^{-18}$	$<3.4 \times 10^{-18}$	$<1.3 \times 10^{-18}$	$<2.0 \times 10^{-18}$	–
G016.7981+00.1264	$<8.0 \times 10^{-18}$	$9 \pm 2 \times 10^{-18}$	$7 \pm 1 \times 10^{-18}$	$6.1 \pm 0.7 \times 10^{-18}$	$<7.3 \times 10^{-18}$	$<1.4 \times 10^{-17}$	$4.8 \pm 0.7 \times 10^{-18}$	$<4.7 \times 10^{-18}$	–
G017.0332+00.7476A	$<5.1 \times 10^{-19}$	$<5.4 \times 10^{-19}$	$<6.6 \times 10^{-19}$	$<6.3 \times 10^{-19}$	$1.14 \pm 0.08 \times 10^{-18}$	$<4.0 \times 10^{-19}$	$<6.2 \times 10^{-19}$	$<4.2 \times 10^{-19}$	–
G017.3765+02.2512	$3.0 \pm 0.5 \times 10^{-17}$	$4.0 \pm 0.8 \times 10^{-17}$	$<3.6 \times 10^{-17}$	$5.0 \pm 0.4 \times 10^{-17}$	$9.2 \pm 0.9 \times 10^{-17}$	$<5.9 \times 10^{-17}$	$<3.0 \times 10^{-17}$	$<7.6 \times 10^{-17}$	–
G018.3412+01.7681	$6.1 \pm 0.8 \times 10^{-18}$	$1.3 \pm 0.4 \times 10^{-18}$	$1.2 \pm 0.2 \times 10^{-18}$	$2.3 \pm 0.3 \times 10^{-18}$	$<1.4 \times 10^{-17}$	$<1.7 \times 10^{-17}$	$<2.4 \times 10^{-18}$	$<6.8 \times 10^{-18}$	–
G018.3706−00.3818	$3.3 \pm 0.9 \times 10^{-17}$	$2.9 \pm 0.7 \times 10^{-17}$	$3.0 \pm 0.5 \times 10^{-17}$	$1.5 \pm 0.4 \times 10^{-17}$	$<8.9 \times 10^{-18}$	$<8.4 \times 10^{-18}$	$<2.1 \times 10^{-17}$	$<9.6 \times 10^{-18}$	–
G018.6608+00.0372	$<1.5 \times 10^{-18}$	$<8.7 \times 10^{-19}$	$<1.2 \times 10^{-18}$	$1.3 \pm 0.3 \times 10^{-18}$	$2.8 \pm 0.2 \times 10^{-18}$	$<1.2 \times 10^{-18}$	$<9.9 \times 10^{-19}$	$<1.1 \times 10^{-18}$	–
G019.8922+00.1023	$4.1 \pm 0.8 \times 10^{-18}$	$<2.4 \times 10^{-18}$	$9 \pm 2 \times 10^{-18}$	$8.4 \pm 0.7 \times 10^{-18}$	$5.3 \pm 0.5 \times 10^{-18}$	$<3.1 \times 10^{-18}$	$<1.6 \times 10^{-18}$	$<2.2 \times 10^{-18}$	–
G019.9224−00.2577	$<1.3 \times 10^{-18}$	$<2.0 \times 10^{-18}$	$<1.8 \times 10^{-18}$	$7.9 \pm 0.5 \times 10^{-18}$	$1.31 \pm 0.05 \times 10^{-17}$	$1.6 \pm 0.5 \times 10^{-18}$	$<1.7 \times 10^{-18}$	$<9.5 \times 10^{-19}$	–
G020.5143+00.4936	$4.1 \pm 0.8 \times 10^{-17}$	$<3.0 \times 10^{-17}$	$<4.1 \times 10^{-17}$	$<3.9 \times 10^{-17}$	$4.1 \pm 0.9 \times 10^{-17}$	$<4.5 \times 10^{-17}$	$<3.6 \times 10^{-17}$	$<3.5 \times 10^{-17}$	–
G021.5624−00.0329	$<2.0 \times 10^{-15}$	$<2.6 \times 10^{-16}$	$<1.7 \times 10^{-16}$	$<1.6 \times 10^{-16}$	$<1.7 \times 10^{-15}$	$<4.5 \times 10^{-15}$	$<1.8 \times 10^{-16}$	$<1.7 \times 10^{-15}$	–
G023.3891+00.1851	$8.0 \pm 0.6 \times 10^{-16}$	$3.4 \pm 0.2 \times 10^{-16}$	$1.7 \pm 0.2 \times 10^{-16}$	$9 \pm 1 \times 10^{-17}$	$<4.2 \times 10^{-16}$	$<4.1 \times 10^{-16}$	$<1.3 \times 10^{-16}$	$<2.9 \times 10^{-16}$	–
G023.6566−00.1273	$<8.4 \times 10^{-17}$	$<1.7 \times 10^{-17}$	$<1.3 \times 10^{-17}$	$<1.3 \times 10^{-17}$	$9 \pm 1 \times 10^{-17}$	$<1.2 \times 10^{-16}$	$<1.5 \times 10^{-17}$	$<5.5 \times 10^{-17}$	–
G024.6343−00.3233	$3.1 \pm 0.5 \times 10^{-17}$	$1.7 \pm 0.2 \times 10^{-17}$	$<5.3 \times 10^{-18}$	$3.7 \pm 1.0 \times 10^{-18}$	$8 \pm 2 \times 10^{-18}$	$<1.4 \times 10^{-17}$	$8 \pm 2 \times 10^{-18}$	$<1.1 \times 10^{-17}$	–
G025.6498+01.0491	$<2.7 \times 10^{-18}$	$<1.3 \times 10^{-18}$	$<1.2 \times 10^{-18}$	$<1.2 \times 10^{-18}$	$8.5 \pm 0.4 \times 10^{-18}$	$<3.8 \times 10^{-18}$	$<1.4 \times 10^{-18}$	$<1.1 \times 10^{-18}$	–
G025.7161+00.0486	$2.7 \pm 0.1 \times 10^{-17}$	$3.2 \pm 0.5 \times 10^{-18}$	$1.9 \pm 0.5 \times 10^{-18}$	$4.7 \pm 0.5 \times 10^{-18}$	$1.4 \pm 0.4 \times 10^{-18}$	$<1.0 \times 10^{-18}$	$<1.1 \times 10^{-18}$	$4 \pm 1 \times 10^{-18}$	–
G025.8015−00.1570 – 1	$2.91 \pm 0.03 \times 10^{-17}$	$4.3 \pm 0.3 \times 10^{-18}$	$1.7 \pm 0.5 \times 10^{-18}$	$4.7 \pm 0.4 \times 10^{-18}$	$1.9 \pm 0.3 \times 10^{-18}$	$<1.5 \times 10^{-18}$	$5 \pm 1 \times 10^{-18}$	$3.1 \pm 0.3 \times 10^{-18}$	–
G025.8015−00.1570 – 2	$8.2 \pm 0.3 \times 10^{-18}$	$1.7 \pm 0.3 \times 10^{-18}$	$1.8 \pm 0.4 \times 10^{-18}$	$2.7 \pm 0.3 \times 10^{-18}$	$2.0 \pm 0.7 \times 10^{-18}$	$<2.3 \times 10^{-18}$	$<8.5 \times 10^{-19}$	$<1.3 \times 10^{-18}$	–
G026.2020+00.2262	$<4.9 \times 10^{-17}$	$<2.2 \times 10^{-17}$	$<1.8 \times 10^{-17}$	$<1.7 \times 10^{-17}$	$<4.8 \times 10^{-17}$	$<4.2 \times 10^{-17}$	$<1.8 \times 10^{-17}$	$<2.6 \times 10^{-17}$	–
G026.3819+01.4057 – 1	$<1.6 \times 10^{-18}$	$<7.7 \times 10^{-19}$	$<9.8 \times 10^{-19}$	$<9.2 \times 10^{-19}$	$1.5 \pm 0.2 \times 10^{-18}$	$<6.7 \times 10^{-19}$	$<8.0 \times 10^{-19}$	$<7.5 \times 10^{-19}$	–
G026.3819+01.4057 – 2	$8.6 \pm 0.6 \times 10^{-18}$	$6.4 \pm 1.0 \times 10^{-18}$	$9 \pm 2 \times 10^{-18}$	$8.2 \pm 1.0 \times 10^{-18}$	$6 \pm 1 \times 10^{-18}$	$<9.6 \times 10^{-18}$	$3 \pm 1 \times 10^{-18}$	$<4.1 \times 10^{-18}$	–
G026.4207+01.6858	$5.7 \pm 0.8 \times 10^{-19}$	$8 \pm 2 \times 10^{-19}$	$8 \pm 2 \times 10^{-19}$	$1.23 \pm 0.08 \times 10^{-18}$	$9 \pm 1 \times 10^{-19}$	$<7.1 \times 10^{-19}$	$3 \pm 1 \times 10^{-19}$	$<4.9 \times 10^{-19}$	–
G026.4958+00.7105 – 1	$4.5 \pm 0.6 \times 10^{-19}$	–	–	–	$<2.9 \times 10^{-19}$	$<3.1 \times 10^{-19}$	–	$<2.5 \times 10^{-19}$	–
G026.4958+00.7105 – 2	$<3.9 \times 10^{-19}$	–	–	–	$<3.1 \times 10^{-19}$	$<2.2 \times 10^{-19}$	–	$<3.5 \times 10^{-19}$	–
G026.5972−00.0241	$2.67 \pm 0.07 \times 10^{-18}$	–	–	–	$<2.9 \times 10^{-19}$	$<4.5 \times 10^{-19}$	–	$1.35 \pm 0.08 \times 10^{-18}$	–
G027.2220+00.1361 – 2	$<3.0 \times 10^{-19}$	$<1.9 \times 10^{-19}$	$<4.0 \times 10^{-19}$	$<3.8 \times 10^{-19}$	$<1.9 \times 10^{-19}$	$<2.2 \times 10^{-19}$	$<3.4 \times 10^{-19}$	$<2.3 \times 10^{-19}$	–
G027.7954−00.2772	$4 \pm 1 \times 10^{-18}$	$<1.6 \times 10^{-18}$	$<2.1 \times 10^{-18}$	$<2.0 \times 10^{-18}$	$<7.4 \times 10^{-18}$	$<1.1 \times 10^{-17}$	$<2.3 \times 10^{-18}$	$<1.5 \times 10^{-17}$	–
G028.2325+00.0394	$<1.9 \times 10^{-18}$	$<3.7 \times 10^{-19}$	$<5.1 \times 10^{-19}$	$<4.9 \times 10^{-19}$	$<1.6 \times 10^{-18}$	$<2.0 \times 10^{-18}$	$<4.2 \times 10^{-19}$	$<8.6 \times 10^{-19}$	–
G028.3046−00.3871A	$5.3 \pm 0.3 \times 10^{-17}$	$2.1 \pm 0.6 \times 10^{-17}$	$3.0 \pm 0.8 \times 10^{-17}$	$1.2 \pm 0.3 \times 10^{-17}$	$1.8 \pm 0.2 \times 10^{-17}$	$<8.6 \times 10^{-18}$	$<8.0 \times 10^{-18}$	$2.5 \pm 0.3 \times 10^{-17}$	–
G028.3373+00.1189	$7.5 \pm 0.8 \times 10^{-17}$	$<2.7 \times 10^{-17}$	$<2.9 \times 10^{-17}$	$<2.8 \times 10^{-17}$	$<2.5 \times 10^{-17}$	$<1.9 \times 10^{-17}$	$<2.9 \times 10^{-17}$	$<2.3 \times 10^{-17}$	–
G028.8621+00.0657	$<7.1 \times 10^{-19}$	$<5.8 \times 10^{-19}$	$<6.8 \times 10^{-19}$	$<6.4 \times 10^{-19}$	$1.2 \pm 0.1 \times 10^{-18}$	$<7.1 \times 10^{-19}$	$<6.9 \times 10^{-19}$	$<7.4 \times 10^{-19}$	–
G030.1981−00.1691	$5.5 \pm 0.7 \times 10^{-17}$	$<8.8 \times 10^{-18}$	$<1.5 \times 10^{-17}$	$<1.4 \times 10^{-17}$	$<3.3 \times 10^{-17}$	$<3.6 \times 10^{-17}$	$<1.4 \times 10^{-17}$	$<2.1 \times 10^{-17}$	–
G030.2971+00.0549	$1.2 \pm 0.3 \times 10^{-19}$	–	–	–	$1.4 \pm 0.4 \times 10^{-19}$	$<2.0 \times 10^{-19}$	–	$<2.1 \times 10^{-19}$	–
G030.4117−00.2277	$2.08 \pm 0.09 \times 10^{-17}$	$6 \pm 1 \times 10^{-18}$	$7 \pm 1 \times 10^{-18}$	$4.7 \pm 0.7 \times 10^{-18}$	$<4.7 \times 10^{-18}$	$5 \pm 1 \times 10^{-18}$	$4.2 \pm 0.8 \times 10^{-18}$	$5.3 \pm 0.9 \times 10^{-18}$	–
G030.5942−00.1273	$1.72 \pm 0.04 \times 10^{-16}$	$1.34 \pm 0.09 \times 10^{-16}$	$1.6 \pm 0.1 \times 10^{-16}$	$7.9 \pm 0.7 \times 10^{-17}$	$<1.9 \times 10^{-17}$	$<1.1 \times 10^{-17}$	$<1.6 \times 10^{-17}$	$1.4 \pm 0.3 \times 10^{-17}$	P
G030.8185+00.2729	$4 \pm 1 \times 10^{-18}$	$<1.2 \times 10^{-18}$	$<9.5 \times 10^{-19}$	$<9.0 \times 10^{-19}$	$<3.9 \times 10^{-18}$	$<3.7 \times 10^{-18}$	$<9.3 \times 10^{-19}$	$<2.3 \times 10^{-18}$	–
G030.9726−00.1410	$<4.9 \times 10^{-19}$	$<4.8 \times 10^{-19}$	$<5.5 \times 10^{-19}$	$<5.2 \times 10^{-19}$	$7 \pm 2 \times 10^{-19}$	$<4.5 \times 10^{-19}$	$<5.4 \times 10^{-19}$	$<4.7 \times 10^{-19}$	–
G030.9727+00.5620	$<1.7 \times 10^{-17}$	$<9.1 \times 10^{-18}$	$<2.1 \times 10^{-17}$	$<2.0 \times 10^{-17}$	$8 \pm 2 \times 10^{-18}$	$<1.4 \times 10^{-17}$	$<2.0 \times 10^{-17}$	$<7.8 \times 10^{-18}$	–
G030.9959−00.0771	$<7.1 \times 10^{-19}$	$<5.1 \times 10^{-19}$	$<7.3 \times 10^{-19}$	$<6.9 \times 10^{-19}$	$1.3 \pm 0.1 \times 10^{-18}$	$7 \pm 2 \times 10^{-19}$	$<6.6 \times 10^{-19}$	$<5.9 \times 10^{-19}$	–
G032.0451+00.0589	$<4.8 \times 10^{-19}$	–	–	–	$3.6 \pm 0.6 \times 10^{-19}$	$<4.2 \times 10^{-19}$	–	$<3.9 \times 10^{-19}$	–
G032.0518−00.0902	$<9.4 \times 10^{-19}$	$<1.2 \times 10^{-18}$	$<9.4 \times 10^{-19}$	$<8.9 \times 10^{-19}$	$1.26 \pm 0.05 \times 10^{-17}$	$1.4 \pm 0.2 \times 10^{-18}$	$<7.7 \times 10^{-19}$	$<4.8 \times 10^{-19}$	–
G032.4727+00.2041	$4.1 \pm 0.2 \times 10^{-17}$	$3.4 \pm 0.6 \times 10^{-18}$	$4 \pm 1 \times 10^{-18}$	$<3.4 \times 10^{-18}$	$<4.3 \times 10^{-18}$	$<4.5 \times 10^{-18}$	$<3.0 \times 10^{-18}$	$2.1 \pm 0.3 \times 10^{-17}$	–
G032.8205−00.3300	$2.4 \pm 0.5 \times 10^{-18}$	$<2.1 \times 10^{-18}$	$<2.5 \times 10^{-18}$	$<2.4 \times 10^{-18}$	$1.8 \pm 0.2 \times 10^{-18}$	$<1.7 \times 10^{-18}$	$<2.1 \times 10^{-18}$	$<1.3 \times 10^{-18}$	–
G032.9957+00.0415	$9 \pm 1 \times 10^{-18}$	$<2.0 \times 10^{-18}$	$<2.0 \times 10^{-18}$	$<1.9 \times 10^{-18}$	$<1.2 \times 10^{-17}$	$<1.4 \times 10^{-17}$	$<2.1 \times 10^{-18}$	$<5.9 \times 10^{-18}$	–
G033.3891+00.1989	$4.5 \pm 0.5 \times 10^{-16}$	$3.0 \pm 0.2 \times 10^{-16}$	$2.5 \pm 0.2 \times 10^{-16}$	$1.3 \pm 0.1 \times 10^{-16}$	$<9.7 \times 10^{-17}$	$<6.1 \times 10^{-17}$	$<6.8 \times 10^{-17}$	$<5.9 \times 10^{-17}$	–
G034.0126−00.2832	$2.4 \pm 0.2 \times 10^{-16}$	$<3.5 \times 10^{-17}$	$<2.9 \times 10^{-17}$	$<2.7 \times 10^{-17}$	$<5.4 \times 10^{-17}$	$<4.0 \times 10^{-17}$	$<2.7 \times 10^{-17}$	$<3.8 \times 10^{-17}$	–

Table B1 – *continued*

Name	Brγ	Br 10	Br 11	Br 12/[Fe II]	H_2 2.1218 μm	H_2 2.2477 μm	Fluorescent Fe II	He I 2.0587 μm	Pfund?
G034.0500−00.2977	$4.3 \pm 0.2 \times 10^{-17}$	$5 \pm 1 \times 10^{-17}$	$4.5 \pm 0.3 \times 10^{-17}$	$2.7 \pm 0.3 \times 10^{-17}$	$<5.6 \times 10^{-18}$	$<4.7 \times 10^{-18}$	$<5.9 \times 10^{-18}$	$<8.6 \times 10^{-18}$	–
G034.4035+00.2282	$<5.0 \times 10^{-19}$	$<3.3 \times 10^{-19}$	$<3.7 \times 10^{-19}$	$<3.5 \times 10^{-19}$	$6.9 \pm 0.8 \times 10^{-19}$	$<4.8 \times 10^{-19}$	$<3.5 \times 10^{-19}$	$<4.1 \times 10^{-19}$	–
G034.6243−00.1300	$4.5 \pm 0.3 \times 10^{-17}$	$<1.1 \times 10^{-17}$	$<1.7 \times 10^{-17}$	$<1.6 \times 10^{-17}$	$<1.1 \times 10^{-17}$	$<1.1 \times 10^{-17}$	$<1.5 \times 10^{-17}$	$1.5 \pm 0.4 \times 10^{-17}$	–
G034.7569+00.0247	$<1.8 \times 10^{-19}$	–	–	–	$<1.8 \times 10^{-19}$	$<2.5 \times 10^{-19}$	–	$<1.6 \times 10^{-19}$	–
G034.8211+00.3519	$<5.8 \times 10^{-18}$	$<4.9 \times 10^{-18}$	–	–	$<6.5 \times 10^{-18}$	$<7.0 \times 10^{-18}$	$<4.5 \times 10^{-18}$	$<1.9 \times 10^{-17}$	–
G035.1979−00.7427	$3.5 \pm 0.5 \times 10^{-18}$	$<2.6 \times 10^{-18}$	$<2.7 \times 10^{-18}$	$5.2 \pm 0.8 \times 10^{-18}$	$3.6 \pm 0.7 \times 10^{-18}$	$<5.2 \times 10^{-18}$	$<3.1 \times 10^{-18}$	$2.2 \pm 0.2 \times 10^{-18}$	–
G036.8780−00.4728 – 1	$7 \pm 1 \times 10^{-19}$	$<3.3 \times 10^{-19}$	$<4.6 \times 10^{-19}$	$<4.4 \times 10^{-19}$	$3.6 \pm 0.8 \times 10^{-19}$	$<5.9 \times 10^{-19}$	$<3.4 \times 10^{-19}$	$<4.2 \times 10^{-19}$	–
G036.8780−00.4728 – 2	$7.3 \pm 1.0 \times 10^{-19}$	$<2.9 \times 10^{-19}$	$<1.9 \times 10^{-18}$	$<1.8 \times 10^{-18}$	$2.8 \pm 0.9 \times 10^{-19}$	$<6.1 \times 10^{-19}$	$<1.7 \times 10^{-18}$	$<4.5 \times 10^{-19}$	–
G036.9194+00.4825A	$5 \pm 1 \times 10^{-19}$	$<2.8 \times 10^{-19}$	$<3.7 \times 10^{-19}$	$<3.5 \times 10^{-19}$	$1.6 \pm 0.5 \times 10^{-19}$	$<3.8 \times 10^{-19}$	$<3.2 \times 10^{-19}$	$<2.4 \times 10^{-19}$	–
G037.5536+00.2008	$<1.2 \times 10^{-18}$	$<3.7 \times 10^{-19}$	$<5.8 \times 10^{-19}$	$<5.5 \times 10^{-19}$	$4.4 \pm 0.7 \times 10^{-19}$	$<1.7 \times 10^{-18}$	$<6.2 \times 10^{-19}$	$<5.4 \times 10^{-19}$	–
G039.4943−00.9933	$5.62 \pm 0.07 \times 10^{-17}$	$9.9 \pm 0.5 \times 10^{-18}$	$6 \pm 1 \times 10^{-18}$	$4.1 \pm 0.5 \times 10^{-18}$	$<7.6 \times 10^{-18}$	$<7.8 \times 10^{-18}$	$2.6 \pm 0.7 \times 10^{-18}$	$<4.5 \times 10^{-18}$	P
G042.0341+00.1905A	$6.5 \pm 0.5 \times 10^{-17}$	$<1.2 \times 10^{-17}$	$<1.5 \times 10^{-17}$	$<1.4 \times 10^{-17}$	$<3.3 \times 10^{-17}$	$<2.9 \times 10^{-17}$	$<1.1 \times 10^{-17}$	$<1.9 \times 10^{-17}$	–
G042.0977+00.3521	$8 \pm 2 \times 10^{-19}$	$<6.8 \times 10^{-19}$	$<9.7 \times 10^{-19}$	$<9.2 \times 10^{-19}$	$9 \pm 1 \times 10^{-19}$	$<3.8 \times 10^{-19}$	$<8.6 \times 10^{-19}$	$<5.3 \times 10^{-19}$	–
G042.1099−00.4466	$4.1 \pm 0.9 \times 10^{-18}$	$<1.5 \times 10^{-18}$	$<1.5 \times 10^{-18}$	$<1.4 \times 10^{-18}$	$<1.5 \times 10^{-18}$	$<2.4 \times 10^{-18}$	$<1.6 \times 10^{-18}$	$<1.3 \times 10^{-17}$	–
G043.1635−00.0697A	$6.7 \pm 0.1 \times 10^{-18}$	$5.1 \pm 0.5 \times 10^{-18}$	$5.0 \pm 0.9 \times 10^{-18}$	$2.8 \pm 0.3 \times 10^{-18}$	$<6.4 \times 10^{-19}$	$<6.3 \times 10^{-19}$	$1.6 \pm 0.2 \times 10^{-18}$	$<7.5 \times 10^{-19}$	P
G043.5216−00.6476	$6.4 \pm 0.5 \times 10^{-18}$	$2.5 \pm 0.3 \times 10^{-18}$	$<3.3 \times 10^{-18}$	$<3.1 \times 10^{-18}$	$4.6 \pm 0.9 \times 10^{-18}$	$<3.1 \times 10^{-18}$	$3.7 \pm 0.7 \times 10^{-18}$	$<2.9 \times 10^{-18}$	–
G043.9956−00.0111	$1.7 \pm 0.2 \times 10^{-17}$	$1.9 \pm 0.3 \times 10^{-17}$	$8 \pm 2 \times 10^{-18}$	$1.0 \pm 0.1 \times 10^{-17}$	$1.3 \pm 0.1 \times 10^{-17}$	$<4.9 \times 10^{-18}$	$8 \pm 1 \times 10^{-18}$	$<4.7 \times 10^{-18}$	–
G044.3103+00.0416	$5.2 \pm 0.1 \times 10^{-18}$	$1.9 \pm 0.3 \times 10^{-18}$	$8 \pm 2 \times 10^{-19}$	$9 \pm 1 \times 10^{-19}$	$1.4 \pm 0.4 \times 10^{-18}$	$<4.4 \times 10^{-19}$	$<4.6 \times 10^{-19}$	$6 \pm 2 \times 10^{-19}$	–
G045.1894−00.4387	$3.78 \pm 0.07 \times 10^{-16}$	$7 \pm 1 \times 10^{-17}$	$6 \pm 2 \times 10^{-17}$	$3 \pm 1 \times 10^{-17}$	$<6.4 \times 10^{-17}$	$<6.5 \times 10^{-17}$	$2.5 \pm 0.8 \times 10^{-17}$	$4 \pm 1 \times 10^{-17}$	–
G045.4641+00.0284	$1.20 \pm 0.09 \times 10^{-19}$	$<4.4 \times 10^{-20}$	$<4.4 \times 10^{-20}$	$<4.1 \times 10^{-20}$	$3.7 \pm 0.8 \times 10^{-20}$	$<4.8 \times 10^{-20}$	$<4.8 \times 10^{-20}$	$<4.6 \times 10^{-20}$	–
G048.9897−00.2992A	$1.2 \pm 0.3 \times 10^{-18}$	$<7.0 \times 10^{-19}$	$<8.8 \times 10^{-19}$	$2.4 \pm 0.2 \times 10^{-18}$	$4.3 \pm 0.2 \times 10^{-18}$	$<8.9 \times 10^{-19}$	$<7.5 \times 10^{-19}$	$<8.8 \times 10^{-19}$	–
G049.0431−01.0787	$<9.9 \times 10^{-19}$	$<6.8 \times 10^{-19}$	$<5.4 \times 10^{-19}$	$7 \pm 2 \times 10^{-19}$	$6.6 \pm 0.3 \times 10^{-18}$	$<9.8 \times 10^{-19}$	$<5.5 \times 10^{-19}$	$<9.0 \times 10^{-19}$	–
G049.4227−00.3715	$1.62 \pm 0.08 \times 10^{-16}$	$<1.0 \times 10^{-16}$	$<4.1 \times 10^{-17}$	$<3.9 \times 10^{-17}$	$<3.0 \times 10^{-17}$	$<4.3 \times 10^{-17}$	$<3.6 \times 10^{-17}$	$<4.5 \times 10^{-17}$	–
G049.4883−00.3545B	$<6.7 \times 10^{-18}$	$<7.2 \times 10^{-18}$	$<8.1 \times 10^{-18}$	$<7.7 \times 10^{-18}$	$<5.8 \times 10^{-18}$	$<6.0 \times 10^{-18}$	$<9.0 \times 10^{-18}$	$<9.1 \times 10^{-18}$	–
G050.0721+00.5591	$1.6 \pm 0.2 \times 10^{-18}$	$<7.4 \times 10^{-19}$	$<1.8 \times 10^{-18}$	$<1.7 \times 10^{-18}$	$2.0 \pm 0.2 \times 10^{-18}$	$<7.7 \times 10^{-19}$	$<1.4 \times 10^{-18}$	$<7.9 \times 10^{-19}$	–
G050.2213−00.6063	$2.9 \pm 0.2 \times 10^{-18}$	$1.1 \pm 0.2 \times 10^{-18}$	$9 \pm 2 \times 10^{-19}$	$9 \pm 2 \times 10^{-19}$	$<5.1 \times 10^{-18}$	$<6.4 \times 10^{-18}$	$7 \pm 2 \times 10^{-19}$	$<2.9 \times 10^{-18}$	–
G050.2844−00.3925A	$9 \pm 1 \times 10^{-18}$	$<7.0 \times 10^{-18}$	$<1.0 \times 10^{-17}$	$<9.8 \times 10^{-18}$	$5 \pm 1 \times 10^{-18}$	$<1.2 \times 10^{-17}$	$<8.6 \times 10^{-18}$	$5 \pm 1 \times 10^{-18}$	–
G052.2025+00.7217A	$<2.0 \times 10^{-17}$	$<4.1 \times 10^{-18}$	$<3.1 \times 10^{-18}$	$6 \pm 1 \times 10^{-18}$	$<1.1 \times 10^{-17}$	$<1.6 \times 10^{-17}$	$2.8 \pm 0.9 \times 10^{-18}$	$8 \pm 1 \times 10^{-18}$	–
G052.2078+00.6890	$1.7 \pm 0.1 \times 10^{-17}$	$<6.7 \times 10^{-18}$	$<7.7 \times 10^{-18}$	$<7.2 \times 10^{-18}$	$1.1 \pm 0.2 \times 10^{-17}$	$<6.8 \times 10^{-18}$	$<8.0 \times 10^{-18}$	$<6.1 \times 10^{-18}$	–
G052.5405−00.9272	$<6.5 \times 10^{-18}$	$<5.6 \times 10^{-18}$	$<6.6 \times 10^{-18}$	$<6.2 \times 10^{-18}$	$<6.0 \times 10^{-18}$	$<7.3 \times 10^{-18}$	$<5.4 \times 10^{-18}$	$<9.3 \times 10^{-18}$	–
G052.9217+00.4142	$1.1 \pm 0.4 \times 10^{-18}$	$<1.9 \times 10^{-18}$	$<3.1 \times 10^{-18}$	$<2.9 \times 10^{-18}$	$1.9 \pm 0.6 \times 10^{-18}$	$<5.9 \times 10^{-18}$	$<2.6 \times 10^{-18}$	$<2.9 \times 10^{-18}$	–
G053.1417+00.0705	$<1.5 \times 10^{-18}$	$<4.4 \times 10^{-19}$	$<6.0 \times 10^{-19}$	$<5.7 \times 10^{-19}$	$4.1 \pm 0.5 \times 10^{-19}$	$<1.7 \times 10^{-18}$	$<4.4 \times 10^{-19}$	$<5.4 \times 10^{-19}$	–
G053.5343−00.7943	$1.31 \pm 0.05 \times 10^{-17}$	$6.4 \pm 0.6 \times 10^{-18}$	$5.2 \pm 0.7 \times 10^{-18}$	$7.0 \pm 0.9 \times 10^{-18}$	$7.5 \pm 0.5 \times 10^{-18}$	$<1.1 \times 10^{-17}$	$2.4 \pm 0.6 \times 10^{-18}$	$<7.4 \times 10^{-18}$	–
G055.1581−00.2991A	$1.64 \pm 0.09 \times 10^{-17}$	$<2.8 \times 10^{-18}$	$<3.4 \times 10^{-18}$	$<3.2 \times 10^{-18}$	$7.8 \pm 0.9 \times 10^{-18}$	$<4.5 \times 10^{-18}$	$<3.4 \times 10^{-18}$	$<5.8 \times 10^{-18}$	–
G056.3694−00.6333	$1.4 \pm 0.4 \times 10^{-18}$	$<1.1 \times 10^{-18}$	$<1.6 \times 10^{-18}$	$<1.5 \times 10^{-18}$	$2.1 \pm 0.2 \times 10^{-18}$	$<1.2 \times 10^{-18}$	$<1.4 \times 10^{-18}$	$<1.8 \times 10^{-18}$	–
G056.4120−00.0277	$4.8 \pm 0.4 \times 10^{-16}$	$4.5 \pm 0.4 \times 10^{-16}$	$3.6 \pm 0.3 \times 10^{-16}$	$2.0 \pm 0.3 \times 10^{-16}$	$<9.8 \times 10^{-17}$	$<1.2 \times 10^{-16}$	$<8.3 \times 10^{-17}$	$<2.3 \times 10^{-16}$	–
G059.3614−00.2068	$9 \pm 3 \times 10^{-18}$	$7 \pm 2 \times 10^{-18}$	$1.3 \pm 0.3 \times 10^{-17}$	$2.1 \pm 0.2 \times 10^{-17}$	$1.8 \pm 0.2 \times 10^{-17}$	$<9.3 \times 10^{-18}$	$8 \pm 2 \times 10^{-18}$	$<8.7 \times 10^{-18}$	–
G059.6403−00.1812A	$5.48 \pm 0.04 \times 10^{-17}$	$1.47 \pm 0.05 \times 10^{-17}$	$9.7 \pm 0.9 \times 10^{-18}$	$9.2 \pm 0.5 \times 10^{-18}$	$<8.4 \times 10^{-19}$	$<1.2 \times 10^{-18}$	$<9.7 \times 10^{-19}$	$2.8 \pm 0.4 \times 10^{-18}$	P
G059.7831+00.0648	$<2.8 \times 10^{-18}$	$<1.2 \times 10^{-18}$	$<1.5 \times 10^{-18}$	$<1.4 \times 10^{-18}$	$4.5 \pm 0.2 \times 10^{-18}$	$9 \pm 1 \times 10^{-19}$	$<1.5 \times 10^{-18}$	$<1.4 \times 10^{-18}$	–
G059.8329+00.6729	$4.2 \pm 0.4 \times 10^{-18}$	$<9.2 \times 10^{-19}$	$<2.3 \times 10^{-18}$	$<2.2 \times 10^{-18}$	$5.7 \pm 0.2 \times 10^{-18}$	$<9.9 \times 10^{-19}$	$<9.9 \times 10^{-19}$	$<7.5 \times 10^{-19}$	–
G060.5750−00.1861	$<3.6 \times 10^{-18}$	$<2.9 \times 10^{-18}$	$<2.1 \times 10^{-18}$	$<2.0 \times 10^{-18}$	$1.0 \pm 0.2 \times 10^{-17}$	$<2.9 \times 10^{-18}$	$<2.1 \times 10^{-18}$	$<1.8 \times 10^{-17}$	–
G063.1140+00.3416	$3.4 \pm 0.3 \times 10^{-16}$	$4.9 \pm 0.3 \times 10^{-17}$	$<3.4 \times 10^{-17}$	$3.5 \pm 0.3 \times 10^{-17}$	$<1.7 \times 10^{-16}$	$<2.1 \times 10^{-16}$	$9 \pm 2 \times 10^{-18}$	$<1.2 \times 10^{-16}$	–
G065.7798−02.6121	$4.4 \pm 0.3 \times 10^{-17}$	$1.2 \pm 0.2 \times 10^{-17}$	$1.9 \pm 0.3 \times 10^{-17}$	$1.0 \pm 0.1 \times 10^{-17}$	$1.5 \pm 0.2 \times 10^{-17}$	$<8.3 \times 10^{-18}$	$<8.8 \times 10^{-18}$	$1.0 \pm 0.2 \times 10^{-17}$	–
G068.2040+00.2387	$8.3 \pm 0.4 \times 10^{-18}$	$<2.1 \times 10^{-18}$	$<3.7 \times 10^{-18}$	$2.5 \pm 0.7 \times 10^{-18}$	$<3.7 \times 10^{-18}$	$<1.9 \times 10^{-18}$	$<2.8 \times 10^{-18}$	$<2.9 \times 10^{-18}$	–
G071.8944+01.3107	$5.4 \pm 0.8 \times 10^{-18}$	$<2.7 \times 10^{-18}$	$<3.3 \times 10^{-18}$	$<3.1 \times 10^{-18}$	$<9.8 \times 10^{-18}$	$<2.0 \times 10^{-17}$	$<3.5 \times 10^{-18}$	$<1.8 \times 10^{-18}$	–
G072.2479+00.2617B	$6 \pm 1 \times 10^{-19}$	$<4.3 \times 10^{-19}$	$<3.8 \times 10^{-19}$	$<3.6 \times 10^{-19}$	$5.9 \pm 0.9 \times 10^{-19}$	$3.2 \pm 0.9 \times 10^{-19}$	$<4.7 \times 10^{-19}$	$<3.7 \times 10^{-19}$	–
G073.0633+01.7958	$<2.6 \times 10^{-18}$	$<5.6 \times 10^{-18}$	$<2.8 \times 10^{-18}$	$4.9 \pm 0.5 \times 10^{-18}$	$3.46 \pm 0.08 \times 10^{-17}$	$5.4 \pm 0.6 \times 10^{-18}$	$<2.9 \times 10^{-18}$	$<3.3 \times 10^{-18}$	–
G073.6525+00.1944	$6 \pm 1 \times 10^{-18}$	$2.7 \pm 0.8 \times 10^{-18}$	$1.7 \pm 0.4 \times 10^{-17}$	$2.5 \pm 0.1 \times 10^{-17}$	$3.1 \pm 0.1 \times 10^{-17}$	$<8.6 \times 10^{-18}$	$1.0 \pm 0.3 \times 10^{-17}$	$<1.3 \times 10^{-17}$	–
G073.6952−00.9996	$3.5 \pm 0.2 \times 10^{-17}$	$5.5 \pm 0.3 \times 10^{-18}$	$6.1 \pm 0.5 \times 10^{-18}$	$4.0 \pm 0.3 \times 10^{-18}$	$<3.9 \times 10^{-17}$	$<3.8 \times 10^{-17}$	$<1.4 \times 10^{-17}$	$-1.3 \pm 0.3 \times 10^{-17}$	–
G075.6014+01.6394	$2.2 \pm 0.1 \times 10^{-18}$	$<5.5 \times 10^{-19}$	$<4.8 \times 10^{-19}$	$1.1 \pm 0.1 \times 10^{-18}$	$2.0 \pm 0.1 \times 10^{-18}$	$7 \pm 1 \times 10^{-19}$	$<4.5 \times 10^{-19}$	$<4.0 \times 10^{-19}$	–
G075.7666+00.3424 – 1	$1.6 \pm 0.2 \times 10^{-16}$	$1.3 \pm 0.1 \times 10^{-16}$	$5 \pm 1 \times 10^{-17}$	$4.4 \pm 0.9 \times 10^{-17}$	$<2.1 \times 10^{-17}$	$<2.2 \times 10^{-17}$	$3.7 \pm 1.0 \times 10^{-17}$	$<7.7 \times 10^{-17}$	–
G075.7666+00.3424 – 2	$3.37 \pm 0.07 \times 10^{-17}$	$3.8 \pm 0.7 \times 10^{-18}$	$3.3 \pm 0.9 \times 10^{-18}$	$2.5 \pm 0.8 \times 10^{-18}$	$<4.3 \times 10^{-18}$	$<5.5 \times 10^{-18}$	$<2.5 \times 10^{-18}$	$<3.1 \times 10^{-18}$	–

Table B1 – *continued*

Name	Brγ	Br 10	Br 11	Br 12/[Fe II]	H_2 2.1218 μm	H_2 2.2477 μm	Fluorescent. Fe II	He I 2.0587 μM	Pfund?
G076.0902+00.1412	$2.94 \pm 0.10 \times 10^{-18}$	$<7.2 \times 10^{-19}$	$<8.0 \times 10^{-19}$	$<7.6 \times 10^{-19}$	$<1.6 \times 10^{-18}$	$<1.7 \times 10^{-18}$	$<7.5 \times 10^{-19}$	$<1.2 \times 10^{-18}$	–
G076.3829−00.6210	$1.83 \pm 0.04 \times 10^{-15}$	$5.8 \pm 0.3 \times 10^{-16}$	$<2.0 \times 10^{-16}$	$3.08 \pm 0.07 \times 10^{-16}$	$<1.6 \times 10^{-16}$	$<7.7 \times 10^{-17}$	$2.3 \pm 0.2 \times 10^{-16}$	$-3.0 \pm 0.4 \times 10^{-16}$	–
G077.4052−01.2136	$1.97 \pm 0.02 \times 10^{-17}$	$2.8 \pm 0.2 \times 10^{-18}$	$2.0 \pm 0.4 \times 10^{-18}$	$8 \pm 2 \times 10^{-19}$	$1.5 \pm 0.2 \times 10^{-18}$	$<9.0 \times 10^{-19}$	$<7.4 \times 10^{-19}$	$6 \pm 1 \times 10^{-19}$	–
G077.4622+01.7600 – 1	$2.9 \pm 0.4 \times 10^{-18}$	$2.3 \pm 0.5 \times 10^{-18}$	$3.4 \pm 0.7 \times 10^{-18}$	$6.1 \pm 0.5 \times 10^{-18}$	$3.7 \pm 0.4 \times 10^{-18}$	$<1.3 \times 10^{-18}$	$<1.6 \times 10^{-18}$	$<1.3 \times 10^{-18}$	–
G077.4622+01.7600 – 2	$1.3 \pm 0.2 \times 10^{-18}$	$<9.1 \times 10^{-19}$	$<9.6 \times 10^{-18}$	$5.1 \pm 0.4 \times 10^{-18}$	$7.3 \pm 0.2 \times 10^{-18}$	$<1.1 \times 10^{-18}$	$<7.4 \times 10^{-19}$	$<8.6 \times 10^{-19}$	–
G077.8999+01.7678	$4.9 \pm 0.5 \times 10^{-18}$	$2.4 \pm 0.8 \times 10^{-18}$	$4.1 \pm 0.7 \times 10^{-18}$	$<3.0 \times 10^{-18}$	$<1.1 \times 10^{-17}$	$<1.3 \times 10^{-17}$	$<3.1 \times 10^{-18}$	$3.7 \pm 0.4 \times 10^{-18}$	–
G078.1224+03.6320	$<3.2 \times 10^{-18}$	$<5.2 \times 10^{-18}$	$<5.9 \times 10^{-19}$	$<5.5 \times 10^{-19}$	$7.99 \pm 0.08 \times 10^{-17}$	$7.2 \pm 0.8 \times 10^{-18}$	$1.6 \pm 0.1 \times 10^{-18}$	$<1.1 \times 10^{-18}$	–
G078.4373+02.6584B	$<5.0 \times 10^{-18}$	$<1.2 \times 10^{-18}$	$<1.8 \times 10^{-18}$	$<1.7 \times 10^{-18}$	$4.3 \pm 0.4 \times 10^{-18}$	$<3.9 \times 10^{-18}$	$<9.6 \times 10^{-19}$	$<2.6 \times 10^{-18}$	–
G078.4705−00.1830	$2.23 \pm 0.06 \times 10^{-18}$	$<2.4 \times 10^{-19}$	$<3.4 \times 10^{-19}$	$<3.2 \times 10^{-19}$	$<2.7 \times 10^{-19}$	$<4.0 \times 10^{-19}$	$<2.8 \times 10^{-19}$	$<3.8 \times 10^{-19}$	–
G078.4754+01.0421	$9.4 \pm 0.9 \times 10^{-18}$	$<4.7 \times 10^{-18}$	$<2.5 \times 10^{-18}$	$<2.4 \times 10^{-18}$	$<3.7 \times 10^{-17}$	$<4.7 \times 10^{-17}$	$<3.1 \times 10^{-18}$	$4 \pm 1 \times 10^{-18}$	–
G078.7641+01.6862	$<5.5 \times 10^{-19}$	$<3.5 \times 10^{-19}$	$<5.4 \times 10^{-19}$	$<5.1 \times 10^{-19}$	$2.4 \pm 0.1 \times 10^{-18}$	$<3.4 \times 10^{-19}$	$<4.7 \times 10^{-19}$	$<3.7 \times 10^{-19}$	–
G078.8867+00.7087	$<4.1 \times 10^{-16}$	$<5.7 \times 10^{-17}$	$<3.3 \times 10^{-17}$	$<3.2 \times 10^{-17}$	$2.2 \pm 0.1 \times 10^{-17}$	$<3.6 \times 10^{-16}$	$<3.7 \times 10^{-17}$	$<1.6 \times 10^{-16}$	–
G078.9761+00.3567	$1.00 \pm 0.03 \times 10^{-15}$	$8.4 \pm 0.6 \times 10^{-16}$	$7 \pm 1 \times 10^{-16}$	$5.9 \pm 0.5 \times 10^{-16}$	$1.1 \pm 0.3 \times 10^{-16}$	$<4.8 \times 10^{-17}$	$2.1 \pm 0.2 \times 10^{-16}$	$<5.9 \times 10^{-17}$	P
G079.1272+02.2782	$4.2 \pm 0.3 \times 10^{-17}$	$<5.1 \times 10^{-18}$	$<8.2 \times 10^{-18}$	$<7.8 \times 10^{-18}$	$1.1 \pm 0.2 \times 10^{-17}$	$<8.9 \times 10^{-18}$	$<6.0 \times 10^{-18}$	$<6.5 \times 10^{-18}$	–
G080.0467+00.3101	$6.1 \pm 0.9 \times 10^{-18}$	$3.4 \pm 0.6 \times 10^{-18}$	$<1.7 \times 10^{-17}$	$1.06 \pm 0.09 \times 10^{-17}$	$4.0 \pm 0.1 \times 10^{-17}$	$6 \pm 1 \times 10^{-18}$	$2.7 \pm 0.6 \times 10^{-18}$	$<6.6 \times 10^{-18}$	–
G080.1909+00.5353	$1.16 \pm 0.08 \times 10^{-17}$	$<1.3 \times 10^{-17}$	$<1.2 \times 10^{-17}$	$1.2 \pm 0.2 \times 10^{-17}$	$9 \pm 2 \times 10^{-18}$	$<2.3 \times 10^{-17}$	$<1.0 \times 10^{-17}$	$2.0 \pm 0.1 \times 10^{-17}$	–
G080.8282+00.5670A	$<5.0 \times 10^{-17}$	$<1.8 \times 10^{-17}$	$1.9 \pm 0.4 \times 10^{-18}$	$<1.5 \times 10^{-17}$	$<3.6 \times 10^{-17}$	$<4.1 \times 10^{-17}$	$<1.6 \times 10^{-17}$	$<2.9 \times 10^{-17}$	–
G080.8645+00.4197	$1.39 \pm 0.08 \times 10^{-18}$	–	–	–	$<9.2 \times 10^{-19}$	$<1.5 \times 10^{-18}$	–	$<4.1 \times 10^{-19}$	–
G081.5168+00.1926	$<4.8 \times 10^{-18}$	$<1.8 \times 10^{-18}$	$<1.8 \times 10^{-18}$	$<1.7 \times 10^{-18}$	$5.0 \pm 0.4 \times 10^{-18}$	$<3.4 \times 10^{-18}$	$<1.8 \times 10^{-18}$	$<2.1 \times 10^{-18}$	–
G081.7131+00.5792	$3.40 \pm 0.06 \times 10^{-16}$	$1.20 \pm 0.04 \times 10^{-16}$	$<3.2 \times 10^{-17}$	$8.7 \pm 0.3 \times 10^{-17}$	$<1.1 \times 10^{-17}$	$<1.2 \times 10^{-17}$	$2.1 \pm 0.3 \times 10^{-17}$	$3.5 \pm 0.2 \times 10^{-17}$	P
G081.7624+00.5916	$7.8 \pm 0.3 \times 10^{-18}$	$<6.7 \times 10^{-19}$	$<7.1 \times 10^{-19}$	$<6.8 \times 10^{-19}$	$<2.5 \times 10^{-18}$	$<3.5 \times 10^{-18}$	$<6.6 \times 10^{-19}$	$<1.2 \times 10^{-18}$	P
G082.5682+00.4040A	$1.74 \pm 0.04 \times 10^{-16}$	$1.1 \pm 0.1 \times 10^{-16}$	$1.46 \pm 0.08 \times 10^{-16}$	$1.35 \pm 0.09 \times 10^{-16}$	$<2.8 \times 10^{-17}$	$<3.4 \times 10^{-17}$	$<3.3 \times 10^{-17}$	$2.4 \pm 0.6 \times 10^{-17}$	–
G083.7071+03.2817	$3.0 \pm 0.2 \times 10^{-16}$	$1.60 \pm 0.07 \times 10^{-16}$	$8.7 \pm 0.6 \times 10^{-17}$	$5.3 \pm 0.5 \times 10^{-17}$	$<9.9 \times 10^{-17}$	$<8.8 \times 10^{-17}$	$<4.6 \times 10^{-17}$	$<4.8 \times 10^{-17}$	–
G084.3065+01.8933	$1.31 \pm 0.03 \times 10^{-16}$	$5.4 \pm 0.5 \times 10^{-17}$	$6.5 \pm 0.5 \times 10^{-17}$	$2.2 \pm 0.3 \times 10^{-17}$	$<1.9 \times 10^{-17}$	$<1.7 \times 10^{-17}$	$<1.0 \times 10^{-17}$	$<1.3 \times 10^{-17}$	P
G085.4102+00.0032A	$4.9 \pm 0.4 \times 10^{-18}$	$<1.0 \times 10^{-18}$	$<1.3 \times 10^{-18}$	$<1.2 \times 10^{-18}$	$<4.0 \times 10^{-18}$	$<5.1 \times 10^{-18}$	$<1.2 \times 10^{-18}$	$<2.0 \times 10^{-18}$	–
G089.6368+00.1732	$3.17 \pm 0.09 \times 10^{-17}$	$5.6 \pm 0.7 \times 10^{-18}$	$3.5 \pm 0.5 \times 10^{-18}$	$2.5 \pm 0.4 \times 10^{-18}$	$<8.7 \times 10^{-18}$	$<8.4 \times 10^{-18}$	$<2.1 \times 10^{-18}$	$<4.4 \times 10^{-18}$	P
G090.2095+02.0405	$7 \pm 1 \times 10^{-17}$	$<7.5 \times 10^{-17}$	$<8.2 \times 10^{-17}$	$<7.8 \times 10^{-17}$	$<6.7 \times 10^{-17}$	$<6.9 \times 10^{-17}$	$<7.8 \times 10^{-17}$	$<6.1 \times 10^{-17}$	–
G094.3228−00.1671	$7.0 \pm 0.5 \times 10^{-17}$	$1.5 \pm 0.3 \times 10^{-17}$	$1.1 \pm 0.2 \times 10^{-17}$	$8 \pm 2 \times 10^{-18}$	$<5.0 \times 10^{-17}$	$<7.0 \times 10^{-18}$	$<7.0 \times 10^{-18}$	$<7.3 \times 10^{-18}$	P
G094.4637−00.8043	$<1.6 \times 10^{-18}$	$<6.0 \times 10^{-19}$	$<2.9 \times 10^{-18}$	$4.1 \pm 0.3 \times 10^{-18}$	$4.9 \pm 0.2 \times 10^{-18}$	$6 \pm 2 \times 10^{-19}$	$<8.8 \times 10^{-19}$	$<8.4 \times 10^{-19}$	–
G095.0026−01.5779	$<1.0 \times 10^{-18}$	$<9.7 \times 10^{-19}$	$<8.2 \times 10^{-19}$	$6 \pm 2 \times 10^{-19}$	$4.2 \pm 0.2 \times 10^{-18}$	$<1.1 \times 10^{-18}$	$<9.7 \times 10^{-19}$	$<7.1 \times 10^{-19}$	–
G095.0531+03.9724	$<5.1 \times 10^{-19}$	$<4.2 \times 10^{-19}$	$<1.7 \times 10^{-18}$	$<1.6 \times 10^{-18}$	$4.8 \pm 0.2 \times 10^{-18}$	$<4.2 \times 10^{-19}$	$<7.6 \times 10^{-19}$	$<4.0 \times 10^{-19}$	–
G096.3597+01.2982	$4.2 \pm 0.3 \times 10^{-17}$	$<1.6 \times 10^{-17}$	$<1.8 \times 10^{-17}$	$<1.7 \times 10^{-17}$	$2.9 \pm 0.4 \times 10^{-17}$	$<1.0 \times 10^{-17}$	$<1.8 \times 10^{-17}$	$<1.3 \times 10^{-17}$	–
G096.4353+01.3233A – 1	$3.25 \pm 0.09 \times 10^{-17}$	$1.6 \pm 0.1 \times 10^{-17}$	$2.2 \pm 0.2 \times 10^{-17}$	$1.3 \pm 0.1 \times 10^{-17}$	$3.3 \pm 0.8 \times 10^{-18}$	$<2.4 \times 10^{-18}$	$<2.1 \times 10^{-18}$	$<2.7 \times 10^{-18}$	–
G096.4353+01.3233A – 2	$9.4 \pm 0.3 \times 10^{-18}$	$3.1 \pm 0.4 \times 10^{-18}$	$2.9 \pm 0.5 \times 10^{-18}$	$4.7 \pm 0.4 \times 10^{-18}$	$7.5 \pm 0.3 \times 10^{-18}$	$<2.3 \times 10^{-18}$	$<1.5 \times 10^{-18}$	$<1.6 \times 10^{-18}$	–
G097.5268+03.1837C	$1.4 \pm 0.1 \times 10^{-17}$	$6 \pm 2 \times 10^{-18}$	$3.9 \pm 1.0 \times 10^{-18}$	$<2.7 \times 10^{-18}$	$<3.3 \times 10^{-18}$	$<7.0 \times 10^{-18}$	$<2.6 \times 10^{-18}$	$<2.2 \times 10^{-18}$	–
G097.9978+01.4688	$9.6 \pm 0.2 \times 10^{-17}$	$3.2 \pm 0.2 \times 10^{-17}$	$<1.2 \times 10^{-17}$	$2.1 \pm 0.1 \times 10^{-17}$	$4.0 \pm 0.3 \times 10^{-18}$	$<6.6 \times 10^{-18}$	$1.61 \pm 0.08 \times 10^{-17}$	$5 \pm 1 \times 10^{-18}$	–
G098.8555+02.9344	$<1.0 \times 10^{-18}$	$<8.1 \times 10^{-18}$	$<2.1 \times 10^{-18}$	$1.93 \pm 0.04 \times 10^{-17}$	$6.5 \pm 0.1 \times 10^{-17}$	$6.5 \pm 0.5 \times 10^{-18}$	$4.4 \pm 0.4 \times 10^{-18}$	$<1.5 \times 10^{-18}$	–
G100.1620+01.6647	$<1.4 \times 10^{-18}$	$<2.3 \times 10^{-18}$	$<4.2 \times 10^{-18}$	$<4.0 \times 10^{-18}$	$1.8 \pm 0.4 \times 10^{-18}$	$<1.3 \times 10^{-18}$	$<4.6 \times 10^{-18}$	$<1.2 \times 10^{-18}$	–
G100.1685+02.0266	$7 \pm 1 \times 10^{-18}$	$<3.5 \times 10^{-18}$	$<1.1 \times 10^{-17}$	$6.2 \pm 0.8 \times 10^{-18}$	$1.5 \pm 0.1 \times 10^{-17}$	$4 \pm 1 \times 10^{-18}$	$<5.7 \times 10^{-18}$	$<3.1 \times 10^{-18}$	–
G100.2124+01.8829	$1.4 \pm 0.1 \times 10^{-17}$	$<2.8 \times 10^{-18}$	$<4.2 \times 10^{-18}$	$5.8 \pm 0.8 \times 10^{-18}$	$1.37 \pm 0.06 \times 10^{-17}$	$2.0 \pm 0.6 \times 10^{-18}$	$<3.6 \times 10^{-18}$	$<3.5 \times 10^{-18}$	–
G100.3779−03.5784	$<3.9 \times 10^{-18}$	$<2.0 \times 10^{-18}$	$2.2 \pm 0.6 \times 10^{-18}$	$1.4 \pm 0.2 \times 10^{-18}$	$1.48 \pm 0.06 \times 10^{-17}$	$<3.8 \times 10^{-18}$	$<2.2 \times 10^{-18}$	$<2.8 \times 10^{-18}$	–
G102.3533+03.6360	$1.2 \pm 0.3 \times 10^{-17}$	$<1.7 \times 10^{-17}$	$4.4 \pm 0.9 \times 10^{-17}$	$2.9 \pm 0.6 \times 10^{-17}$	$1.0 \pm 0.2 \times 10^{-17}$	$<3.8 \times 10^{-17}$	$<1.3 \times 10^{-17}$	$-4 \pm 1 \times 10^{-17}$	–
G103.8034+00.4062	$<9.9 \times 10^{-19}$	$<8.3 \times 10^{-19}$	$<7.9 \times 10^{-19}$	$<7.5 \times 10^{-19}$	$3.1 \pm 0.2 \times 10^{-18}$	$<5.8 \times 10^{-19}$	$<7.0 \times 10^{-19}$	$<9.5 \times 10^{-19}$	–
G103.8744+01.8558	$<5.2 \times 10^{-18}$	$<2.1 \times 10^{-18}$	$<2.8 \times 10^{-18}$	$<2.7 \times 10^{-18}$	$<5.1 \times 10^{-18}$	$<5.3 \times 10^{-18}$	$<2.6 \times 10^{-18}$	$<3.1 \times 10^{-18}$	–
G105.5072+00.2294	$9 \pm 2 \times 10^{-19}$	$<1.5 \times 10^{-18}$	$<1.3 \times 10^{-18}$	$<1.3 \times 10^{-18}$	$4.9 \pm 0.3 \times 10^{-18}$	$<1.3 \times 10^{-18}$	$<1.2 \times 10^{-18}$	$<1.1 \times 10^{-18}$	–
G107.6823−02.2423A	$7.0 \pm 0.1 \times 10^{-17}$	$1.5 \pm 0.1 \times 10^{-17}$	$<4.7 \times 10^{-18}$	$1.62 \pm 0.10 \times 10^{-17}$	$2.1 \pm 0.2 \times 10^{-18}$	$<1.6 \times 10^{-18}$	$9.5 \pm 0.5 \times 10^{-18}$	$4.7 \pm 0.7 \times 10^{-18}$	–
G108.7575−00.9863	$2.8 \pm 0.2 \times 10^{-18}$	$<1.2 \times 10^{-18}$	$<1.1 \times 10^{-18}$	$<1.0 \times 10^{-18}$	$<1.0 \times 10^{-17}$	$<1.6 \times 10^{-17}$	$<9.3 \times 10^{-19}$	$<5.0 \times 10^{-18}$	–
G110.8038−02.5649	$1.76 \pm 0.09 \times 10^{-17}$	$6.3 \pm 0.6 \times 10^{-18}$	$<6.6 \times 10^{-18}$	$7.5 \pm 0.9 \times 10^{-18}$	$7 \pm 2 \times 10^{-18}$	$<6.4 \times 10^{-18}$	$4.0 \pm 0.7 \times 10^{-18}$	$<4.9 \times 10^{-18}$	–
G111.2348−01.2385	$1.38 \pm 0.10 \times 10^{-17}$	$1.3 \pm 0.1 \times 10^{-17}$	$9 \pm 1 \times 10^{-18}$	$6 \pm 1 \times 10^{-18}$	$8.4 \pm 0.1 \times 10^{-17}$	$8 \pm 1 \times 10^{-18}$	$6.1 \pm 1.0 \times 10^{-18}$	$<4.4 \times 10^{-18}$	–
G139.9091+00.1969A	$2.46 \pm 0.05 \times 10^{-17}$	$1.9 \pm 0.2 \times 10^{-17}$	$2.2 \pm 0.2 \times 10^{-17}$	$2.2 \pm 0.2 \times 10^{-17}$	$8.1 \pm 0.7 \times 10^{-18}$	$<2.3 \times 10^{-18}$	$8 \pm 2 \times 10^{-18}$	$<3.4 \times 10^{-18}$	–
G141.9996+01.8202	$1.27 \pm 0.05 \times 10^{-15}$	$4.2 \pm 0.2 \times 10^{-16}$	$<3.7 \times 10^{-16}$	$3.8 \pm 0.2 \times 10^{-16}$	$<4.0 \times 10^{-16}$	$<3.7 \times 10^{-16}$	$1.9 \pm 0.2 \times 10^{-16}$	$<2.1 \times 10^{-16}$	–
G142.2446+01.4299	$4.2 \pm 0.1 \times 10^{-18}$	$<5.5 \times 10^{-19}$	$<8.2 \times 10^{-19}$	$<7.8 \times 10^{-19}$	$1.3 \pm 0.1 \times 10^{-18}$	$<1.3 \times 10^{-18}$	$<7.0 \times 10^{-19}$	$<6.0 \times 10^{-19}$	–

Table B1 – *continued*

Name	Brγ	Br 10	Br 11	Br 12/[Fe II]	H_2 2.1218 μm	H_2 2.2477 μm	Fluorescent Fe II	He I 2.0587 μM	Pfund?
G144.6678−00.7136	$7.8 \pm 0.5 \times 10^{-18}$	$6.1 \pm 0.8 \times 10^{-18}$	$5.1 \pm 0.7 \times 10^{-18}$	$3.5 \pm 0.6 \times 10^{-18}$	$5.6 \pm 0.7 \times 10^{-18}$	$<2.2 \times 10^{-18}$	$1.8 \pm 0.6 \times 10^{-18}$	$<3.9 \times 10^{-18}$	–
G145.1975+02.9870 – 1	$<8.5 \times 10^{-19}$	$<8.6 \times 10^{-19}$	$<1.2 \times 10^{-18}$	$<1.1 \times 10^{-18}$	$1.1 \pm 0.1 \times 10^{-18}$	$<8.2 \times 10^{-19}$	$<9.7 \times 10^{-19}$	$<9.4 \times 10^{-19}$	–
G145.1975+02.9870 – 2	$1.5 \pm 0.2 \times 10^{-18}$	$<1.9 \times 10^{-18}$	$<1.8 \times 10^{-18}$	$<1.8 \times 10^{-18}$	$<1.4 \times 10^{-18}$	$<1.3 \times 10^{-18}$	$<1.6 \times 10^{-18}$	$<1.7 \times 10^{-18}$	–
G148.1201+00.2928	$4.1 \pm 0.3 \times 10^{-18}$	$6 \pm 1 \times 10^{-19}$	$<1.7 \times 10^{-18}$	$<1.6 \times 10^{-18}$	$<4.8 \times 10^{-18}$	$<4.9 \times 10^{-18}$	$<1.3 \times 10^{-18}$	$<2.5 \times 10^{-18}$	–
G150.6862−00.6887	$1.30 \pm 0.02 \times 10^{-16}$	$1.04 \pm 0.07 \times 10^{-16}$	$9.2 \pm 0.7 \times 10^{-17}$	$9.2 \pm 0.7 \times 10^{-17}$	$1.6 \pm 0.3 \times 10^{-17}$	$<9.2 \times 10^{-18}$	$2.2 \pm 0.7 \times 10^{-17}$	$<1.9 \times 10^{-17}$	–
G151.6120−00.4575	$1.93 \pm 0.04 \times 10^{-16}$	$9.8 \pm 0.7 \times 10^{-17}$	$<7.7 \times 10^{-17}$	$1.41 \pm 0.09 \times 10^{-16}$	$<4.7 \times 10^{-17}$	$<4.9 \times 10^{-17}$	$5.1 \pm 0.5 \times 10^{-17}$	$<5.6 \times 10^{-17}$	–
G168.0627+00.8221	$9.6 \pm 0.5 \times 10^{-18}$	$4.7 \pm 0.3 \times 10^{-18}$	$5.4 \pm 0.4 \times 10^{-18}$	$6.9 \pm 0.4 \times 10^{-18}$	$8.7 \pm 0.5 \times 10^{-18}$	$<6.8 \times 10^{-18}$	$1.1 \pm 0.3 \times 10^{-18}$	$<3.0 \times 10^{-18}$	–
G169.6459−00.0687	$4.77 \pm 0.04 \times 10^{-17}$	$2.96 \pm 0.04 \times 10^{-17}$	$2.71 \pm 0.04 \times 10^{-17}$	$2.34 \pm 0.04 \times 10^{-17}$	$1.2 \pm 0.4 \times 10^{-18}$	$<9.2 \times 10^{-19}$	$3.8 \pm 0.4 \times 10^{-18}$	$<1.9 \times 10^{-18}$	P
G173.4815+02.4459	$1.5 \pm 0.3 \times 10^{-18}$	$<7.2 \times 10^{-19}$	$<1.1 \times 10^{-18}$	$<1.1 \times 10^{-18}$	$2.7 \pm 0.1 \times 10^{-18}$	$<8.3 \times 10^{-19}$	$<1.1 \times 10^{-18}$	$<1.7 \times 10^{-18}$	–
G173.4839+02.4317	$3.42 \pm 0.06 \times 10^{-16}$	$1.25 \pm 0.07 \times 10^{-16}$	$<3.7 \times 10^{-17}$	$7.2 \pm 0.2 \times 10^{-17}$	$1.9 \pm 0.4 \times 10^{-17}$	$<2.0 \times 10^{-17}$	$4.9 \pm 0.3 \times 10^{-17}$	$7.5 \pm 0.7 \times 10^{-17}$	–
G173.6328+02.8064	$1.1 \pm 0.2 \times 10^{-17}$	$<2.4 \times 10^{-17}$	$1.8 \pm 0.5 \times 10^{-17}$	$1.8 \pm 0.2 \times 10^{-17}$	$1.13 \pm 0.08 \times 10^{-17}$	$<4.1 \times 10^{-17}$	$<2.2 \times 10^{-17}$	$<3.0 \times 10^{-17}$	–
G173.6339+02.8218	$2.72 \pm 0.06 \times 10^{-16}$	$1.11 \pm 0.07 \times 10^{-16}$	$1.0 \pm 0.2 \times 10^{-16}$	$6.5 \pm 0.7 \times 10^{-17}$	$<8.4 \times 10^{-17}$	$<7.9 \times 10^{-17}$	$<6.4 \times 10^{-17}$	$<5.5 \times 10^{-17}$	–
G173.7215+02.6924	$1.196 \pm 0.006 \times 10^{-15}$	$5.9 \pm 0.3 \times 10^{-16}$	$5.3 \pm 0.3 \times 10^{-16}$	$4.4 \pm 0.3 \times 10^{-16}$	$<1.7 \times 10^{-17}$	$<9.3 \times 10^{-18}$	$8.1 \pm 0.3 \times 10^{-17}$	$<3.3 \times 10^{-17}$	P
G177.7291−00.3358	$3.5 \pm 0.2 \times 10^{-16}$	$1.9 \pm 0.5 \times 10^{-16}$	$5.6 \pm 0.5 \times 10^{-16}$	$6.1 \pm 0.5 \times 10^{-16}$	$<1.0 \times 10^{-16}$	$<1.8 \times 10^{-16}$	$<1.5 \times 10^{-16}$	$<3.5 \times 10^{-16}$	–
G178.7540+01.1609	$7.45 \pm 0.08 \times 10^{-16}$	$3.59 \pm 0.05 \times 10^{-16}$	$<1.1 \times 10^{-16}$	$2.63 \pm 0.03 \times 10^{-16}$	$<1.2 \times 10^{-17}$	$<1.6 \times 10^{-17}$	$6.1 \pm 0.4 \times 10^{-17}$	$<3.8 \times 10^{-17}$	P
G179.0380+04.3003	$1.1 \pm 0.1 \times 10^{-18}$	$<6.2 \times 10^{-18}$	$<2.0 \times 10^{-18}$	$2.4 \pm 0.2 \times 10^{-18}$	$8.7 \pm 0.9 \times 10^{-19}$	$<2.9 \times 10^{-18}$	$<2.3 \times 10^{-18}$	$<2.7 \times 10^{-18}$	–
G183.4530−01.7774	$1.9 \pm 0.4 \times 10^{-18}$	$<1.6 \times 10^{-18}$	$<2.0 \times 10^{-18}$	$3.4 \pm 0.7 \times 10^{-18}$	$<3.5 \times 10^{-18}$	$<5.1 \times 10^{-18}$	$<1.9 \times 10^{-18}$	$<2.0 \times 10^{-18}$	–
G184.8704−01.7329	$1.86 \pm 0.04 \times 10^{-16}$	$2.0 \pm 0.2 \times 10^{-16}$	$2.0 \pm 0.1 \times 10^{-16}$	$1.5 \pm 0.1 \times 10^{-16}$	$7 \pm 1 \times 10^{-17}$	$<2.1 \times 10^{-17}$	$1.55 \pm 0.09 \times 10^{-16}$	$<4.4 \times 10^{-17}$	–
G188.8120+01.0686	$-2.4 \pm 0.4 \times 10^{-18}$	$-2.5 \pm 0.5 \times 10^{-18}$	$<2.5 \times 10^{-18}$	$<2.3 \times 10^{-18}$	$1.1 \pm 0.1 \times 10^{-18}$	$<1.4 \times 10^{-18}$	$<2.4 \times 10^{-18}$	$<9.3 \times 10^{-19}$	–
G188.9479+00.8871	$<2.6 \times 10^{-16}$	$<8.5 \times 10^{-17}$	$<6.7 \times 10^{-17}$	$6.1 \pm 0.6 \times 10^{-17}$	$<1.9 \times 10^{-16}$	$<3.5 \times 10^{-16}$	$<7.9 \times 10^{-17}$	$<1.7 \times 10^{-16}$	–
G188.9696−01.9380	$1.4 \pm 0.3 \times 10^{-18}$	$<1.5 \times 10^{-18}$	$<9.3 \times 10^{-19}$	$2.4 \pm 0.3 \times 10^{-18}$	$1.37 \pm 0.03 \times 10^{-17}$	$<1.9 \times 10^{-18}$	$<1.1 \times 10^{-18}$	$<1.0 \times 10^{-18}$	–
G189.0307+00.7821	$1.82 \pm 0.07 \times 10^{-16}$	$1.3 \pm 0.2 \times 10^{-17}$	$<7.7 \times 10^{-18}$	$<7.3 \times 10^{-18}$	$<1.2 \times 10^{-16}$	$<2.1 \times 10^{-16}$	$<7.4 \times 10^{-18}$	$<8.0 \times 10^{-17}$	–
G189.0323+00.8092	$1.05 \pm 0.03 \times 10^{-15}$	$1.6 \pm 0.2 \times 10^{-16}$	$<1.0 \times 10^{-16}$	$1.37 \pm 0.06 \times 10^{-16}$	$<2.5 \times 10^{-16}$	$<4.9 \times 10^{-16}$	$1.0 \pm 0.1 \times 10^{-16}$	$<3.9 \times 10^{-16}$	–
G192.6005−00.0479	$<1.2 \times 10^{-17}$	$<2.5 \times 10^{-18}$	$<2.4 \times 10^{-18}$	$<2.3 \times 10^{-18}$	$1.20 \pm 0.06 \times 10^{-17}$	$2.5 \pm 0.7 \times 10^{-18}$	$<2.1 \times 10^{-18}$	$<4.0 \times 10^{-18}$	–
G192.9089−00.6259	$3.0 \pm 0.9 \times 10^{-18}$	$<2.9 \times 10^{-18}$	$<3.9 \times 10^{-18}$	$<3.7 \times 10^{-18}$	$1.2 \pm 0.1 \times 10^{-17}$	$4 \pm 1 \times 10^{-18}$	$<3.5 \times 10^{-18}$	$<3.3 \times 10^{-18}$	–
G194.9349−01.2224	$9.2 \pm 1.0 \times 10^{-18}$	$3.5 \pm 0.6 \times 10^{-18}$	$8 \pm 2 \times 10^{-18}$	$<5.1 \times 10^{-18}$	$9 \pm 1 \times 10^{-18}$	$<1.1 \times 10^{-17}$	$<7.1 \times 10^{-18}$	$-1.52 \pm 0.08 \times 10^{-17}$	–
G196.1620−01.2546	$1.9 \pm 0.2 \times 10^{-18}$	$<6.3 \times 10^{-19}$	–	–	$<1.6 \times 10^{-18}$	$<2.1 \times 10^{-18}$	$<8.3 \times 10^{-19}$	$<9.1 \times 10^{-19}$	–
G196.4542−01.6777	$4.6 \pm 0.2 \times 10^{-18}$	$1.8 \pm 0.3 \times 10^{-18}$	$<1.4 \times 10^{-18}$	$3.9 \pm 0.5 \times 10^{-18}$	$6.2 \pm 0.3 \times 10^{-18}$	$<3.5 \times 10^{-18}$	$<1.4 \times 10^{-18}$	$2.4 \pm 0.6 \times 10^{-18}$	–
G200.0789−01.6323	$1.6 \pm 0.2 \times 10^{-18}$	$<8.3 \times 10^{-19}$	$<1.4 \times 10^{-18}$	$<1.3 \times 10^{-18}$	$4.2 \pm 0.2 \times 10^{-18}$	$1.4 \pm 0.2 \times 10^{-18}$	$<1.2 \times 10^{-18}$	$<1.0 \times 10^{-18}$	–
G203.3166+02.0564	$9.9 \pm 0.3 \times 10^{-16}$	$4.0 \pm 0.3 \times 10^{-16}$	$3.2 \pm 0.4 \times 10^{-16}$	$1.7 \pm 0.3 \times 10^{-16}$	$<7.0 \times 10^{-16}$	$<6.3 \times 10^{-16}$	$1.8 \pm 0.3 \times 10^{-16}$	$<5.6 \times 10^{-16}$	–
G207.2654−01.8080 – 1	$9.8 \pm 0.2 \times 10^{-17}$	$2.6 \pm 0.1 \times 10^{-17}$	$2.0 \pm 0.1 \times 10^{-17}$	$1.15 \pm 0.09 \times 10^{-17}$	$<7.0 \times 10^{-18}$	$<6.6 \times 10^{-18}$	$7.9 \pm 1.0 \times 10^{-18}$	$<4.0 \times 10^{-18}$	–
G207.2654−01.8080 – 2	$3.00 \pm 0.06 \times 10^{-16}$	$1.34 \pm 0.08 \times 10^{-16}$	$1.15 \pm 0.08 \times 10^{-16}$	$8.6 \pm 0.8 \times 10^{-17}$	$<3.3 \times 10^{-17}$	$<2.0 \times 10^{-17}$	$4.7 \pm 0.9 \times 10^{-17}$	$<3.6 \times 10^{-17}$	–
G211.8957−01.2025	$2.92 \pm 0.10 \times 10^{-18}$	$1.4 \pm 0.3 \times 10^{-18}$	$6 \pm 1 \times 10^{-19}$	$<7.1 \times 10^{-19}$	$1.27 \pm 0.08 \times 10^{-18}$	$<5.6 \times 10^{-19}$	$<7.1 \times 10^{-19}$	$<5.8 \times 10^{-19}$	–
G212.0641−00.7395	$7.0 \pm 0.8 \times 10^{-18}$	$<2.0 \times 10^{-18}$	$5 \pm 2 \times 10^{-18}$	$2.5 \pm 0.4 \times 10^{-18}$	$1.6 \pm 0.1 \times 10^{-17}$	$<6.9 \times 10^{-18}$	$<1.5 \times 10^{-18}$	$<3.2 \times 10^{-18}$	–
G212.2344−03.5038	$9.3 \pm 0.2 \times 10^{-17}$	$5.4 \pm 0.8 \times 10^{-17}$	$<1.5 \times 10^{-17}$	$4.1 \pm 0.2 \times 10^{-17}$	$<9.3 \times 10^{-18}$	$<1.1 \times 10^{-17}$	$2.2 \pm 0.2 \times 10^{-17}$	$<6.1 \times 10^{-18}$	–
G212.9626+01.2954	$2.1 \pm 0.3 \times 10^{-16}$	$1.0 \pm 0.1 \times 10^{-16}$	$5.0 \pm 0.9 \times 10^{-17}$	$1.0 \pm 0.2 \times 10^{-16}$	$2.3 \pm 0.6 \times 10^{-16}$	$<1.8 \times 10^{-16}$	$<4.4 \times 10^{-17}$	$<1.3 \times 10^{-16}$	–
G213.9180+00.3786	$2.13 \pm 0.05 \times 10^{-17}$	$8.6 \pm 1.0 \times 10^{-18}$	$1.8 \pm 0.2 \times 10^{-17}$	$8.1 \pm 0.5 \times 10^{-18}$	$<6.4 \times 10^{-18}$	$<6.9 \times 10^{-18}$	$<5.1 \times 10^{-18}$	$-3.4 \pm 0.8 \times 10^{-18}$	–
G215.8902−02.0094	$9.0 \pm 0.2 \times 10^{-18}$	$4.2 \pm 0.6 \times 10^{-18}$	$<2.4 \times 10^{-18}$	$2.6 \pm 0.4 \times 10^{-18}$	$<2.4 \times 10^{-18}$	$<2.7 \times 10^{-18}$	$1.6 \pm 0.2 \times 10^{-18}$	$<2.1 \times 10^{-18}$	–
G217.6047−02.6170	$2.31 \pm 0.04 \times 10^{-17}$	$5.8 \pm 0.5 \times 10^{-18}$	$<1.7 \times 10^{-18}$	$4.6 \pm 0.3 \times 10^{-18}$	$9.4 \pm 0.3 \times 10^{-18}$	$<9.0 \times 10^{-19}$	$1.7 \pm 0.3 \times 10^{-18}$	$<1.7 \times 10^{-18}$	–
G224.6075−01.0063	$1.7 \pm 0.3 \times 10^{-16}$	$5 \pm 1 \times 10^{-17}$	$1.1 \pm 0.3 \times 10^{-16}$	$2.2 \pm 0.1 \times 10^{-16}$	$1.8 \pm 0.3 \times 10^{-16}$	$<2.0 \times 10^{-16}$	$<6.9 \times 10^{-17}$	$<1.2 \times 10^{-16}$	–
G232.6207+00.9959	$3.7 \pm 0.2 \times 10^{-17}$	$1.6 \pm 0.2 \times 10^{-17}$	$<1.1 \times 10^{-17}$	$8.0 \pm 0.8 \times 10^{-18}$	$<1.0 \times 10^{-17}$	$<8.6 \times 10^{-18}$	$8.8 \pm 0.7 \times 10^{-18}$	$<1.0 \times 10^{-17}$	–

Table B2. Equivalent widths (in Å) of CO 2–0 bandhead emission for the YSOs, with the mean continuum flux density (in W m^{-2} μm^{-1}) in the 2.2825–2.2875 μm region just to the blue end of the bandhead. A positive EW indicates emission. The errors are quoted to 1σ; the limits are 3σ limits. The negative for G032.4727+00.2041 is used to indicate that while looking at the spectrum there appears to be absorption, but the detection is not above the 3σ threshold. All other limits are limits on emission.

Name	CO EW (Å)	Continuum flux density	Name	CO EW (Å)	Continuum flux density	Name	CO EW (Å)	Continuum flux density
G010.8411−02.5919	2.2 ± 0.4	$2.87 \pm 0.02 \times 10^{-14}$	G032.9957+00.0415	<1.3	$4.72 \pm 0.05 \times 10^{-14}$	G071.8944+01.3107	<2.4	$1.33 \pm 0.01 \times 10^{-14}$
G010.8856+00.1221	<0.8	$5.63 \pm 0.03 \times 10^{-14}$	G033.3891+00.1989	<1.5	$8.18 \pm 0.03 \times 10^{-13}$	G072.2479+00.2617B	3.9 ± 0.8	$2.37 \pm 0.03 \times 10^{-15}$
G011.9019+00.7265	<8.8	$1.04 \pm 0.04 \times 10^{-12}$	G034.0126−00.2832	<0.7	$4.39 \pm 0.01 \times 10^{-13}$	G073.0633+01.7958	<3.2	$1.16 \pm 0.02 \times 10^{-14}$
G016.7122+01.3119 – 1	<2.0	$2.72 \pm 0.02 \times 10^{-13}$	G034.0500−00.2977	<1.6	$7.25 \pm 0.03 \times 10^{-14}$	G073.6525+00.1944	4.5 ± 0.8	$8.38 \pm 0.04 \times 10^{-14}$
G016.7122+01.3119 – 2	<1.8	$1.52 \pm 0.02 \times 10^{-14}$	G034.4035+00.2282	6.0 ± 1.2	$1.862 \pm 0.010 \times 10^{-15}$	G073.6952−00.9996	3.0 ± 0.6	$2.37 \pm 0.01 \times 10^{-13}$
G016.7981+00.1264	<1.6	$4.93 \pm 0.04 \times 10^{-14}$	G034.6243−00.1300	<4.4	$2.41 \pm 0.03 \times 10^{-14}$	G075.6014+01.6394	<4.7	$1.64 \pm 0.02 \times 10^{-15}$
G017.0332+00.7476A	<12.1	$3.9 \pm 0.4 \times 10^{-16}$	G034.7569+00.0247	<6.1	$2.8 \pm 0.1 \times 10^{-16}$	G075.7666+00.3424 – 1	<1.2	$1.95 \pm 0.01 \times 10^{-13}$
G017.3765+02.2512	<1.5	$3.59 \pm 0.04 \times 10^{-13}$	G034.8211+00.3519	<2.5	$1.85 \pm 0.08 \times 10^{-14}$	G075.7666+00.3424 – 2	<2.1	$2.27 \pm 0.02 \times 10^{-14}$
G018.3412+01.7681	<1.4	$6.87 \pm 0.05 \times 10^{-14}$	G035.1979−00.7427	9.1 ± 0.9	$2.62 \pm 0.02 \times 10^{-14}$	G076.0902+00.1412	<1.3	$6.79 \pm 0.05 \times 10^{-15}$
G018.3706−00.3818	<1.3	$7.82 \pm 0.02 \times 10^{-14}$	G036.8780−00.4728 – 1	<4.4	$1.43 \pm 0.01 \times 10^{-15}$	G076.3829−00.6210	6.5 ± 0.8	$1.189 \pm 0.007 \times 10^{-12}$
G018.6608+00.0372	<2.0	$5.75 \pm 0.04 \times 10^{-15}$	G036.8780−00.4728 – 2	<4.3	$1.36 \pm 0.04 \times 10^{-15}$	G077.4052−01.2136	<2.1	$4.17 \pm 0.06 \times 10^{-15}$
G019.8922+00.1023	<0.8	$2.332 \pm 0.006 \times 10^{-14}$	G036.9194+00.4825A	<2.7	$1.016 \pm 0.007 \times 10^{-15}$	G077.4622+01.7600 – 1	6.0 ± 0.4	$1.179 \pm 0.008 \times 10^{-14}$
G019.9224−00.2577	9.5 ± 1.1	$4.78 \pm 0.08 \times 10^{-15}$	G037.5536+00.2008	<3.4	$3.54 \pm 0.04 \times 10^{-15}$	G077.4622+01.7600 – 2	<3.8	$3.04 \pm 0.08 \times 10^{-15}$
G020.5143+00.4936	<21.5	$2.6 \pm 0.2 \times 10^{-14}$	G039.4943−00.9933	<0.8	$4.13 \pm 0.02 \times 10^{-14}$	G077.8999+01.7678	<2.2	$5.44 \pm 0.02 \times 10^{-14}$
G021.5624−00.0329	<9.3	$5.8 \pm 0.2 \times 10^{-12}$	G042.0341+00.1905A	<1.1	$1.222 \pm 0.008 \times 10^{-13}$	G078.1224+03.6320	<4.0	$2.76 \pm 0.05 \times 10^{-15}$
G023.3891+00.1851	<2.4	$2.12 \pm 0.02 \times 10^{-12}$	G042.0977+00.3521	<4.0	$1.03 \pm 0.03 \times 10^{-15}$	G078.4373+02.6584B	<1.0	$1.82 \pm 0.02 \times 10^{-14}$
G023.6566−00.1273	−19.1 ± 0.7	$4.17 \pm 0.02 \times 10^{-13}$	G042.1099−00.4466	<2.8	$3.13 \pm 0.05 \times 10^{-15}$	G078.4705−00.1830	<2.8	$1.38 \pm 0.01 \times 10^{-15}$
G024.6343−00.3233	<1.7	$6.47 \pm 0.06 \times 10^{-14}$	G043.1635−00.0697A	<1.5	$3.64 \pm 0.03 \times 10^{-15}$	G078.4754+01.0421	1.9 ± 0.2	$1.59 \pm 0.01 \times 10^{-13}$
G025.6498+01.0491	8.9 ± 0.6	$9.08 \pm 0.07 \times 10^{-15}$	G043.5216−00.6476	<2.3	$1.56 \pm 0.01 \times 10^{-14}$	G078.7641+01.6862	<4.6	$9.2 \pm 0.3 \times 10^{-16}$
G025.7161+00.0486	<2.2	$4.98 \pm 0.04 \times 10^{-15}$	G043.9956−00.0111	<2.0	$3.04 \pm 0.03 \times 10^{-14}$	G078.8867+00.7087	<0.7	$1.425 \pm 0.007 \times 10^{-12}$
G025.8015−00.1570 – 1	<2.1	$7.3 \pm 0.1 \times 10^{-15}$	G044.3103+00.0416	<5.8	$1.48 \pm 0.04 \times 10^{-15}$	G078.9761+00.3567	<0.7	$7.83 \pm 0.02 \times 10^{-13}$
G025.8015−00.1570 – 2	<2.3	$8.80 \pm 0.08 \times 10^{-15}$	G045.1894−00.4387	<0.9	$2.90 \pm 0.02 \times 10^{-13}$	G079.1272+02.2782	<1.2	$5.26 \pm 0.03 \times 10^{-14}$
G026.2020+00.2262	<1.1	$2.868 \pm 0.008 \times 10^{-13}$	G045.4641+00.0284	<4.7	$1.14 \pm 0.02 \times 10^{-16}$	G080.0467+00.3101	20.1 ± 0.2	$7.64 \pm 0.03 \times 10^{-14}$
G026.3819+01.4057 – 1	<1.6	$4.61 \pm 0.06 \times 10^{-15}$	G048.9897−00.2992A	<2.4	$2.95 \pm 0.04 \times 10^{-15}$	G080.1909+00.5353	<0.8	$1.70 \pm 0.03 \times 10^{-13}$
G026.3819+01.4057 – 2	<1.8	$4.81 \pm 0.02 \times 10^{-14}$	G049.0431−01.0787	6.5 ± 0.5	$4.42 \pm 0.03 \times 10^{-15}$	G080.8282+00.5670A	<0.7	$2.35 \pm 0.01 \times 10^{-13}$
G026.4207+01.6858	<1.7	$5.31 \pm 0.03 \times 10^{-15}$	G049.4227−00.3715	<6.6	$8.2 \pm 0.2 \times 10^{-14}$	G080.8645+00.4197	<2.0	$3.37 \pm 0.04 \times 10^{-15}$
G026.4958+00.7105 – 1	<5.2	$6.4 \pm 0.3 \times 10^{-16}$	G049.4883−00.3545B	<8.7	$8.3 \pm 0.2 \times 10^{-15}$	G081.5168+00.1926	<1.2	$1.792 \pm 0.010 \times 10^{-14}$
G026.4958+00.7105 – 2	<13.8	$1.8 \pm 0.3 \times 10^{-16}$	G050.0721+00.5591	<2.4	$3.70 \pm 0.02 \times 10^{-15}$	G081.7131+00.5792	<0.5	$1.220 \pm 0.003 \times 10^{-13}$
G026.5972−00.0241	<27.2	$1.4 \pm 0.2 \times 10^{-16}$	G050.2213−00.6063	<1.2	$2.71 \pm 0.03 \times 10^{-14}$	G081.7624+00.5916	<1.3	$9.76 \pm 0.08 \times 10^{-15}$
G027.2220+00.1361 – 2	<6.8	$3.2 \pm 0.2 \times 10^{-16}$	G050.2844−00.3925A	2.3 ± 0.4	$7.1 \pm 0.2 \times 10^{-14}$	G082.5682+00.4040A	<0.5	$4.54 \pm 0.03 \times 10^{-13}$
G027.7954−00.2772	<3.8	$3.20 \pm 0.03 \times 10^{-14}$	G052.2025+00.7217A	<1.2	$6.86 \pm 0.05 \times 10^{-14}$	G083.7071+03.2817	<0.8	$6.50 \pm 0.03 \times 10^{-13}$
G028.2325+00.0394	<1.2	$6.88 \pm 0.07 \times 10^{-15}$	G052.2078+00.6890	<4.3	$2.27 \pm 0.05 \times 10^{-14}$	G084.3065+01.8933	<0.9	$1.167 \pm 0.010 \times 10^{-13}$
G028.3046−00.3871A	8.3 ± 1.6	$3.98 \pm 0.09 \times 10^{-14}$	G052.5405−00.9272	<2.2	$1.79 \pm 0.06 \times 10^{-14}$	G085.4102+00.0032A	<1.0	$1.75 \pm 0.05 \times 10^{-14}$
G028.3373+00.1189	<4.2	$4.5 \pm 0.1 \times 10^{-14}$	G052.9217+00.4142	<1.8	$1.74 \pm 0.01 \times 10^{-14}$	G089.6368+00.1732	<0.8	$3.70 \pm 0.02 \times 10^{-14}$
G028.8621+00.0657	<4.6	$1.27 \pm 0.02 \times 10^{-15}$	G053.1417+00.0705	<1.1	$4.51 \pm 0.05 \times 10^{-15}$	G090.2095+02.0405	<29.9	$2.1 \pm 0.4 \times 10^{-14}$
G030.1981−00.1691	<3.7	$1.57 \pm 0.01 \times 10^{-13}$	G053.5343−00.7943	<1.0	$7.40 \pm 0.04 \times 10^{-14}$	G094.3228−00.1671	<1.7	$3.17 \pm 0.10 \times 10^{-14}$
G030.2971+00.0549	<21.8	$1.3 \pm 0.2 \times 10^{-16}$	G055.1581−00.2991A	<2.7	$1.75 \pm 0.05 \times 10^{-14}$	G094.4637−00.8043	7.0 ± 0.7	$6.77 \pm 0.03 \times 10^{-15}$
G030.4117−00.2277	<0.8	$2.12 \pm 0.01 \times 10^{-14}$	G056.3694−00.6333	<2.7	$5.3 \pm 0.1 \times 10^{-15}$	G095.0026−01.5779	<2.2	$3.99 \pm 0.05 \times 10^{-15}$
G030.5942−00.1273	<0.3	$1.877 \pm 0.004 \times 10^{-13}$	G056.4120−00.0277	<3.7	$8.9 \pm 0.1 \times 10^{-13}$	G095.0531+03.9724	<5.6	$9.1 \pm 0.2 \times 10^{-16}$
G030.8185+00.2729	<2.3	$1.94 \pm 0.02 \times 10^{-14}$	G059.3614−00.2068	3.2 ± 0.3	$8.02 \pm 0.05 \times 10^{-14}$	G096.3597+01.2982	<7.9	$1.85 \pm 0.08 \times 10^{-14}$
G030.9726−00.1410	<3.6	$1.76 \pm 0.03 \times 10^{-15}$	G059.6403−00.1812A	<1.4	$6.42 \pm 0.06 \times 10^{-15}$	G096.4353+01.3233A – 1	<1.3	$2.07 \pm 0.01 \times 10^{-14}$
G030.9727+00.5620	<1.5	$4.2 \pm 0.1 \times 10^{-14}$	G059.7831+00.0648	<2.3	$9.86 \pm 0.08 \times 10^{-15}$	G096.4353+01.3233A – 2	<2.1	$8.7 \pm 0.1 \times 10^{-15}$
G030.9959−00.0771	<3.8	$1.59 \pm 0.04 \times 10^{-15}$	G059.8329+00.6729	<10.8	$9.2 \pm 0.5 \times 10^{-16}$	G097.5268+03.1837C	<0.7	$2.88 \pm 0.01 \times 10^{-14}$
G032.0451+00.0589	<5.0	$7.7 \pm 0.4 \times 10^{-16}$	G060.5750−00.1861	2.7 ± 0.8	$1.010 \pm 0.007 \times 10^{-14}$	G097.9978+01.4688	7.0 ± 0.3	$5.79 \pm 0.02 \times 10^{-14}$
G032.0518−00.0902	−9.9 ± 0.9	$2.16 \pm 0.02 \times 10^{-15}$	G063.1140+00.3416	<1.6	$8.5 \pm 0.1 \times 10^{-13}$	G098.8555+02.9344	8.5 ± 0.7	$3.90 \pm 0.06 \times 10^{-15}$
G032.4727+00.2041	>−3.2	$2.90 \pm 0.03 \times 10^{-14}$	G065.7798−02.6121	<1.5	$6.85 \pm 0.05 \times 10^{-14}$	G100.1620+01.6647	<8.7	$1.52 \pm 0.07 \times 10^{-15}$
G032.8205−00.3300	<3.1	$5.43 \pm 0.10 \times 10^{-15}$	G068.2040+00.2387	<1.2	$1.69 \pm 0.02 \times 10^{-14}$	G100.1685+02.0266	<4.6	$9.8 \pm 0.1 \times 10^{-15}$

Table B2 – *continued*

Name	CO EW (Å)	Continuum flux density	Name	CO EW (Å)	Continuum flux density
G100.2124+01.8829	4.8 ± 0.4	$2.70 \pm 0.03 \times 10^{-14}$	G178.7540+01.1609	<3.1	$1.473 \pm 0.009 \times 10^{-13}$
G100.3779−03.5784	<1.6	$2.552 \pm 0.010 \times 10^{-14}$	G179.0380+04.3003	1.4 ± 0.2	$2.470 \pm 0.010 \times 10^{-14}$
G102.3533+03.6360	<0.6	$2.639 \pm 0.008 \times 10^{-13}$	G183.4530−01.7774	<1.7	$2.01 \pm 0.03 \times 10^{-14}$
G103.8034+00.4062	<2.8	$2.40 \pm 0.03 \times 10^{-15}$	G184.8704−01.7329	<1.0	$2.47 \pm 0.03 \times 10^{-13}$
G103.8744+01.8558	<3.1	$1.46 \pm 0.02 \times 10^{-14}$	G188.8120+01.0686	<2.6	$5.56 \pm 0.06 \times 10^{-15}$
G105.5072+00.2294	<2.1	$6.94 \pm 0.06 \times 10^{-15}$	G188.9479+00.8871	<3.9	$8.1 \pm 0.1 \times 10^{-13}$
G107.6823−02.2423A	<2.1	$1.875 \pm 0.009 \times 10^{-14}$	G188.9696−01.9380	<1.5	$1.183 \pm 0.008 \times 10^{-14}$
G108.7575−00.9863	<1.0	$4.19 \pm 0.03 \times 10^{-14}$	G189.0307+00.7821	<2.3	$5.43 \pm 0.05 \times 10^{-13}$
G110.8038−02.5649	5.5 ± 0.2	$5.64 \pm 0.02 \times 10^{-14}$	G189.0323+00.8092	<2.1	$1.59 \pm 0.01 \times 10^{-12}$
G111.2348−01.2385	<1.2	$4.77 \pm 0.02 \times 10^{-14}$	G192.6005−00.0479	<1.5	$3.43 \pm 0.04 \times 10^{-14}$
G139.9091+00.1969A	3.5 ± 0.3	$3.64 \pm 0.01 \times 10^{-14}$	G192.9089−00.6259	<3.9	$7.8 \pm 0.1 \times 10^{-15}$
G141.9996+01.8202	<0.7	$3.26 \pm 0.01 \times 10^{-12}$	G194.9349−01.2224	4.7 ± 0.4	$7.34 \pm 0.04 \times 10^{-14}$
G142.2446+01.4299	<1.7	$3.73 \pm 0.05 \times 10^{-15}$	G196.1620−01.2546	3.9 ± 0.5	$5.81 \pm 0.08 \times 10^{-15}$
G144.6678−00.7136	<2.1	$2.99 \pm 0.02 \times 10^{-14}$	G196.4542−01.6777	<2.2	$1.71 \pm 0.01 \times 10^{-14}$
G145.1975+02.9870 – 1	<11.0	$1.30 \pm 0.05 \times 10^{-15}$	G200.0789−01.6323	<12.2	$9.2 \pm 0.5 \times 10^{-16}$
G145.1975+02.9870 – 2	<2.8	$8.39 \pm 0.04 \times 10^{-15}$	G203.3166+02.0564	<0.6	$4.867 \pm 0.009 \times 10^{-12}$
G148.1201+00.2928	<0.6	$2.51 \pm 0.02 \times 10^{-14}$	G207.2654−01.8080 – 1	<2.0	$3.30 \pm 0.02 \times 10^{-14}$
G150.6862−00.6887	11.9 ± 0.4	$1.14 \pm 0.01 \times 10^{-13}$	G207.2654−01.8080 – 2	2.2 ± 0.4	$2.473 \pm 0.010 \times 10^{-13}$
G151.6120−00.4575	2.5 ± 0.2	$5.34 \pm 0.02 \times 10^{-13}$	G211.8957−01.2025	<3.1	$2.65 \pm 0.04 \times 10^{-15}$
G168.0627+00.8221	2.6 ± 0.3	$2.48 \pm 0.02 \times 10^{-14}$	G212.0641−00.7395	<3.9	$1.33 \pm 0.02 \times 10^{-14}$
G169.6459−00.0687	<4.0	$5.13 \pm 0.03 \times 10^{-15}$	G212.2344−03.5038	<0.6	$1.048 \pm 0.004 \times 10^{-13}$
G173.4815+02.4459	<2.2	$3.33 \pm 0.03 \times 10^{-15}$	G212.9626+01.2954	<2.9	$4.54 \pm 0.10 \times 10^{-13}$
G173.4839+02.4317	<1.9	$2.15 \pm 0.01 \times 10^{-13}$	G213.9180+00.3786	<0.7	$5.63 \pm 0.03 \times 10^{-14}$
G173.6328+02.8064	<0.6	$3.166 \pm 0.009 \times 10^{-13}$	G215.8902−02.0094	2.0 ± 0.5	$2.29 \pm 0.03 \times 10^{-14}$
G173.6339+02.8218	<1.6	$7.24 \pm 0.01 \times 10^{-13}$	G217.6047−02.6170	<2.0	$4.09 \pm 0.06 \times 10^{-15}$
G173.7215+02.6924	<1.5	$1.29 \pm 0.01 \times 10^{-13}$	G224.6075−01.0063	<3.9	$4.10 \pm 0.08 \times 10^{-13}$
G177.7291−00.3358	3.5 ± 0.4	$1.67 \pm 0.01 \times 10^{-12}$	G232.6207+00.9959	1.4 ± 0.2	$1.055 \pm 0.003 \times 10^{-13}$

Table B3. List of objects for which either or both of the Brγ or He I 2.0587 μm emission lines have P-Cygni profiles.

Object	P-Cygni profile
G017.3765+02.2512	Both Brγ and He I
G018.3412+01.7681	Brγ only
G023.3891+00.1851	He I only
G027.7954−00.2772	Brγ only
G056.4120−00.0277	Both Brγ and He I
G073.6525+00.1944	Brγ only
G073.6952−00.9996	He I only
G076.3829−00.6210	He I only
G077.8999+01.7678	Brγ only
G102.3533+03.6360	Both Brγ and He I
G141.9996+01.8202	Both Brγ and He I
G151.6120−00.4575	He I only
G168.0627+00.8221	He I only
G173.6328+02.8064	He I only
G177.7291−00.3358	Both Brγ and He I
G189.0307+00.7821	Both Brγ and He I
G189.0323+00.8092	Both Brγ and He I
G194.9349−01.2224	He I only
G203.3166+02.0564	Brγ only
G213.9180+00.3786	Both Brγ and He I

This paper has been typeset from a TEX/LATEX file prepared by the author.